Summer 2017

Development of a variogram approach to spatial outlier detection using a supplemental digital elevation model dataset

Zane Daniel Helwig

Department:

DEVELOPMENT OF A VARIOGRAM APPROACH TO SPATIAL OUTLIER DETECTION USING A SUPPLEMENTAL DIGITAL ELEVATION MODEL DATASET

by

ZANE DANIEL HELWIG

A THESIS

Presented to the Faculty of the Graduate School of the

MISSOURI UNIVERSITY OF SCIENCE AND TECHNOLOGY

In Partial Fulfillment of the Requirements for the Degree

MASTER OF SCIENCE IN GEOLOGICAL ENGINEERING

2017

Approved by

Dr. Joe Guggenberger, Advisor
Dr. Andrew Curtis Elmore
Dr. Cesar Mendoza

PUBLICATION THESIS OPTION

This thesis consists of the following article which has been submitted for publication:

Paper I: Pages 17-46 have been submitted to the Journal of Hydrology.

ABSTRACT

When developing a ground water model, the quality of the dataset should first be evaluated. Spatial outliers can lead to predictions which are not representative of actual conditions. In order to isolate misrepresentative points, a method is presented which examines the experimental variogram of a ground water elevation dataset. To define a threshold variance between pairs of ground water elevation measures, ground elevation values from a digital elevation model (DEM) are used to determine a maximum reasonable variance expected to occur on the experimental variogram. To determine appropriate DEM parameters, a separate study was also done which observed characteristic behavior of gradient calculations for a DEM with fluctuating resolution and extent. This method is applied first to a synthetic dataset and then to a monitoring well network at Fort Leonard Wood, Missouri. Results of the analysis show that all points targeted as spatial outliers in the case study are justified for removal. This approach can readily be incorporated into the development of a regional groundwater model by kriging. The strengths of this method are that it incorporates supplemental DEM building of the concept that the groundwater surface is a smoothed version of the topographic surface. This method also takes advantage of every point pair relationship in that both neighboring points and distant pairs are compared.

ACKNOWLEDGEMENTS

A special thanks to Dr. Curtis Elmore for presenting the opportunity to pursue my Master's Degree and for the help and guidance throughout my research. A special thanks also to Dr. Joe Guggenberger for guidance on my thesis and encouragement along the way. Lastly a thanks to my sponsors at the Army Corps of Engineers for sponsoring this research.

TABLE OF CONTENTS

Page

LIST OF ILLUSTRATIONS

SECTION Page

PAPER

LIST OF TABLES

1. INTRODUCTION

1.1. REVIEW OF SPATIAL OUTLIER DETECTION APPROACHES

Two general types of outliers are presented by Shekhar et al. (2003). Global outliers are values that are inconsistent with the remainder of the dataset or do not follow the standard distribution of the dataset. Spatial outliers are values which do not follow the assumed continuity of nearby values or the underlying structure of the surface which is being considered. The key difference between these two definition's is that global outliers do not consider the spatial attribute of a point, therefore global methods are not suited to compare values which are samples of an surface that varies with space, such as terrain or groundwater elevation (GWE) data. The focus of this study will be to present a method to identify spatial outliers from a GWE dataset. Spatial outliers can be caused by natural variability that occurs in the system, such as sources of sinks due to karst, or from other sources of error in the acquisition of the data value. Therefore it is important to be able to identify these errors, so non-representative measures are excluded from a regional groundwater model and repetition of errors is mitigated. Shekhar et al. (2003) and Chen et al. (2008) identify two general methods which are designed to detect spatial outliers. The first is a graphical method which is based on the visualization of spatial data which highlights spatial outliers. The second is a quantitative method which provides a precise test to distinguish spatial outliers from the remainder of the data (Shekhar et al., 2003; Chen et al., 2008).

Miller et al. (1997) presented a quantitative approach to scanning for potential spatial outliers by examining the prediction error from kriging divided by the root of the kriging estimation variance, referred to as the z-score. Points with a high z-score indicated they needed further inspection. A similar approach was taken by Bardossy and Kundzewicz (1990) using a jack-knifing technique, where the point of interest is temporarily removed from the dataset, then neighboring points are used to predict the value at that location. The residual of the predicted and observed value is divided by the standard deviation of the estimation error. The resulting value is the criterion used to highlight spatial outliers. This process of comparing observed values to a value predicted at that same location by neighboring values in called cross validation. Tremblay and others (2015) presented a semi-automated filtering approach to detecting outliers from large public groundwater databases. The automated portion of the approach first identified depth to static water level measurements that were greater than a threshold determined by a high quality dataset. The second automated step calculated moving averages of neighboring wells and highlighted points that deviated significantly from the local average. For a final processing step the data identified as potential outliers was visually examined where qualitative hydrogeological knowledge was applied to determine if the points were truly outliers. Liu and others (2001) presented another quantitative technique using super block based spatial sorting and searching scheme to identify nearest neighbors. They applied an inverse distance weighted technique to interpolate from the identified nearest neighbors and compared the interpolated value to observed values. Points with high residuals were identified as spatial outliers. This technique was made more robust and overcame the shortcomings of typical cross

validation techniques by using a jackknifing technique to determine which neighbors had the greatest effect on the interpolated value, and subsequently dropping the two values which contributed the most to the estimation. Similarly Liu and others (2001) also calculated the gradient of the triangles formed by the neighboring points and the observation point and applied the same robust technique by dropping out the two most influential values. The robust gradient was compared to the non-robust method to determine if the observation point was a potential outlier. Shekhar et al. (2003) did a comprehensive study of a number of spatial outlier detection algorithms to identify the key components or building blocks of a spatial outlier detection algorithm. The authors first identified S-outliers as spatial objects lying in a spatial framework that can be described by an attribute function which has a statistically significant arithmetic difference from a neighborhood aggregate function. Where an aggregate function describes a group of data by a single representative value, such as the median or mean. Using this core definition an efficient algorithm was designed to minimize computer time in detection of S-outliers. Hannah (1981) presented an interesting approach to identifying errors in elevation data for digital terrain models. The approach was based on the assumption that a terrain model represents a continuous surface, which for the most part, varies smoothly with elevation. Therefore any points causing sharp discontinuities in the elevation or sudden changes in the surface slope can be suspected of being in error. Therefore a number of tests were done which looked the slopes between a central observation point and surrounding neighbor points. If the observation point caused a significant difference in the slope of surrounding points it was identified as a potential source of error.

Bardossy and Kundzewicz (1990) and Shekhar et al. (2003) identified that outliers can be detected during the development of a semivariogram by examining the cloud and selecting the points on the cloud with the highest squared differences. Shekhar et al. (2003) points out that this graphical approach lacks precise criteria to distinguish outliers from true values. A common practice in developing a groundwater model is to supplement sparse groundwater elevation (GWE) data with ground surface elevation data from a digital elevation model (DEM). This practice is based off the assumption that for unconfined conditions, the groundwater is a smoothed version of the topographic surface (King, 1899; Domenico and Schwartz, 1998; Blauvelt and Fullmer, 2011). Following this same assumption, this paper presents an approach that uses the variogram of a DEM to define a threshold on the experimental variogram of GWE values to provide precise criteria for identification. A key advantage to using relationships from an experimental variogram is that every pair of points is plotted so more information is used than tradition quantitative outlier detection approaches that only consider neighboring points. This approach provides new contributions by providing precise criteria for a graphical method.

1.2. GEOSTATISTICAL CONCEPTS

Geostatistical theory is based on the observation that the variability of measured quantities with a spatial attribute, called regionalized variables, have a particular structure (Journel and Huijbregts, 1978). The variogram, also referred to in some texts as the semi-variogram, is a common geostatistical tool used to describe this structure by quantifying the relation of point pairs, which possess spatial attributes, based on the

distance between the pair of points. The variogram function is expressed by Goovaerts (1997) as:

$$\gamma(s) = \frac{1}{2N(s)} \sum_{\alpha=1}^{N} (h(u_\alpha) - h(u_\alpha + s))^2 \quad (1)$$

Where:

$h = a\ measurement\ of\ some\ scaler\ quantity$

$s = a\ vector\ separating\ two\ data\ values$

$N(s) = number\ of\ data\ pairs\ separated\ by\ the\ vector\ s$

$u_a = vector\ of\ spatial\ coordinates\ of\ the\ \alpha^{th}\ individual$

An intrinsic hypothesis of the variogram is that the variogram function is not a function of the location u_a, but only a function of the separation, *s*. This intrinsic hypothesis is the hypothesis of second order stationarity of the differences. This means that within the domain of *h*, the variability between $\left(h(u_\alpha) - h(u_\alpha + s)\right)$ is constant and independent of u_a (Journel and Huijbregts, 1978). While the formal definition of the variance follows Equation (2), Goovaerts (1997) states that the semivariogram value at a given separation, *s*, is sometimes referred to as the semivariance. Following this established convention the value of the variogram function will be referred to here as the variance.

$$\sigma^2 = \frac{1}{n} \sum_{\alpha=1}^{n} (z(\alpha) - m)^2 \quad (2)$$

$where$

$\sigma^2 = variance$

$m = mean$

$z(\alpha) = measure\ of\ the\ continuous\ attribute\ z\ on\ indivuals, \alpha$

$n = number\ of\ individuals, \alpha$

The first step in the development of any variogram is plotting the experimental variogram, or the variogram cloud. The variogram cloud plots the variance for every possible pair of points on the domain, so *N* is always equal to one and every s is considered. To summarize the experimental variogram a binned variogram is developed. The binned variogram accounts for spatial anisotropy by setting an angular tolerance for the angle of separation, *s*. The semivariogram is symmetric with respect to its first bisector (Goovaerts, 1997), so the variogram value computed in opposite directions are identical. Therefore, the number of different directions considered on the variogram is the angular tolerance divided by 90°. As an example from Goovaerts (1997), for a semivariogram with an angular tolerance of 22.5°, there would be a total of four directional bins with directions of 22.5°, 67.5°, 112.5°, and 157.5°. In each direction the average variance is calculated for each increment of $|s|$. The size of the increment of separation distance,$|s|$, is referred to as the lag size.

2. METHOD DEVELOPMENT

For the same location on the topographic and potentiometric surface, it can be assumed that the gradient of the topographic surface should be greater than or equal to the gradient of the potentiometric surface. This follows the assumption of unconfined conditions for the groundwater surface. The equation for the gradient of a field of scalar values (a) is presented by Domenico and Schwartz (1998) as:

$$\nabla a = \frac{\partial a}{\partial x} i + \frac{\partial a}{\partial y} j + \frac{\partial a}{\partial z} k \tag{3}$$

The true gradient of a planar surface is calculated using the three point problem as presented by Vacher (2005). A good approximation of the gradient for the same planar surface can be found by computing the difference, or residual, of every pair of points on the domain, as presented in Equation (4) and (5). The magnitude of the gradient corresponds to the greatest residual and the direction of the gradient is parallel to vector separating the point pair with the greatest magnitude.

$$|\nabla a| = \frac{R_{max}}{|s_{max}|} \tag{4}$$

with

$$R_{max} = \max(R_i) \tag{5}$$

Where:

$R_i = The\ residual\ of\ the\ i^{th}\ pair\ of\ points\ lying\ on\ a\ plane$

$s_{max} =\ vector\ separating\ a\ pair\ of\ points\ corresponding\ to\ R_{max}$

To relate the gradient approximation from Equation (4) to the variogram function in Equation (1) it must be recognized that both equations consider the difference between each pair of points on the entire domain. Therefore from Equation (4), we expect that the

largest difference for the variogram function, $h(u_\alpha) - h(u_\alpha + s)$, for each lag interval to correspond to the average gradient for that lag over the domain. To get a more conservative average estimate of the aggregate gradient for each lag, only the greatest anisotropy direction should be considered. Because of the inherent variability in the gradient vector field over the domain, the use of this conservative average is an appropriate method to represent the gradient of the entire domain. When computing the binned variogram function for each direction, the variogram threshold is defined by the maximum variance (γ_{max}) for each lag interval of $|s|$.

$$\gamma_{max}(|s|, \theta_{max}) = \frac{1}{2N(|s|,\theta_{max})} \sum_{\alpha=1}^{N} (h(u_\alpha) - h(u_\alpha + |s|))^2 \quad (6)$$

Where:

$\theta_{max} = direction\ of\ s\ corresponding\ to\ the\ greatest\ value\ of\ \gamma(s)$ for each $|s|$

2.1. GRADIENT SCALE RELATIONSHIPS

Figure 2.1 shows that the location of the boundary formed by the binned variogram of the DEM points was found to be dependent on both the resolution of the DEM as well as its extent about the GWE dataset of interest. Therefore a study was done following the work of Silliman and Frost (1998) to determine the response of the range of gradient magnitudes and directions for gradient calculations using the solution to the three point problem presented by Vacher (2005). For the three point problem calculations, the acute angle of the triangle formed by the three points was limited to be greater than or equal to 30°. This reduced the number of required iterations (thus reducing computation time) and improved the convergence of calculations, as shown in Figure 2.2.

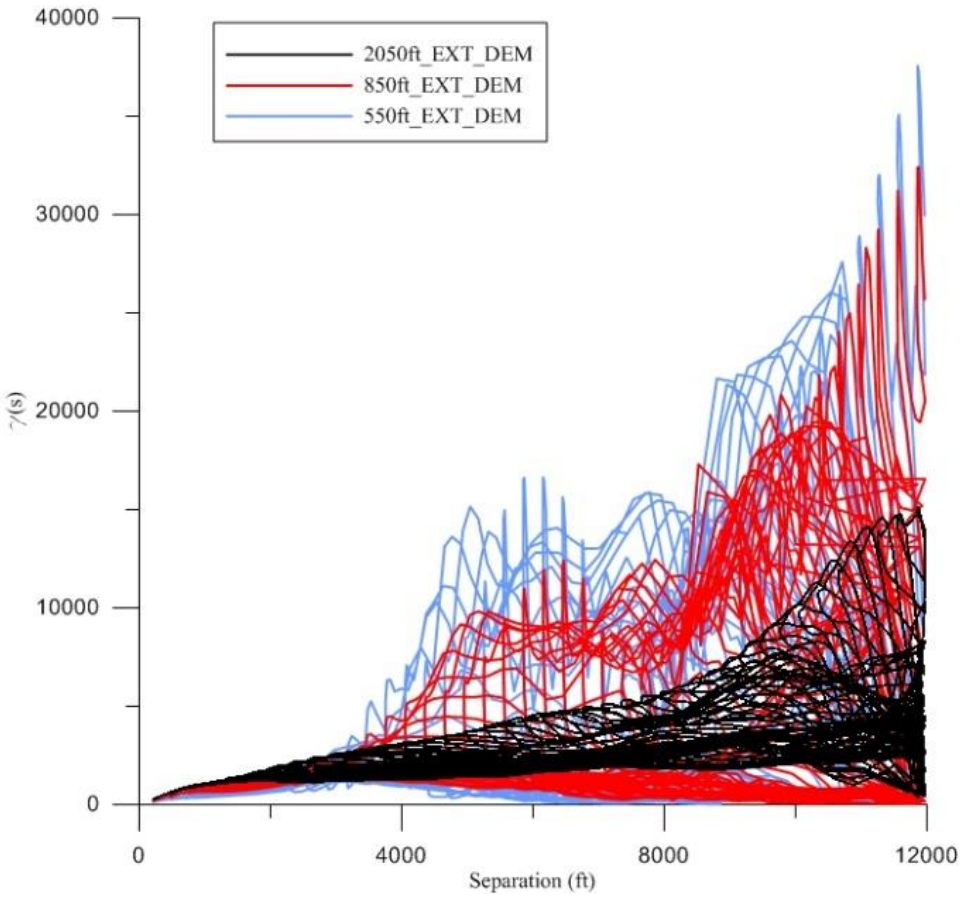

Figure 2.1. Variations in DEM threshold with changing extent.

To look at the scale effects of DEM parameters two different cases were considered to observe effects on both gradient magnitude and direction:

1) Constant resolution with variable extent
2) Constant extent with variable resolution

The extent was determined by selecting DEM points that where within a specified radial distance from the MW points. The different resolutions were based from a DEM with a 30ft (10m) grid size. To decrease the resolution, the grid sized was increased by mean aggregation in ArcGIS. For both cases the gradient magnitude and direction were plotted against the area of the triangle formed the by the three points used for the

calculation to determine the effects of scale. This study was done for two different locations to evaluate if relationships where location specific.

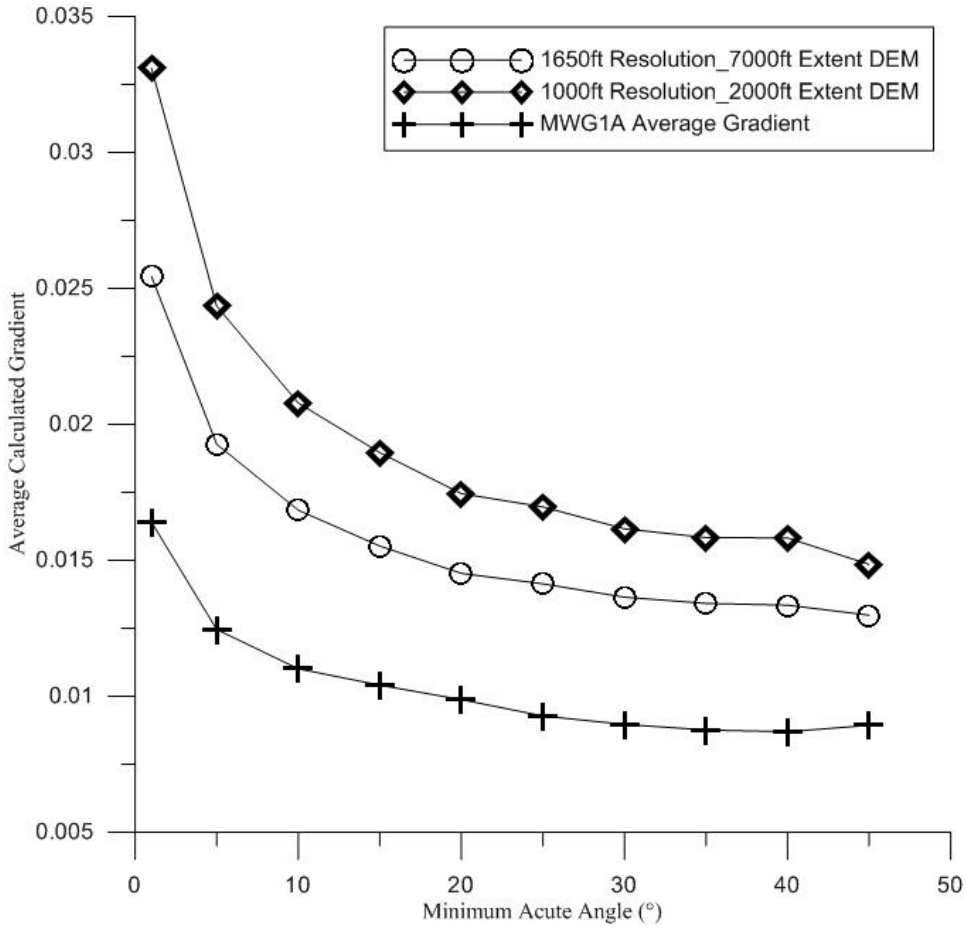

Figure 2.2. Establishing a minimum acute angle for three point problem.

For the same DEM resolution the extent about the MW points of interest was gradually increased to see the effects of the domain of the DEM on the calculated gradient direction. The calculated gradient direction, expressed in degrees azimuth, was plotted against the triangular area used for the gradient calculations in the figures

following. On the gradient direction plot, for every trio of points the direction of the gradient was calculated and then plotted against the area of the triangle formed by the three points. The figure shows that for larger areas there is a decreasing range of gradient directions. This transition from where gradient direction does not depend upon the area to where the direction begins to converge to a single value with increasing area can be interpreted as the transition from the local scale to the regional scale. The gradient at the local scale reflects the true gradient at a point. The gradient at the regional scale reflects an underlying trend of the entire gradient field. The transition point is represented by the area coinciding with the vertical dashed line. As shown in Figure 2.3, for a constant resolution it was found that:

- As the extent increases the size of the local scale also increases
- The median gradient direction stays relatively constant as extent increases

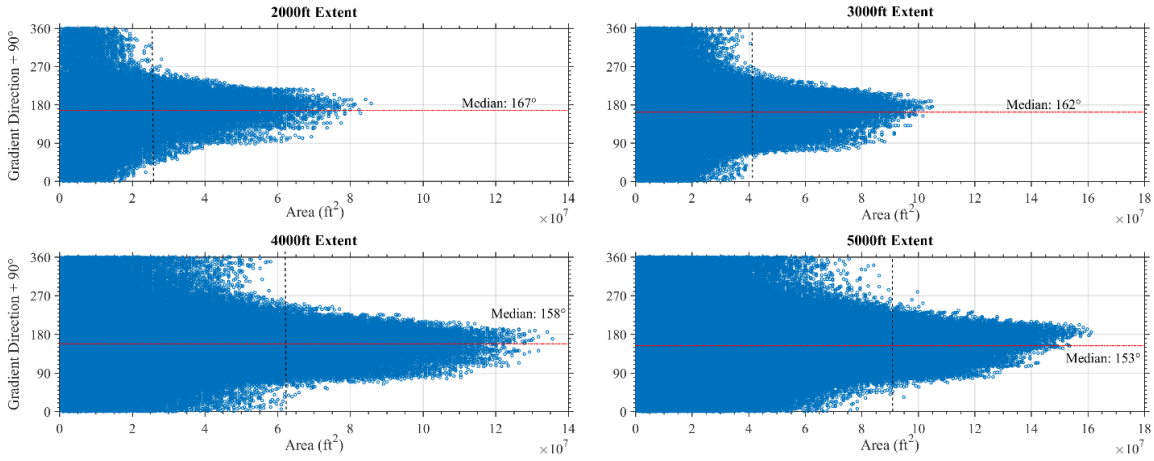

Figure 2.3. Constant resolution 1000ft (300m) with increasing extent.

The same procedure was applied again only the extent was held constant and the resolution was increased. A similar trend, shown in Figure 2.4, was found for a constant extent with increasing resolution:

- As the DEM grid size increases there is a decrease in the size of the local scale.
- The gradient direction stayed nearly constant with a variable resolution

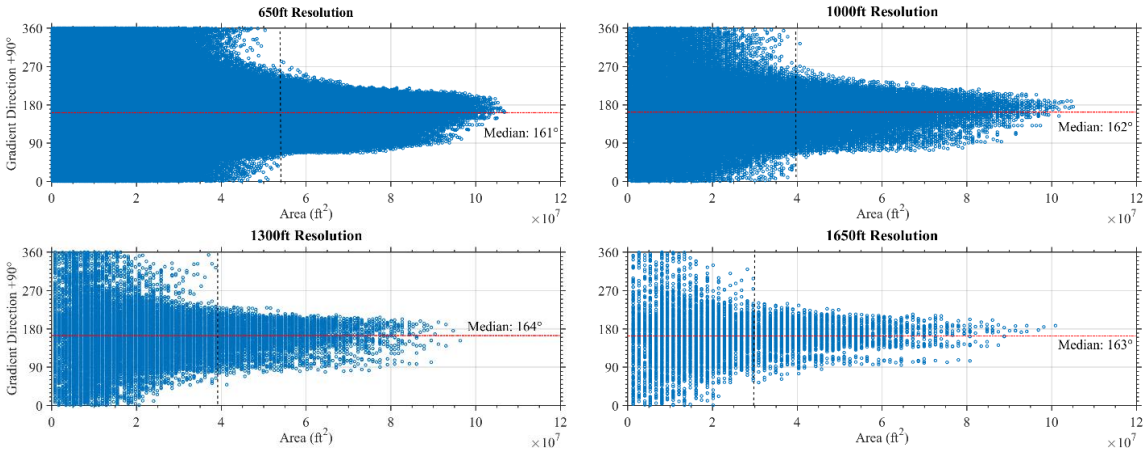

Figure 2.4. Constant extent (3000ft) with increasing grid size

Case 1 and 2 were again considered, now looking at effects of scale on calculated gradient magnitude, as shown in Figure 2.5 and 2.6. The following relationships were found to hold true for variable extents.

- The range of calculated gradient magnitudes at smaller areas decreases as the DEM resolution decreases.
- As the area increases the gradient converges to a much smaller range which is expected to be the regional value.
- As the resolution decreases the median of the gradient magnitude values decrease.

- As the resolution decreases the median follows closer with the converged gradient value.

The final analysis was on the effect of variable extent with a fixed resolution on the calculated gradient magnitude, as shown in Figure 2.6. Results from the study show the following patterns:

- The range of gradient magnitudes increase as the domain of the DEM decreases.
- The median of the calculated gradient magnitude decreases as the domain of the DEM increases

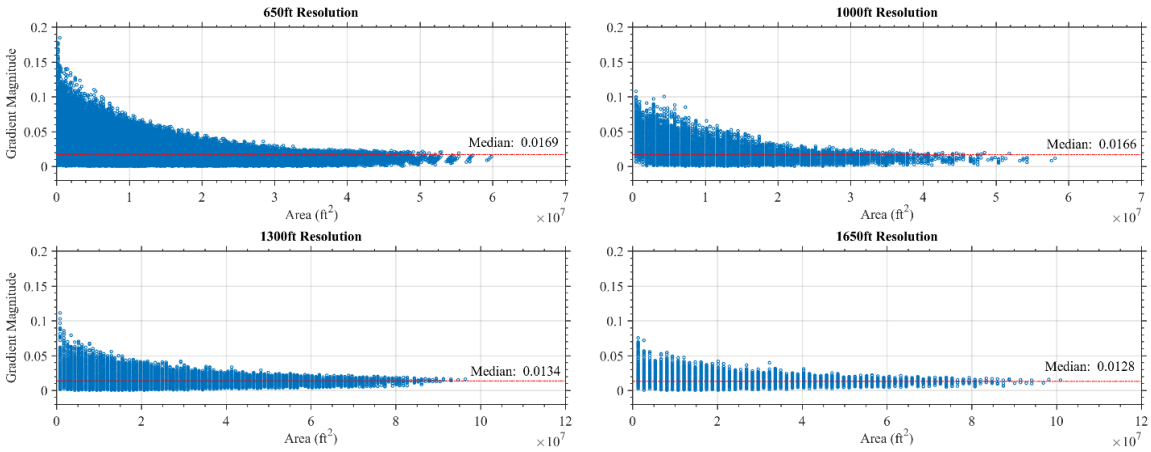

Figure 2.5. Gradient Magnitude: 3000ft extent with increasing grid size

Results from this study replicated those from Silliman and Frost (1998), where it was shown that with increased area the gradient magnitude and direction converge to a regional value. This study showed what should already be apparent, that the gradient at the local scale is highly variable, as it is dependent upon location. To fully capture the

variability in gradient at each location the DEM extent about each point should be approximately equal to the maximum area of the local scale of the GWE gradient.

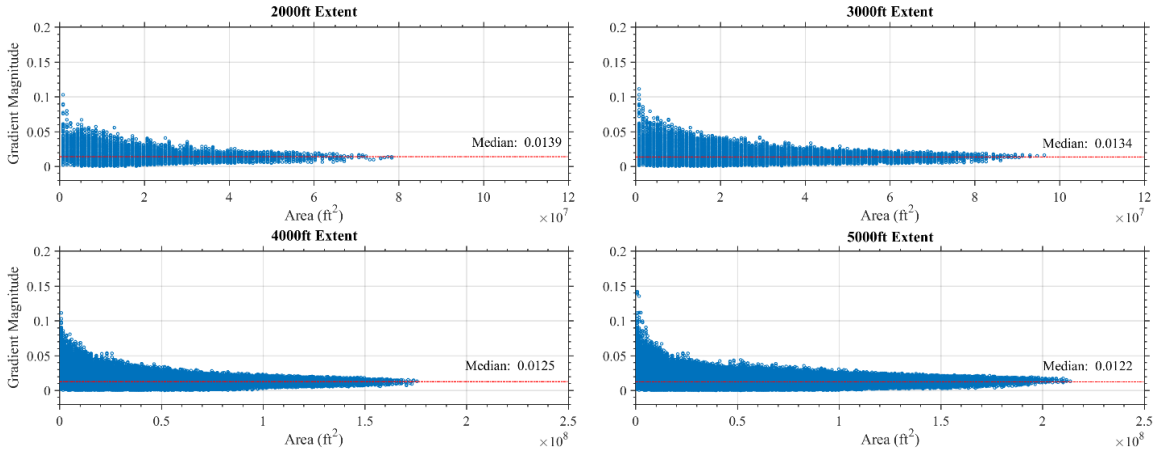

Figure 2.6. Gradient magnitude: 1300ft (400m) resolution with increasing extent

2.2. MODEL VERIFICATION

The characteristic structure of the gradient calculations over the entire domain shown in this study can be seen in the variogram as well. For one, the local scale and regional scale that are identified in the gradient direction plots are also shown on the binned variogram of the DEM. In Figure 2.7, for each separation distance, the variogram function is computed for different directions. On the binned variogram for each separation distance the average variance for each direction is plotted. The same behavior exhibited in the gradient direction and magnitude plots is shown here. For small separation distances, analogous to a smaller calculation area, the variogram function is relatively independent of the direction. As the separation distance increases, the value of

the variogram function starts to become far more dependent on the direction, replicating the scale characteristics identified in the gradient direction plot.

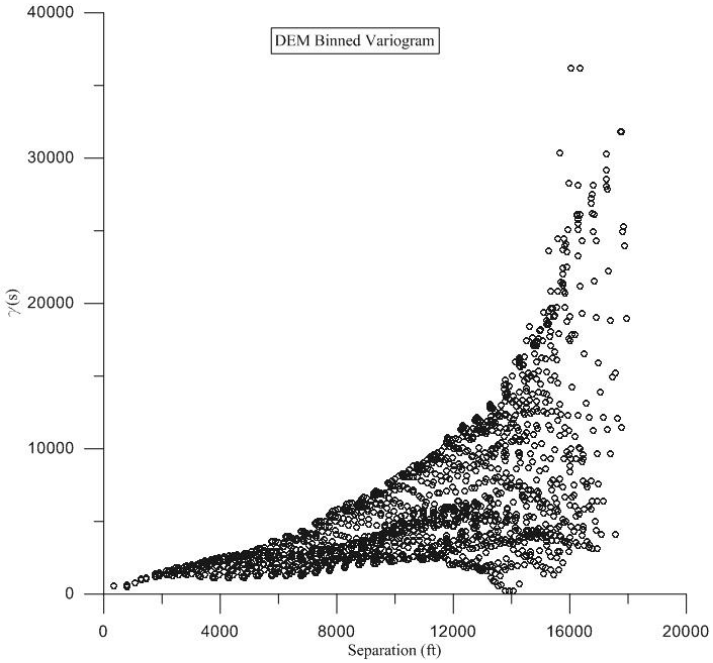

Figure 2.7. Illustration of scale effects shown on binned variogram

In addition, the assertion that the maxed binned variance is representative of the average gradient can be verified with the gradient magnitude plots. With the magnitude of the gradient representing the largest change that will occur on some surface per unit length, to check how well the developed threshold matches with the average calculated gradient, Equation (7) was formulated to calculate the equivalent variance that would occur between two points separated by a distance s parallel to the gradient, ∇a . In order to compare the values at the same scale, the area of calculation for the three point problem should be related to the separation distance on the variogram. Because the

variogram and gradient plot were calculated on the same domain, the maximum area should correspond to the greatest separation distance and the smallest area correspond to the smallest separation distance. With this established, both the range of areas and separation distances were divided into 20 equal sized bins. For each area bin the average gradient was determined and multiplied by the separation distance associated with the same bin number. The resulting variance that would occur on a plane with gradient $|\nabla a|$ is shown in Equation (7).

$$\gamma_{grad}(s) = \frac{1}{2}(|\nabla a| * s)^2 \quad (7)$$

Equation 7 is plotted with the DEM variogram threshold to see how well the threshold follows the average gradient from the three point problem computation for the same points over the same domain. Figure 2.8 shows that the max binned threshold provides a reasonable estimate of the average variance on the domain. .

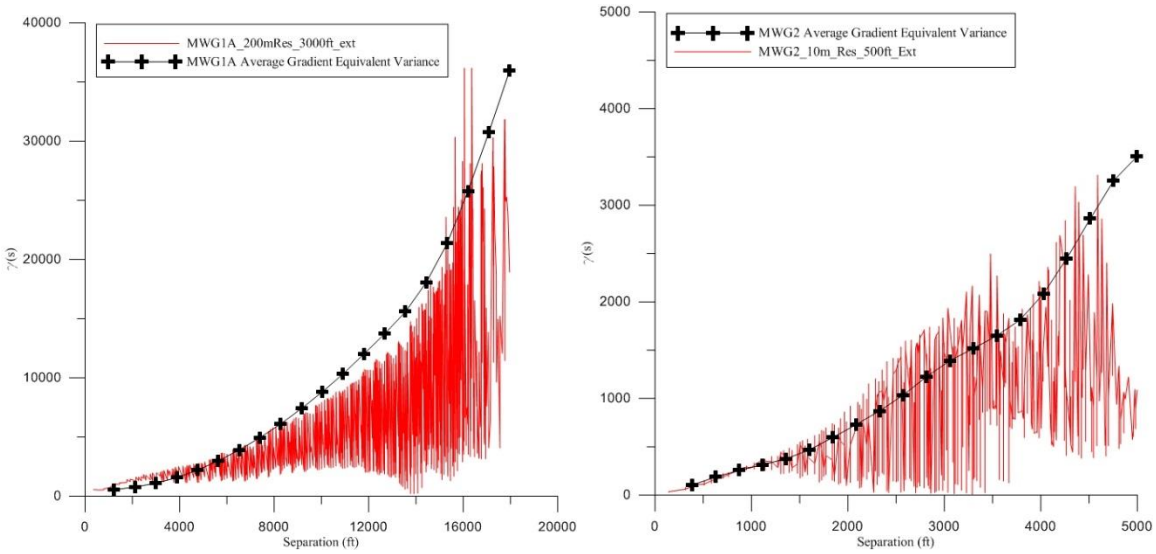

Figure 2.8. Equivalent variance from three point calculations

PAPER

I. DEVELOPMENT OF A VARIOGRAM PROCEDURE TO IDENTIFY SPATIAL OUTLIERS USING A SUPPLEMENTAL DIGITAL ELEVATION MODEL

Keywords: outlier detection, spatial outlier, variogram, supplemental topographic data, gradient

Authors: Zane D. Helwig[*], E.I.[1]; Joe Guggenberger Ph.D., P.E. M. EWRI, M. ASCE[2], Andrew Curtis Elmore Ph.D., P.E., F.EWRI, F.ASCE[3]; Rachel Uetrecht, E.I[4]

[1]Graduate Student in Geological Engineering, Missouri University of Science and Technology, 266 McNutt Hall, Rolla, MO 65409; PH (816) 262-5564; email: zhx9d@mst.edu

[2]Assistant Professor of Geological Engineering, Missouri University of Science and Technology, 318 McNutt Hall, Rolla, MO 65409; PH (573) 341-4466; F: (573) 341-6935 email: jguggenb@mst.edu

[3]Professor Emeritus of Geological Engineering, Missouri University of Science and Technology, 205 Straumanis James Hall, Rolla, MO 65409; PH (573) 341-6784; email: elmoreac@mst.edu

[4] Graduate Student in Geological Engineering, Missouri University of Science and Technology, 266 McNutt Hall, Rolla, MO 65409; PH (816) 308-5798; email: rmu5y2@mst.edu

[*]Corresponding Author

ABSTRACT:

When using a ground water elevation dataset for the development of a groundwater model, it is prudent to first evaluate the quality of the data before using it in a ground water model. However, it may not be practical to evaluate every data point when working with large datasets associated with a regional model. To isolate misrepresentative points in a large data set, a graphical technique has been developed which examines the experimental variogram of ground water elevation values to identify points with high variogram function values. The potential outliers identified using the graphical variogram process are subsequently evaluated by reviewing well borings, well installation records, and available time series of water level measurements to retain or reject outlier status. Supplemental ground elevation data from a digital elevation model is used to create a threshold on the experimental variogram of the ground water elevation data. This process is verified using a developed synthetic ground water dataset, then applied to a case study at the Fort Leonard Wood Military Reservation, Missouri. The method showed good results in identifying points that were justified for removal upon inspection of the available records and provides recommendations based on common causes of error. With this methods reliance on both an experimental variogram of measured water levels and a binned variogram of ground elevation measures, it naturally fits as a preprocessing step that can be applied prior to kriging.

Keywords: outlier detection, spatial outlier, variogram, supplemental topographic data, gradient

1. INTRODUCTION

Pucci and Murashige (1987) state that before a groundwater resource investigation is established or a hydraulic model developed, existing groundwater measurements should first be evaluated for their usefulness. There are many potential sources of error in measures of the potentiometric surface including human error in measuring of depth to static water level, inaccurate well coordinates, measurements taken directly after well completion before the water level has stabilized, and non-representative measurements in wells with long completion intervals and significant vertical gradients (Hill-Rowley et al., 2003; Snyder, 2008; Arihood, 2009; Tremblay et al., 2015; Elci et al., 2003). All these sources of error may be present in databases that are not always systematically validated, with quality control often absent, and reliability in the measurements highly variable depending on where the data is sourced (Tremblay et. al. 2015). In addition to sampling errors, there are naturally occurring (for example, sources or sinks from karst) and/or anthropogenic features, such as leaking water from supply pipelines, which can create a localized effect on the potentiometric surface which may skew the characterization of the more regional surface, especially when monitoring locations are relatively sparse. When this is the case, points reflecting such local variability should be considered for exclusion from a regional model. Such data points that differ significantly from neighboring points for the reasons given above are referred to as spatial outliers (Shekhar et al., 2003; Chen et al. 2008; Liu et al., 2001). Spatial outliers differ from global outliers in that global outliers are identified by comparison

with the aggregate of the entire population while spatial outliers are those that go against regional trends or do not maintain local continuity.

There are two general methods applied to detect spatial outliers. The most common approach is a quantitative method which looks at the residual between a point and a predicted value at the same location then applies some mathematical method to determine if the residual is significant (Tremblay et al., 2015; Shekhar et al., 2013; Miller et al., 1997; Bardossy and Kundzewicz, 1990; Liu et. al., 2001). The second is identified by Shekhar et al. (2003) and Chen et al. (2008) as a graphical method which is based on the visualization of spatial data to highlight spatial outliers. Graphical methods rely on the qualitative identification of outliers which appear to fall outside of the grouping of the remainder of the data, and thus lack defined criteria for when a point on the graphic qualifies as an outlier. When discussing different outlier detection methods, Bardossy and Kundzewicz (1990) and Shekhar et al. (2003) discuss the conceptual use of an experimental variogram as a way of identifying outlying points, however, the presentation of a systemic approach to selecting outlying points on a variogram is absent.

A common assumption in the development of groundwater models is that for unconfined conditions the groundwater is a smoothed version of the topographic surface (King, 1899; Domenico and Schwartz, 1998; Blauvelt and Fullmer, 2011). This assumption enables the incorporation of a ground elevation dataset to supplement sparse groundwater elevation (GWE) measurements when developing a model of the potentiometric surface (Desbarats et al., 2002; Boezio et al., 2005; Boezio et al., 2006; Hoeksema et al., 1989). The purpose of this paper is to present a new graphical approach to identifying potential spatial outliers which use a digital elevation model (DEM) dataset

to establish criteria for detecting spatial outliers. Unlike those in the literature review, this approach addresses regional trends at the site in addition to comparing each individual data point to its neighbors, thus fully using all point-to-point relationships. To demonstrate the applicability of the approach, it is used to perform an outlier analysis on a dataset collected at Fort Leonard Wood, Missouri where multiple monitoring well (MW) networks have been established to sample the quality of the regional aquifer.

2. METHODS

A common geostatistical tool used to describe the difference between pairs of points based on the distance between the point pairs is the variogram. Goovaerts (1997) presents the variogram function as

$$\gamma(s) = \frac{1}{2N(s)} \sum_{\alpha=1}^{N} (h(u_\alpha) - h(u_\alpha + s))^2 \quad (1)$$

Where:

$h = a\ measurement\ of\ some\ scaler\ quantity$

$s = a\ vector\ separating\ two\ data\ values$

$N(s) = number\ of\ data\ pairs\ within\ the\ class\ of\ distance\ and\ direction\ of\ s$

$u_a = vector\ of\ spatial\ coordinates\ of\ the\ \alpha^{th}\ individual$

The $\gamma(s)$ values from Equation 1 will be referred to here as the variance, although other authors refer to it as the variability (Journel and Huijbregts, 1997), or the semi-variance (Goovaerts, 1997). The variogram is usually either expressed as a binned variogram or a variogram cloud. A variogram cloud (also referred to as an experimental variogram) plots half the squared difference of every pair of points against the separation

distance for that pair, so every separation vector *s* is considered and *N* is always one. For the binned variogram, point pairs are separated into distance bins which only include pairs separated by a specified range of the magnitude of *s*. Within each distance bin, pairs are further classified by the direction in which they are separated. Half the average variance of each directional class is plotted within each bin of separation distance. Each possible GWE pair are plotted in order to isolate GWE values as potential spatial outliers. This is facilitated through the use of the GWE variogram cloud.

The principal assumption used in this analysis is that the potentiometric surface is a smoothed version of the topographic surface. This allows for the development of a threshold comparison to the GWE variogram cloud. We can assume that at the same location on both surfaces, the gradient of the topographic surface should be greater than or equal to the gradient of the potentiometric surface. Domenico and Schwartz (1998) define the gradient of a scalar field of some attribute *a* as:

$$\nabla a = \frac{\partial a}{\partial x} i + \frac{\partial a}{\partial y} j + \frac{\partial a}{\partial z} k \quad (2)$$

The direction of ∇a corresponds to the direction of greatest change in attribute *a*. The magnitude of ∇a for a planar surface is the greatest level of change per unit length that will occur on that surface. The gradient of a planar surface is calculated using any three points that do not fall along a line, and the three point problem can be simplified to a two point problem if the direction of the gradient is known. With a known gradient direction, the magnitude of the gradient can be determined from the residual of two points separated in that direction.

$$|\nabla a| = \frac{R_a}{|s_a|} \quad (3)$$

Where:

$R_a = the\ difference\ between\ a\ pair\ of\ points\ separated\ by\ s_a$

$s_a = vector\ separating\ a\ pair\ of\ points\ in\ the\ gradient\ direction$

When the direction of the gradient is not known, a reasonable approximation of the planar surface gradient can be found by looking at the residual of every pair of points in the domain. The magnitude of the gradient is approximated as the greatest residual between a pair of points in the domain divided by the magnitude of the vector separating the pair of points, and the direction of the gradient is a direction parallel to the vector separating the two points.

$$|\nabla a| = \frac{R_{max}}{|s_{max}|} \tag{4}$$

With

$$R_{max} = \max(R_i) \tag{5}$$

Where:

$R_i = The\ residual\ of\ the\ i^{th}\ pair\ of\ points\ lying\ on\ a\ plane$

$s_{max} = vector\ separating\ a\ pair\ of\ points\ corresponding\ to\ R_{max}$

The variogram function (Equation 1) and gradient approximation (Equation 4) both consider the residual of every point pair on the area of interest so for a set of data on the same domain:

$$R_i = h(u_\alpha) - h(u_\alpha + s) \tag{6}$$

From Equation 4, we expect the variance corresponding to the points separated in the direction of the gradient to be at $R_i = R_{max}$. So the greatest value from $h(u_\alpha) - h(u_\alpha + s)$ should correspond to the greatest variance and is expected to result from a pair of points separated in the direction of the gradient. Thus for each separation distance the largest variance to occur is dependent on the gradient between the point pairs. The

inherent variability of the topographic surface causes the gradient to fluctuate over the entire domain of interest. To find a representative variance which adequately describes the gradient of the entire domain, the average variance corresponding to the greatest directional bin from the binned DEM variogram should be used. Using the maximum of the directional variance averages gives a good estimate of the average calculated gradient for different separation distances. To target values on the GWE variogram cloud, the maximum variance on the binned DEM variogram can be used as a threshold. When multiple points lie above this threshold, the corresponding pairs should coincide with a single point that can be identified as a potential spatial outlier. For points identified as a potential outliers, justification should be provided through inspection of each point in order to retain the point as a spatial outlier.

2.1. MODEL DEVELOPMENT

The location of the boundary formed by the binned variogram of the DEM points was found to be dependent on both the resolution of the DEM as well as its extent about the GWE dataset of interest. A 30ft (10m) resolution DEM was found to have the highest data density for a best approximation of the topographic surface evaluated in this study. To find the DEM extent which adequately characterized the area about each MW, a study was done, which followed the work of Silliman and Frost (1998) that looked at the response of the calculated gradient to changes in the extent and resolution of the DEM. In this study, the gradient magnitude and direction for every point trio were calculated from the three point problem as presented by Vacher (2005). To rule out point trios that were close to falling along a line, only trios with an inner acute angle greater than a

prescribed tolerance were used in the computation. The gradient direction, expressed in degrees azimuth, and magnitude were then plotted against the area of the triangle formed by the three points in the problem. Figure 1, shows that the local and regional scale of the gradient could be differentiated using gradient direction plots. This matches the results of Silliman and Frost (1998). Figure 1 shows that for larger areas there is a decreasing range of gradient directions. The area at which at which the gradient direction is no longer independent of the calculation area marks the transition from the local scale to the regional scale. The gradient at the local scale reflects the true gradient at a point and is more dependent upon location and any localized gradient variations, and the gradient at the regional scale reflects an underlying trend of the entire gradient field. The area at which this transition occurs is represented by the vertical dashed line on Figure 1. The DEM dataset more clearly shows the scale than the GWE dataset due to the higher density of points and is used to illustrate the relationship.

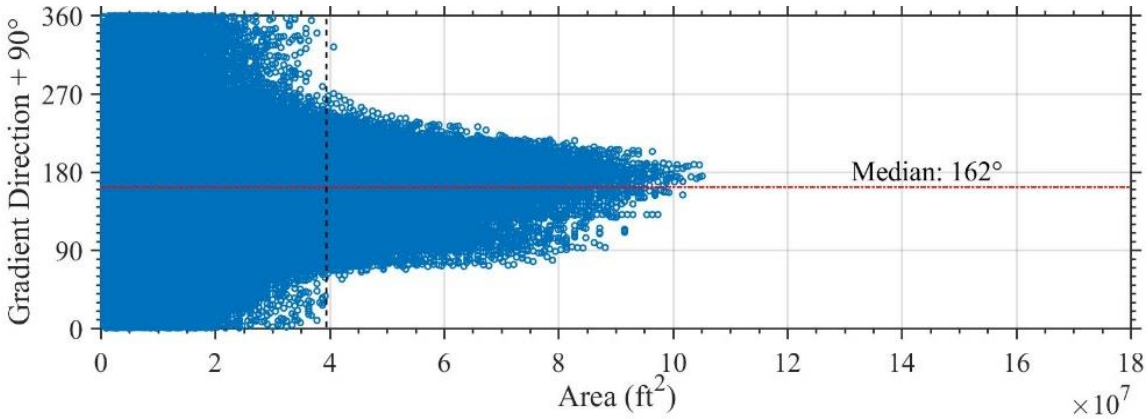

Figure 1. Estimation of local scale from gradient direction plot. The gradient direction for each point trio from a 300m (1000ft) resolution DEM with a 3000ft extent was computed and plotted against the triangular area defined by the three points. The maximum area of the local scale is approximately 4x107 ft^2, represented by the black vertical dashed line.

To best capture the maximum DEM variance at each separation distance at a point of interest, points separated in each direction must be considered. So the extent of DEM data needed to capture the gradient at each scale is encompassed by a circular area about the point of interest. The local scale is dependent upon location, which is why the range is much larger than the regional scale when calculating gradient for every three point combination. The gradient at the regional scale is not dependent on location, so long as it is in the same domain. Therefore when comparing DEM variance to the GWE cloud, only DEM points in an extent about the GWE points equal to the local scale are needed to fully capture a gradient estimate. Because the extent of the DEM is defined by a radius about each MW, to define the radial extent for the DEM, the radius of a circle with an area equal to the area of the maximum local scale of the GWE points was used.

The binned variogram of the DEM is plotted with the variogram cloud of the GWE values as the first step in identifying potential spatial outliers. Lines are drawn on a site map between pairs of GWE measures corresponding to each point lying above the DEM threshold. A point cannot be isolated as a potential outlier from a single linkage, therefore at least two linkages are need to identify a point as a potential spatial outlier. However, a point with two links may not be the source of high variance, but rather be linked with two potential outlying points. Ideally, there should be an iterative approach to removing the point with the greatest number of linkages and then recalculating the variogram cloud to repeat the analysis to ensure that only points contributing to the high variance are removed. To replace this time consuming process it can be determined from the first iteration if a link should be associated with a point. Links to a point can be established as significant or not based on if they connect with a higher level candidate,

where a higher level candidate is one with more linkages. A link only significantly contributes to a point if it does not connect with a higher level candidate. A point is identified as a potential spatial outlier if it has at least two significant links.

2.2. DEVELOPMENT OF A SYNTHETIC DATASET

A synthetic dataset was created to test the validity of the method. To create artificial groundwater elevations that represented a smoothed version of the topography, surface elevations gathered from a DEM were divided into 24 equal sized bins, each bin covering 15 feet of elevation. For each of the 34 synthetic points, the surface elevation at that point was multiplied by a coefficient, ranging from 0.95 to 0.75, corresponding to the elevation bin it belonged to. The lowest coefficient was used at points with the highest surface elevation and likewise the highest coefficient was used at the lowest surface elevation. This produced a smoothing effect so that at topographic highs the difference in groundwater and surface elevation was the greatest.

From the average of the original synthetic data set, six potential outlier points where added that corresponded to three levels of error. The first level, being the lowest level of error contained two points corresponding to plus and minus a single standard deviation from the mean of the synthetic dataset. Following this two second level error points were added whose values were plus and minus two standard deviations from the synthetic data mean and the two points with the highest level of error were plus and minus three standard deviations from the mean of the synthetic dataset. The spatial coordinates of the outlying points were constrained to fall inside of the domain of the original synthetic dataset.

3. RESULTS AND DISCUSSION

A 30ft (10m) resolution DEM with a sampling frequency reduced to 160ft (50m) intervals was used to determine the threshold variance of the synthetic GWE dataset. Reducing the sampling frequency allowed for faster computations of the DEM gradient plots and variogram. In addition the gradient may not be an accurate reflection of the surface when calculated between short distances, the increased distance between sampling points reduces anonymously high or low gradients due to embankments or flat areas from human development, such as parking lots.

The scale of the synthetic dataset was determined from the gradient direction plot, with the local scale defined by an area to the left of the vertical dashed line in Figure 2. The radial extent of the DEM used for comparison was determined from the radius of a circle with an area equal to the maximum area at the local scale. The resulting extent of the DEM was a 2400ft radius about the synthetic data points. The binned variogram of the DEM was laid over the variogram cloud of the synthetic data, as shown in Figure 3.

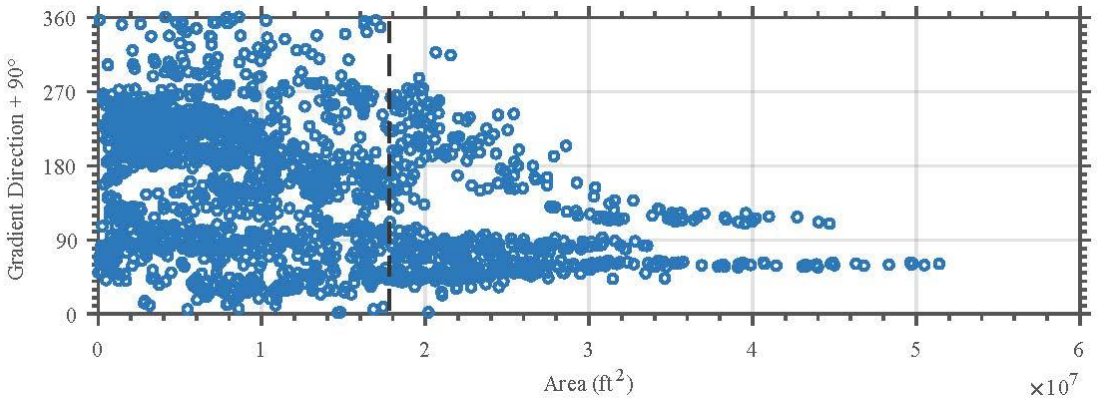

Figure 2. Gradient direction plot for the synthetic dataset. The local scale is estimated by the black vertical dashed line.

The data pair links corresponding to GWE points lying above the variogram threshold are illustrated in Figure 4 to identify points with the highest variability. When multiple linkages are drawn to the same point, it indicates the point is the source of the high variance and should be further investigated, that is, it is a potential outlier.

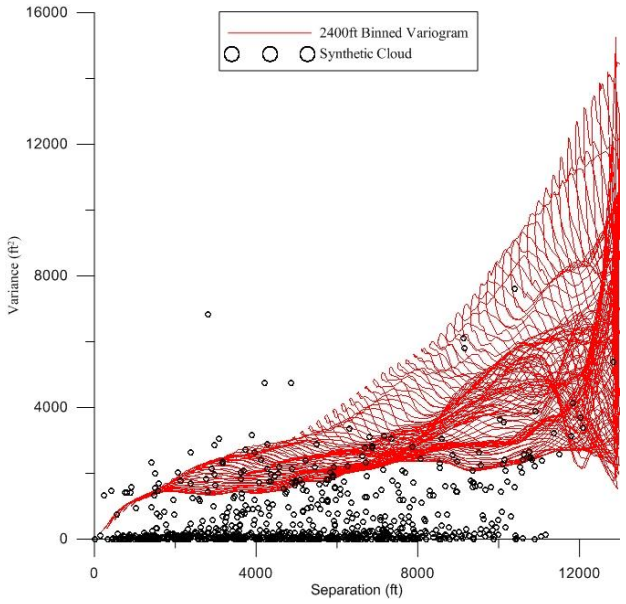

Figure 3. Synthetic Dataset variogram threshold comparison. The binned variogram of a DEM with 30ft resolution, sampled at 160ft intervals, with a 2400ft radial extent about the monitoring wells was overlaid over the synthetic GWE variogram cloud. Each point from the synthetic cloud lying about the DEM binned variogram corresponds to a point pair that contains an outlying point.

Inspection of Figure 4 shows that point C has 3 linkages. The link connecting to point B should not be considered because B has a greater number of linkages than C, so it is a higher level candidate. This leaves point C with 2 significant linkages, so it still qualifies as a potential spatial outlier. In addition to point C, points A and B are also identified as potential spatial outliers. Both A and B have at least 5 linkages so can easily

be identified as potential spatial outliers. All three of the points identified corresponded to the introduced outlier points. Points A and B were the highest level error points and point C was a second level error point. The remaining second level error point is relatively far away from other points. Due to this points distance from neighboring points a higher residual is tolerated, so it was not identified as an outlier. The two points with the lowest level of error (a single standard deviation from the original mean) were not identified either. The first level error points are least likely to significantly deviate from neighbors and regional trends and thus were not identified as outliers in this case. With a greater number of significant linkages corresponding to higher level error points, this synthetic study shows that the number of significant linkages can be used as degree of confidence in positive identification of spatial outliers.

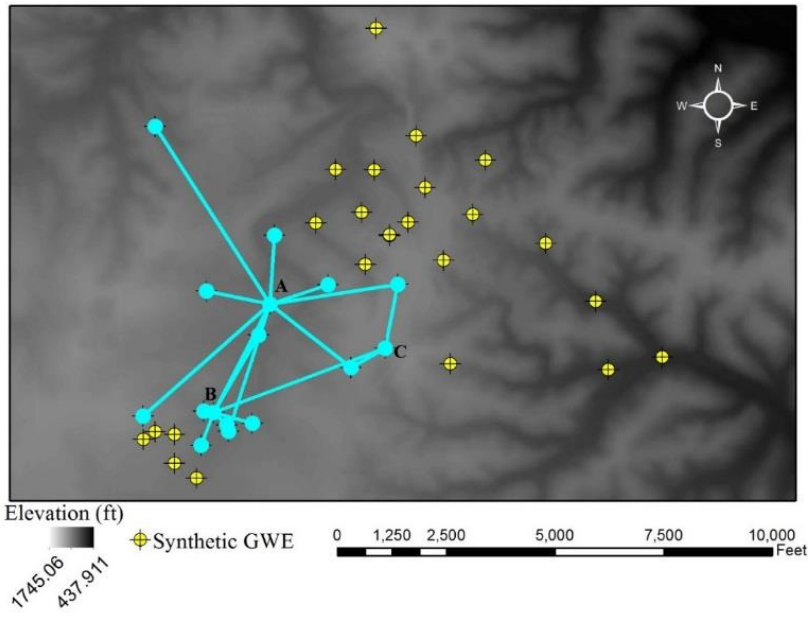

Figure 4. Synthetic data outlier identification. Links between point pairs, shown in blue, corresponding to points lying above the threshold, aid in targeting which points are the cause of the high variation. Points A, B, and C are identified as spatial outliers.

3.1. FORT LEONARD WOOD CASE STUDY RESULTS

A case study was performed using groundwater elevation data collected at Fort Leonard Wood Military Reservation (FLWMR) in south-central Missouri. The regional aquifer is unconfined and is within the Gasconade Formation, consisting of Ordovician aged dolomite. A number of detailed investigations have been carried out at the FLWMR which discuss the site geological and groundwater flow mechanisms (Kleeschulte and Imes, 1997; Mugel and Imes, 2003; Harrison et al., 1996; Imes et al., 1996). The dataset is from a set of 69 monitoring wells installed for environmental sampling. Measures of depth from top of casing were all collected within a 24 hour period in January of 2015 using an electronic water-level meter. The measured depth to water ranges from 3ft to 326ft below top of casing, and screened intervals ranged from 10ft to 206ft in length.

The site was divided into three subsites based on the geographic separation of the monitoring wells, as shown in Figure 5. For each subsite, the binned variogram from a 30ft (10m) resolution DEM sampled at 160ft (50m) intervals was used to establish the threshold on the variogram cloud of the GWE values. For brevity, only the analysis for MWG1 is shown here, however, the procedure was the same for the remaining sites. After creating the gradient direction plot for MWG1, it was observed that the regional gradient converged in two directions as shown in Figure 6. A potential reason for this is that the northern most points belonged to a different flow regime and thus should be considered separately. Therefore MWG1 was divided into two separate subsites, MWG1A and MWG1B, as shown in Figure 7.

The resulting gradient direction plots for MWG1A and MWG1B are shown in Figure 8. The maximum area corresponding to the local scale at MWG1A is shown and

the regional value now converges to a single direction. The local scale was not readily determined for MWG1B because it was a relatively small dataset, so the scale was assumed to the greatest calculated area for the MWG1B site. By using the greatest calculated area, a larger extent DEM is used which results in a lower variogram threshold. With this approach more linkages are drawn, so a point may be identified with greater confidence. While this approach may lead to the identification of more potential outliers, this places more reliance on the individual analysis of each point to determine if an outlier should be retained.

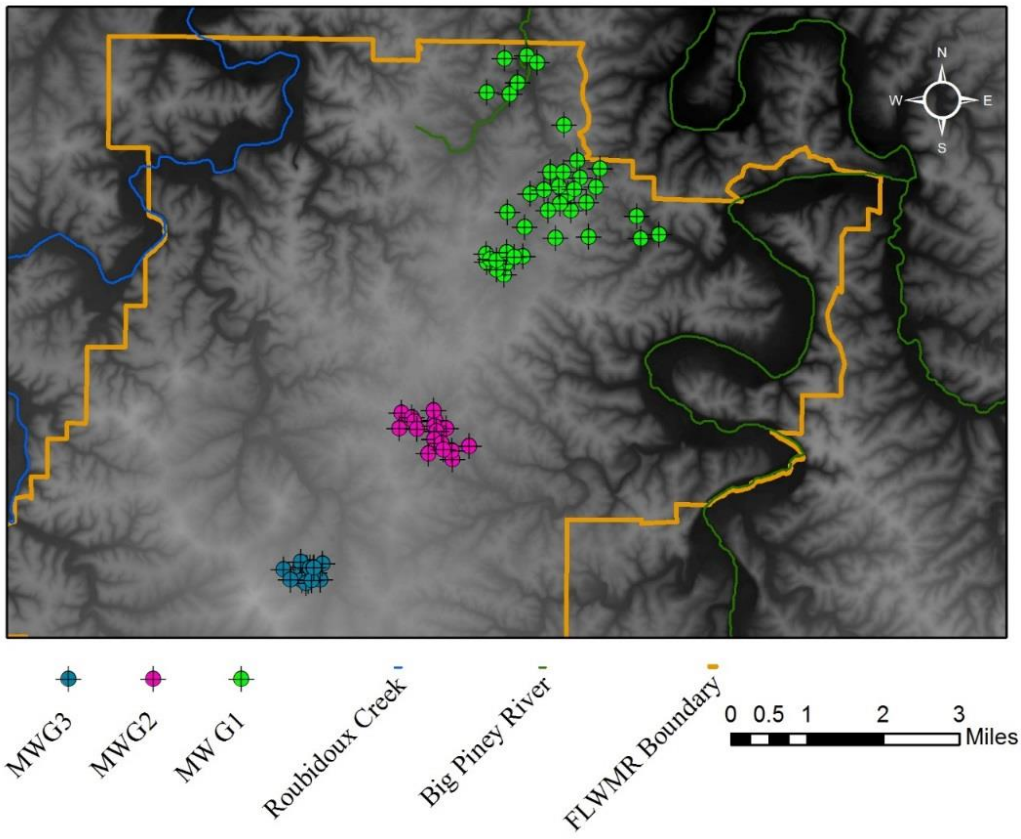

Figure 5. Overview of the FLWMR monitoring well groupings.

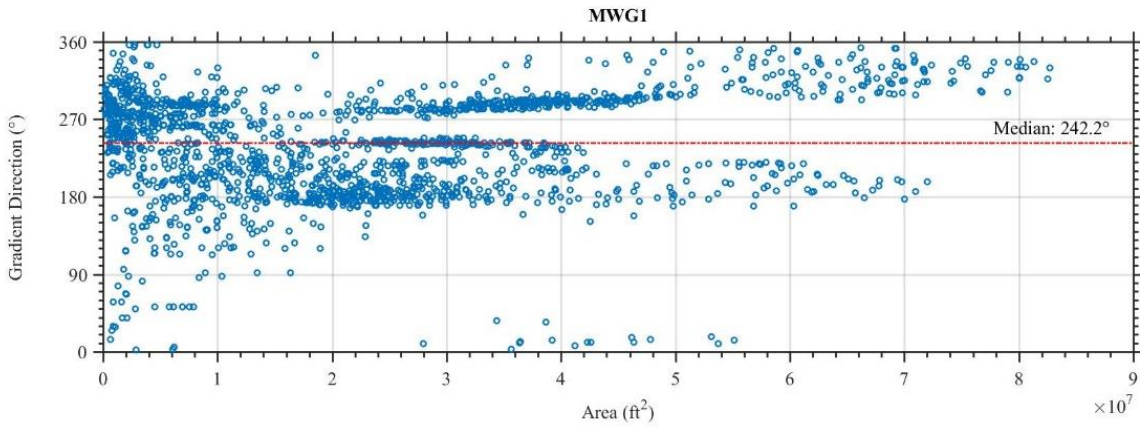

Figure 6. MWG1 gradient direction plot. The site was divided into two subsites, MWG1A and MWG1B to address convergence in two different directions at the regional scale.

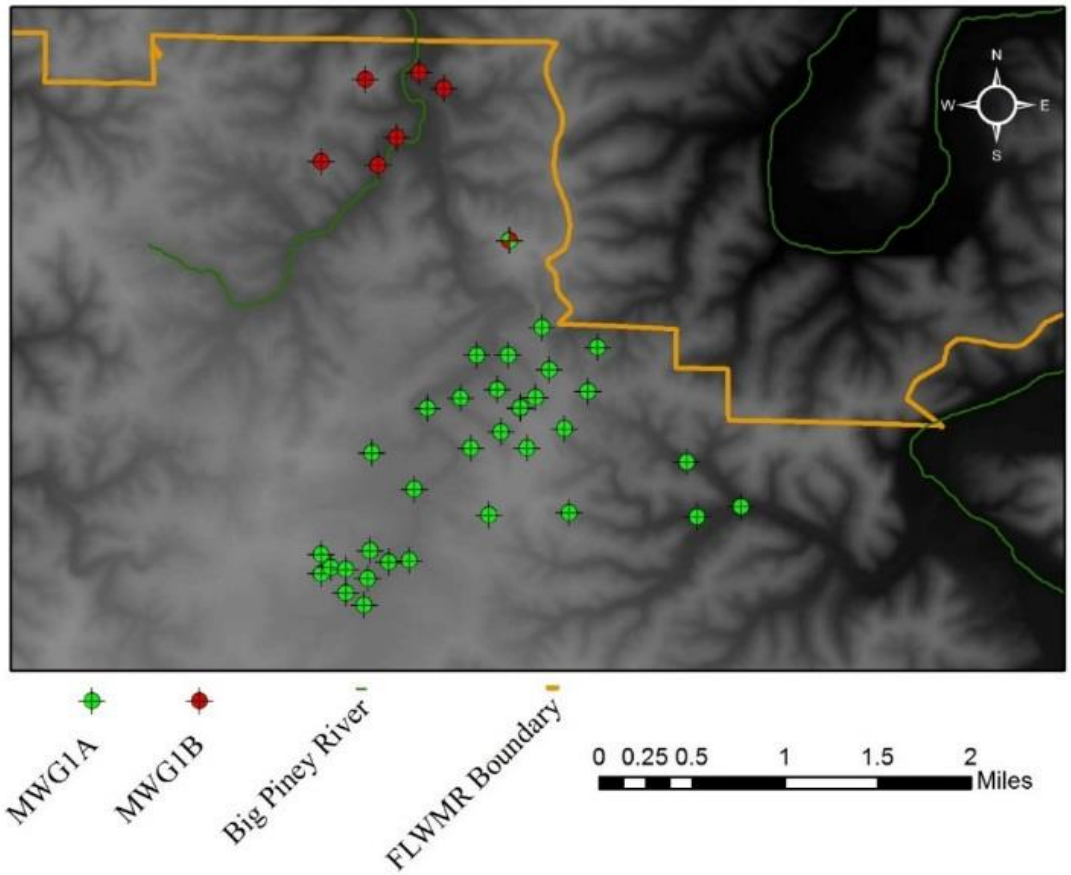

Figure 7. MWG1 divided into two subsites. The point lying between MWG1A and MWG1B was considered in the analysis for both sites.

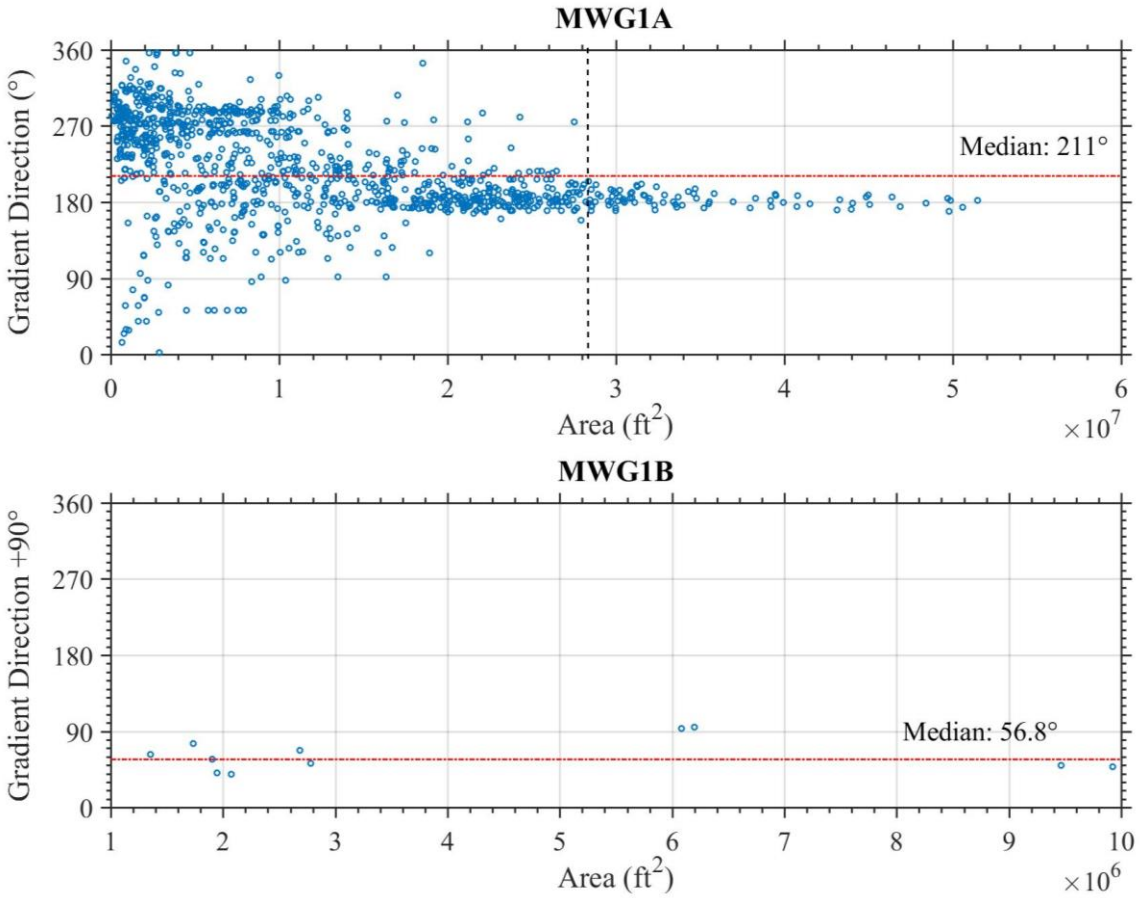

Figure 8. Gradient direction plots for MWG1A and MWG1B. It should be noted the area for MWG1B is an order of magnitude smaller than the area on the MWG1A plot. Sparse GWE data at MWG1B leads to a lack of structure on the gradient direction plot and thus poor interpretation.

With the calculated area corresponding to the local scale determined, the binned variogram of the DEM with corresponding radial extent about each point in MWG1A and MWG1B was overlaid over the GWE variogram cloud, shown in Figure 8. Figure 9 shows the linkages to the data pairs corresponding to the points above the variogram threshold. MW-1207 was included in both subsites since its location fell approximately in the middle of the two sites. From the results of both subsites MWG1A and MWG1B, MW-1207 was identified as a spatial outlier. From MWG1B two additional potential

outliers are identified, with both MW-1204 and MW-1205 having at least two significant linkages. The small number of points in MWG1B showed to be low quality, with nearly half of the points on the site identified as potential outliers.

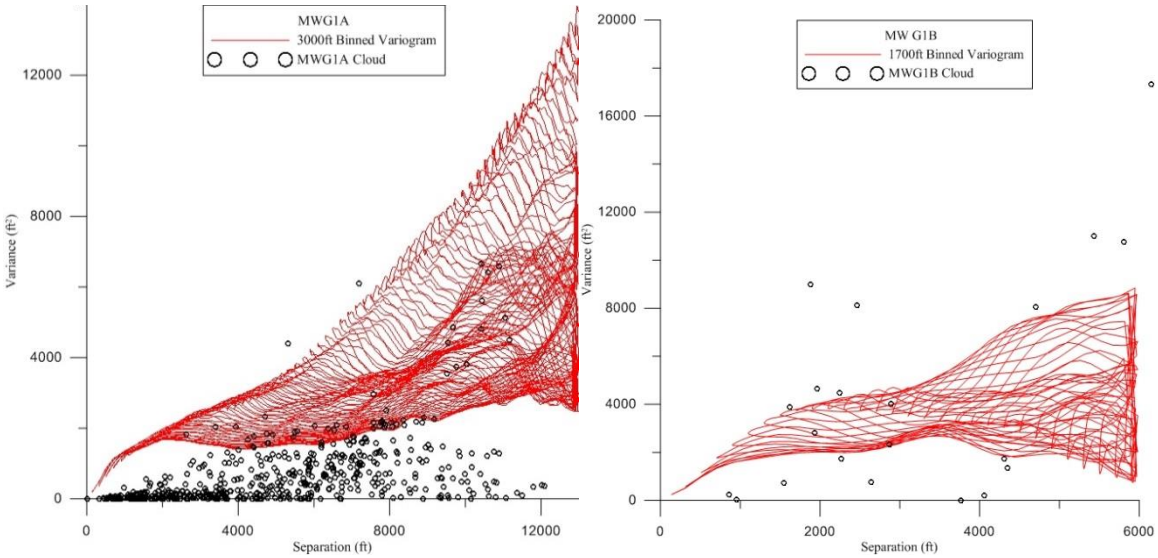

Figure 9. Variogram threshold comparison for MWG1A and MWG1B**.** A 3000ft extent DEM was used for MWG1A comparison and a 1700ft extent DEM was used for MWG1B comparison. Outlying points are found from points lying above the binned DEM variogram shown in red.

This procedure was repeated for both MWG2 and MWG3, and a total of 7 more spatial outliers were identified. All points identified from the variogram comparison method have been outlined in Table 1 with the number of links shown to indicate the level of confidence in a positive identification of a potential spatial outlier.

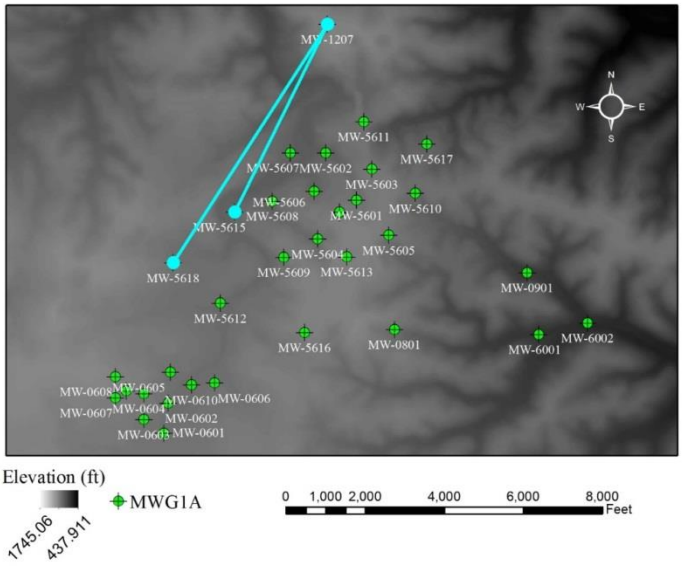

Figure 10. MWG1A potential spatial outlier detection. The lines represent the links between pairs of points. Both points lying above the variogram threshold linked to the same point, providing MW-1207 with the perquisite two significant linkages to qualify as a spatial outlier.

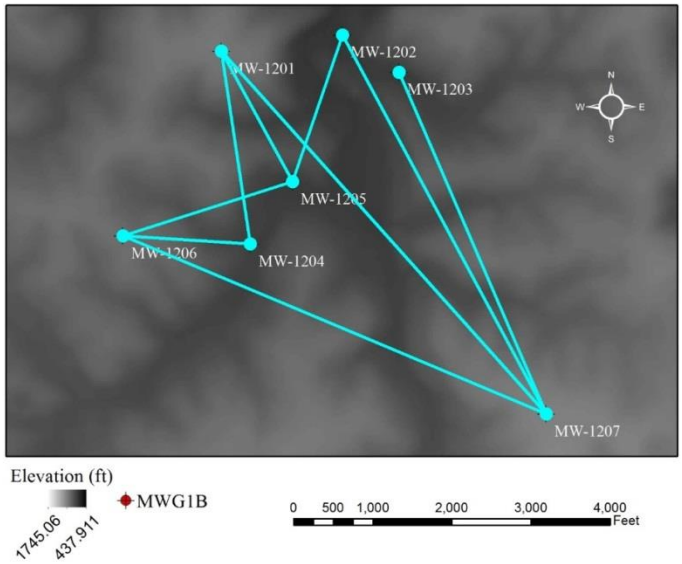

Figure 11. MWG1B spatial outlier detection. The lines show links between data pairs corresponding to points on the variogram. MW-1207 was included in both MWG1A and MWG1B because it was not clearly part of a group of wells. In the analysis for both sites it was identified as a potential spatial outlier. Two other points within MWG1B were also identified as potential spatial outliers.

Table 1. FLWMR Case Study Results

Group Number	Well ID	Significant Links
MWG1A/B	1207	6
MWG1B	1204	2
MWG1B	1205	3
MWG2	309	2
MWG2	401	5
MWG2	307	14
MWG2	305	5
MWG3	211	11

A number of potential causes or indicators of error which might justify retaining a potential outlier were considered for the FLMWR site. After the review of borings logs and well installation records, each well that possessed the specified attribute was indicated by a dot in Table 2, with closed dots indicating that the well which possessed that attribute was retained as a spatial outlier. Highlighted rows correspond to the potential outliers identified in Table 1. Wells with long completion intervals (greater than 50ft in length) were expected to be a potential source of error. Wells with shallow completion were completed above the Gasconade formation (the regional aquifer unit), and thus potentially sampling a different aquifer unit or perched zone. Wells with solution features (voids greater than 5ft) identified in the boring logs were thought to have potential sources or sinks. Wells with any perched zones identified in the boring

log, if not properly completed, may reflect an average of the perched and regional aquifer. Wells with inconsistent initial water levels deviating more than 30ft from the water level measured at the time of drilling, may indicate that the water level might not have stabilized when the initial measurement was taken, or there may be seepage in an improperly completed well. Seasonal variation marks those wells which had a greater water level in January 2015 than the average of the previous four years of spring measures. This goes against the assumption that water levels in spring are greater than in January, and thus a source term, such as a leaky pipe may provide a source to keep the water level in January high.

As shown in Table 2, the most common cause of error was wells completed above the regional aquifer unit, leading to uncharacteristically high water levels. In addition, each well showing unexpected seasonal variation was retained as a spatial outlier. Inspection of boring logs for MW-305 and adjacent wells showed a large void (~14ft) at the same depth in each borehole. However, MW-305 was the only well with no record of grouting the void and thus was retained as a potential outlier. For MW-307, the January water level was more than 40ft higher than the measured water level at time of drilling. As shown in Table 2, MW-309 is the only well that was identified as a potential spatial outlier but not excluded from the regional model. Table 2 shows that despite expectations, long screened wells, perched zones and solution features did not significantly contribute as a source of error.

Table 2. Sources of error for spatial outliers

Well ID	Long Completion Interval	Shallow Completion	Solution Features	Perched Zones	Inconsistent Initial Water Level	Seasonal Variation
MW-1202	O	O[2]		O		
MW-1204		●				
MW-1205		●				
MW-1207		●				
MW-0601	O					
MW-0602	O					
MW-0603	O			O		
MW-0604			O			
MW-0606			O			
MW-0607	O					
MW-0609	O					
MW-0610	O					
MW-209		O[2]		O		
MW-211	●	●		●		
MW-212		O[2]				
MW-303			O			
MW-304			O			
MW-305			●[1]	●		
MW-307					●	●
MW-309			O	O		
MW-401						●
MW-402					O	
MW-502			O			
MW-0801				O		
MW-6002		O		O		
MW-5614D			O			
MW-5614S			O		O	

● = Retained spatial outlier Potential spatial outlier

O = Possesses specified attribute

[1] Adjacent wells with large voids are grouted, however, this was not.

[2] Completion is within 10ft of the top of the Gasconade Formation

When deciding if a point should be removed, the resulting loss of resolution in the model should be considered. If the resolution loss is negligible then even for low confidence points, one can simply drop the targeted outlier (Liu et al., 2001). Likewise, if the inclusion of a targeted outlier that is suspected to be caused by natural variation has significant effects on the development of a groundwater model, then it should be excluded. For example, while it was decided to retain a point identified using this procedure, the scale of the effect of the potential sink on the model may be greater than the actual effects on the potentiometric surface. If this is the case then it could lead to false interpretations of groundwater flow characteristics

In order to test this new approach against more established approaches to data quality analysis, the results of this method were compared against results from a more conventional cross validation approach, specifically the approach presented by Miller et al. Miller at al identified that estimation errors from kriging greater than two kriging standard deviations may indicate an anomaly or erroneous value. Therefore, points with z-scores, the estimation error divided by the kriging standard deviation, greater than 2 are potentially spatial outliers. Results from the z-score method for each site are shown in Table 3.

It is immediately noted that there is little agreeance in the results of the two methods. Notably absent are points identified from the variogram approach that were confirmed to measures of perched aquifers (MW-1204 and MW-1205). Likely the reason these points were not identified is that for the MWG1B area, kriging standard deviation values were so high that the z-score was acceptably low. From Table 2, we see some of the wells identified in MWG1A only with the z-score method, are wells which have long

completion interval and others have solution features present in the borehole. However, the remaining wells (MW-5602,MW-5607,MW-5612, MW-0605) have no justification for removal. The case here may be the opposite than shown for MWG1B, were with a higher density of points in the area, a lower kriging standard deviation causes the method to be overly sensitive in identification of points. The potential outliers in MWG3 agreed for both methods. For MWG2 there were no points with a z-score higher than 2, however, the two points with the highest z-score were potential outliers identified in the variogram approach.

Table 3. Case study results using z-score approach

Group Number	Well ID	Kriging Standardized Error
MWG1A	MW-0601	-2.99
MWG1A	MW-0602	6.00
MWG1A	MW-0604	-3.54
MWG1A	MW-0605	6.14
MWG1A	MW-0606	6.06
MWG1A	MW-0610	-7.10
MWG1A	MW-5602	-2.58
MWG1A	MW-5607	2.28
MWG1A	MW-5612	2.27
MWG1A	MW-1207	2.49
MWG3	MW-211	-3.02

4. CONCLUSIONS

The variogram comparison approach to detecting spatial outliers provided reasonable results with a synthetic dataset and when applied during a case study at Fort Leonard Wood, Missouri. By providing justification as a final step to retaining a spatial outlier, a better understanding of causes of error are gained and there is a chance to introduce best management practices for monitoring well installation and sampling. The results showed that a recommended best practice from this study is to verify the geologic units during well construction and completion. In addition, because every point that showed seasonal variation was identified as an outlier, expected seasonal trends should be considered when evaluating if a measured water level is a good representation of the ground water surface. By using a supplemental DEM and every GWE point relationship, spatial outliers were still able to be identified in small low quality datasets. Other approaches which use cross-validation from some interpolation method may have skewed results based on the structure and density of data points, which ultimately effects the results of the interpolation. Therefore these methods may be overly sensitive for clustered data or the standard deviation from interpolation may be high enough to mask any potential outliers. The approach presented in Miller et al. is presented as only a rapid filtering procedure to identify points to be inspected. Other cross-validation procedures are made more robust, such as was presented in Liu et al. and may not be subject to such shortcomings. This approach overcomes these shortcomings as it is not reliant on placing confidence in neighboring points, but rather compares observations to a secondary high confidence dataset. Tradition spatial outlier detection methods only consider the

expected continuity of a point with its nearest neighbors. This approach looks at the relation of neighboring points along with distant points to see if data pairs also conform to expected regional trends.

Limitations of this method should also be considered. The location of the variogram threshold is dependent upon the qualitative identification of the area of the local scale on the gradient direction plot, leading to non-unique results. In addition, while assuming a single average gradient value for each scale on the variogram was necessary for comparison, in reality the gradient is a vector field and thus unique to each location. In the case study the procedure did not identify outliers in areas with long screened intervals or areas with known leaky pipes. There was concern that these areas may not give representative water levels. While the variation between a pair of points on the groundwater surface may be less than the average variation on the topographic surface, this does not disqualify a point as a spatial outlier. It may be the case that this method is not sensitive enough to the small changes these processes may have on the groundwater table. Lastly, the requirement for a supplementary related dataset limits extended application of this procedure.

This technique is recommended for those already applying geostatistical techniques to develop a groundwater surface. When co-kriging, the development of an experimental variogram of GWE values and a binned variogram of the secondary variable (DEM) are already part of the process. This technique can readily be incorporated as a preliminary step in the kriging process.

ACKNOWLEDGEMENTS

The authors would like to thank Dr. Carlo Salvinelli for his helpful comments on the manuscript. This work was supported by the United States Army Corps of Engineers grant no. W912DQ-14-2-0003-001.

REFERENCES

Arihood, L.D. (2009) Processing, analysis, and general evaluation of well-driller records for estimating hydrogeologic parameters of the glacial sediments in a ground-water flow model of the Lake Michigan Basin. US Geol. Surv. Sci. Invest. Rep. 2008-5184.

Bardossy, A. and Kundzewicz Z. W. (1990). "Geostatistical methods for detection of outliers in groundwater quality spatial fields." *Journal of Hydrology*. 115, 343-359.

Blauvelt, R. P. and Fullmer, D. (2011). "The Use of Topography as an Indicator of Ground Water Flow Direction and Its Implications for Due Diligence." *Journal of ASTM International*, 8(3), 103115.

Boezio, M., Costa, J., and Koppe, J. (2005). "Mapping water table level using piezometers readings and topography as secondary information – Trevo Mine – Brazil." *Application of Computers and Operations Research in the Mineral Industry*, 181–189.

Boezio, M. N. M., Costa, J. F. C. L., and Koppe, J. C. (2006). "Kriging with an external drift versus collocated cokriging for water table mapping." *Applied Earth Science*, 115(3), 103–112.

Chen D., Lu, C.-T., Kou, Y., Chen, F. (2008). "On detecting spatial outliers." *Geoinformatica*. 12, 455-475.

Desbarats, A. J., Logan, C.E., Hinton, M. J., and Sharpe, D. R. (2002). "On the kriging of water table elevations using collateral information from a digital elevation model." *Journal of Hydrology*. 255, 25-38.

Domenico, P. A., and Schwartz, F. W. (1998). *Physical and chemical hydrogeology*. Wiley, New York.

Elçi, A., Flach, G. P., and Molz, F. J. (2003). "Detrimental effects of natural vertical head gradients on chemical and water level measurements in observation wells: identification and control." *Journal of Hydrology*, 281(1-2), 70–81.

Goovaerts, P. (1997). *Geostatistics for natural resources evaluation*. Oxford University press, New York, N.Y.; Oxford.

Harrison, R. W., Orndorff, R. C., and Weems, R. E. (1996). *Geology of the Fort Leonard Wood Military Reservation and adjacent areas, south-central Missouri*. U.S. Dept. of the Interior, U.S. Geological Survey, Reston, VA.

Hill-Rowley, R., McClain, T., Malone, M. (2003). "Static water level mapping in east central Michigan." *J Am Water Resour Assoc*. 39(1), 99-111.

Hoeksema, R. J., Clapp, R. B., Thomas, A. L., Hunley, A. E., Farrow, N. D., and Dearstone, K. C. (1989). "Cokriging model for estimation of water table elevation." *Water Resources Research*, 25(3), 429–438.

Imes, J. L., Schumacher, J. G., and Kleeschulte, M. J. (1996). *Geohydrologic and water-quality assessment of the Fort Leonard Wood Military Reservation, Missouri, 1994-95*. U.S. Dept. of the Interior, U.S. Geological Survey, Rolla, MO.

Journel, A. G., and Huijbregts, C. J. (1997). *Mining geostatistics*. Acad. Press, London.

King, F.H., (1899). Principle and conditions of the movements of groundwater. US Geol. Survey 19th Ann. Rep. Part 2, 59-294.

Kleeschulte, M. J., and Imes, J. L. (1997). *Regional ground-water flow directions and spring recharge areas in and near the Fort Leonard Wood Military Reservation, Missouri*. U.S. Dept. of the Interior, U.S. Geological Survey, Reston, VA.

Liu, H., Jezek, K. C., O'Kelly, M. E. (2001). "Detecting outliers in irregularly distributed spatial data sets by locally adaptive and robust statistical analysis and GIS." *Int. J. Geographical Information Science*. 15(8), 721-741.

Miller. R.D., Davis, J.C., Olea, R.A. (1997). "Acquisition Activity, Statistical Quality Control, and Spatial Quality Control for 1997 Annual Water Level Data Acquired by the Kansas Geological Survey." Open-file Report 97-33, Kansas Geological Survey.

Mugel, D. N., and Imes, J. L. (2003). *Geohydrologic framework, ground-water hydrology, and water use in the Gasconade River basin upstream from Jerome, Missouri, including the Fort Leonard Wood Military Reservation*. U.S. Dept. of the Interior, U.S. Geological Survey, Rolla, MO.

Pucci, Jr. A.A. and Murashige, J. A. E. (1987). "Applications of Universal Kriging to an Aquifer Study in New Jersey." *Groundwater*, 25(6), 672-678.

Schumacher, J. G., and Imes, J. L. (2000). *Geohydrology and water quality at Shanghai Spring and solid-waste management units at the Fort Leonard Wood Military Reservation, Missouri, 1995-98.* , U.S. Dept. of the Interior, U.S. Geological Survey, Rolla, MO.

Shekhar, S., Lu, C.-T., Zhang, P. (2003). "A unified approach to detecting spatial outliers." *GeoInformatica*. 7(2), 139-166.

Silliman, S. E., and Frost, C. (1998). "Monitoring Hydraulic Gradient Using Three-Point Estimator." *Journal of Environmental Engineering*, 124(6), 517–523.

Snyder, D.T. (2008). "Estimated depth to ground water and configuration of the water table in the Portland, Oregon area." US Geol Sur Sci Invest Rep. 2008-5059.

Tremblay, Y., Lemieux, J.-M., Fortier, R. Molson, J., Therrien, R., Therrien, P., Comeau, G., Marie-Catherine, T. P. (2015). "Semi-automated filtering of data outliers to improve spatial analysis of piezometric data." *Hydrogeology Journal*. 23, 851-868.

Vacher, H. L. (2005). "Computational geology 12 - Cramer's Rule and the Three-Point Problem." *Journal of Geoscience Education*, 48(4), 522–532.

SECTION

3. RECOMMENDATIONS FOR FUTURE WORK

The following ideas are presented provide alternative approaches to this procedure and continued research.

- Rather than using the binned DEM variogram as the threshold establish a hypothesized gradient to plot the equivalent variance.
- Rather than establishing a boundary on the variogram, use gradient direction and magnitude plots to identify outlying points.
- The gradient magnitude and direction plots can be used to best fit a trend model in kriging.
- Establish an interval above the threshold that indicates confidence in points.
- Rather than dividing sites by spatial proximity, do a watershed analysis to separate sites for analysis.

APPENDIX A.

MONITORING WELL DATABASE

FLW OU	MW ID	Northing (ft)	Easting (ft)	TOC (ft)	GWE (ft)	GE (ft)
FLW-002	MW-209	13689040.56	1881917.989	1142.72	934.08	1139.86
FLW-002	MW-210	13689014.15	1882397.205	1122.96	934.32	1120.18
FLW-002	MW-211	13689023.91	1882877.546	1120.52	997.77	1117.48
FLW-002	MW-212	13688647.68	1882928.75	1126.54	937.76	1123.85
FLW-002	MW-213	13688196.38	1883302.68	1128.21	934.76	1125.41
FLW-002	MW-214	13689423.67	1881960.476	1143.49	936.74	1140.50
FLW-002	MW-215	13688899.59	1880784.564	1124.04	932.39	1121.75
FLW-002	MW-216	13689291.02	1883456.079	1111.53	954.96	1108.84
FLW-002	MW-217	13688113.43	1882476.949	1135.94	932.42	1133.29
FLW-002	MW-218	13688129.36	1882027.113	1144.19	932.16	1142.05
FLW-002	MW-219	13687951.41	1882325.344	1135.67	932.52	1132.41
FLW-056	MW-5611	13717176.73	1901116.125	1061.44	885.23	1058.90
FLW-056	MW-5612	13712580.31	1897492.867	1054.98	868.58	1052.75
FLW-056	MW-5613	13713751.39	1900695.223	1121.50	894.81	1118.56
FLW-056	MW-5614S	13714872.5	1900503.068	1103.79	889.44	1101.23
FLW-056	MW-5614D	13714890.59	1900508.793	1102.95	889.22	1100.11
FLW-056	MW-5615	13714885.54	1897855.171	1050.64	851.70	1048.06
FLW-006	MW-0601	13709285.83	1896060.853	1076.71	850.80	1073.93
FLW-006	MW-0602	13710045.74	1896170.801	1078.62	847.37	1075.40
FLW-006	MW-0603	13709632.7	1895551.404	1087.00	844.18	1087.01
FLW-008	MW-0801	13711916.95	1901901.506	1063.64	874.66	1060.00
FLW-003	MW-305	13699195.28	1891303.694	1078.97	895.24	1076.18
FLW-003	MW-306	13699740.36	1888954.619	1145.06	865.35	1142.67
FLW-003	MW-307	13699870.05	1891169.695	1099.73	919.04	1097.03
FLW-003	MW-308	13698670.75	1892058.491	1103.00	845.12	1100.61
FLW-003	MW-309	13697444.77	1893632.247	1076.57	814.97	1073.57
FLW-006	MW-0607	13710180.6	1894838.858	1118.84	830.79	1119.11
FLW-006	MW-0608	13710717.41	1894834.544	1133.54	830.02	1134.16
FLW-012	MW-1204	13721797.69	1896454.337	927.20	886.81	924.08
FLW-012	MW-1205	13722584.88	1896986.312	912.31	893.49	909.68
FLW-060	MW-6001	13711786.33	1905542.49	888.66	861.40	885.68
FLW-060	MW-6002	13712078.7	1906781.158	863.99	858.07	860.63
FLW-056	MW-5603	13715976.1	1901323.36	1084.69	896.88	1082.69
FLW-056	MW-5604	13714207.12	1899950.387	1070.73	886.46	1068.48
FLW-056	MW-5605	13714301.36	1901755.532	1095.56	896.52	1092.46
FLW-056	MW-5606	13715415.57	1899861.191	1049.40	887.55	1046.82
FLW-056	MW-5607	13716390.76	1899261.509	1029.37	881.72	1029.38
FLW-056	MW-5608	13715164.69	1898806.955	1053.15	877.07	1049.98
FLW-003	MW-301	13698676.33	1888781.22	1136.71	863.69	1133.71

FLW-003	MW-302	13699394.84	1889641.814	1130.22	875.68	1128.02
FLW-003	MW-303	13699113.69	1889832.392	1122.04	875.62	1120.24
FLW-003	MW-304	13698608.86	1890031.811	1100.55	877.05	1097.85
FLW-006	MW-0609	13710352.39	1895112.356	1114.70	832.35	1114.96
FLW-003	MW-310	13696501.53	1892478.455	1121.59	842.04	1118.70
FLW-003	MW-311	13696924.99	1890805.827	1109.90	856.19	1106.90
FLW-006	MW-0604	13710291.06	1895551.588	1097.29	839.49	1097.72
FLW-006	MW-0605	13710829.82	1896231.26	1077.15	847.00	1077.25
FLW-006	MW-0606	13710556.04	1897347.379	1071.20	851.42	1071.30
FLW-056	MW-5609	13713746.1	1899091.677	1094.32	881.33	1090.81
FLW-056	MW-5610	13715361.89	1902421.506	1064.57	898.05	1061.07
FLW-002	MW-201R	13688165	1881265.157	1155.51	931.80	1153.07
FLW-006	MW-0610	13710509.9	1896758.56	1067.14	859.09	1064.86
FLW-056	MW-5601	13715187.83	1900937.159	1078.19	895.61	1076.20
FLW-056	MW-5602	13716383	1900159.514	1022.58	895.78	1019.98
FLW-003	MW-505	13697110.62	1892424.892	1093.80	842.72	1091.11
FLW-003	MW-401	13698819.02	1891195.597	1073.80	889.28	1070.80
FLW-003	MW-402	13698446.59	1891353.609	1070.32	858.02	1067.12
FLW-003	MW-502	13697889.38	1891196.509	1078.06	853.36	1075.06
FLW-003	MW-503	13697638.11	1891723.422	1068.79	856.08	1066.30
FLW-003	MW-504	13697194.99	1891829.911	1085.91	860.01	1082.92
FLW-056	MW-5616	13711836.42	1899620.945	1117.52	880.22	1115.08
FLW-012	MW-1201	13724233.16	1896087.956	1088.69	759.39	1085.81
FLW-012	MW-1202	13724440.97	1897620.584	889.93	797.18	886.40
FLW-012	MW-1203	13723969.89	1898334.432	909.51	818.51	906.63
FLW-056	MW-5618	13713603	1896291.972	1080.08	835.09	0.00
FLW-060	MW-0901	13713354.72	1905251.322	908.86	881.72	909.13
FLW-056	MW-5617	13716612.46	1902710.509	1040.78	881.70	0.00
FLW-012	MW-1206	13721902.04	1894841.926	1066.41	798.72	1064.12
FLW-012	MW-1207	13719650.96	1900194.967	1125.97	945.53	1123.01

APPENDIX B.

GRADIENT CALCULATIONS MATLAB CODE

```
%Calculates true gradient on a plane defined by three points for each
%unique three point combination from xyz data.  0 degrees is north.

clear
clc
close all
format long

%input file location for spatial data.  Data should be in three columns
%with no headings.  The first two columns should be x and y data
respectively with the
%third column being the head or elevation

data = xlsread('x_validation_olea_comparison','xyz');
%easting should be in first column and northing in second column

%N is the number of data points
%C is the total number of unique 3 point combinations; formula to find
C
%can be found in accompanying three point problem mathcad file.

N = 69;
C = 52394;
ext = 3000;             %labels for graph
res = 500;              %labels for graph
season = 'January ';    %labels for graph
year = 2015;            %labels for graph
site = 'MWG1B ';        %labels for graph


Z = zeros(C,1);
G = zeros(C,1);
AT = zeros(C,1);
counter = 0;
for i = 1:N-2
        for j = i+1:N-1
                for k = j+1:N

                    xi = data(i,1);
                    xj = data(j,1);
                    xk = data(k,1);
                    yi = data(i,2);
                    yj = data(j,2);
                    yk = data(k,2);
                    zi = data(i,3);
                    zj = data(j,3);
                    zk = data(k,3);

                    if xi == xj && xj == xk
                        continue
                    end

                    if yi == yj && yj == yk
                        continue
                    end
```

```
A = [xi,yi,0];
B = [xj,yj,0];
C = [xk,yk,0];

BA = B-A;
CB = C-B;
CA = C-A;
AB = A-B;
AC = A-C;
BC = B-C;


thetaA = atan2d(norm(cross(BA,CA)),dot(BA,CA));
thetaB = atan2d(norm(cross(AB,CB)),dot(AB,CB));
thetaC = atan2d(norm(cross(AC,BC)),dot(AC,BC));

thetas = [thetaA(:), thetaB(:), thetaC(:)];
D= min(thetas(:));

%filters acute angle values less than input
if D <= 30
    continue
end


a = -[zi yi 1; zj yj 1; zk yk 1];
b = -[xi zi 1; xj zj 1; xk zk 1];
c = [xi yi 1; xj yj 1; xk yk 1];

me = det(-a)/det(c);
mn = det(-b)/det(c);

Area = norm(cross(CA,CB))/2;
strike = atand(-det(b)/det(a));
dzdx=-det(a)/det(c);

%for the theta value below, north is 0 degrees and
east
%is 90
if strike<90
   if dzdx < 0
       theta = strike+90;
   else
       theta = strike +270;
   end
end

if strike >= 90
    if dzdx >0
        theta = strike+90;
    else
        theta = strike-90;
    end
```

```
                    end

                    %translation of deta 90 degrees clockwise moves 0
                    %degrees from N to E.  However, angles still
increase
                    %clockwise, remove comments to include code

                    %theta=theta+90;
                    %if theta >360
                    %    theta = theta-360;
                    %end

                    delH = ((me)^2 + (mn)^2)^0.5;
                    counter = counter +1;
                    Z(counter,1)=(theta);
                    AT(counter,1) = Area;
                    G(counter,1) = delH;


                end
        end
end

P = Z(1:find(Z,1,'last'));      %Gradient direction matrix
AP = AT(1:find(AT,1,'last'));   %Area matrix
GF = G(1:find(G,1,'last'));     %Gradient magnitude matrix

%Change variable input dependent on plotting gradient or direction and
%seasonal

s=scatter(AP,P,10);  %input
s.LineWidth=0.5;
x=xlabel('Area (ft^2)','FontSize',7,'fontname','Times New Roman');
y=ylabel('Gradient Direction (°)','FontSize',7,'fontname','Times New
Roman');
%title([num2str(res) 'm DEM ' num2str(ext) 'ft Gradient Direction vs.
Area'])
%title(['MW G1B Gradient Direction'])
t = title([(site) (season) num2str(year)
],'FontSize',7,'fontname','Times New Roman');
%Average = mean(GF)
Median = median(P)  %input
s=sprintf('45%c',char(176));
mdlabel=sprintf('Median: %0.1f' ,[Median]);
%h=annotation('textbox',[0.78 0.72 0.105 0.06],'String',[mdlabel
char(176)],'linestyle','none','FontSize',20,'FontName','Times New
Roman');
ax=gca;
ax.PlotBoxAspectRatio=[1 0.3 0.3427];
ax.ActivePositionProperty = 'position';
set(gca,'Units','centimeters','position',[1.5 1 12.5 4]);
%set(gca,'Units','centimeters','outerposition',[1 1 14 5]);
set(y,'Units','Normalized','Position',[-0.07, 0.5, 0]);
set(x,'Units','Normalized','Position',[0.5, -0.16, 0]);
set(t,'Units','Normalized','Position',[0.5, 1.05, 0]);
```

```
ax.FontName='Times New Roman';
ax.FontSize=7;
ax.XMinorTick='on';
ax.YMinorTick='on';
set(gca,'TickDir','out');
ax.YLim = [0 360];
ax.YTick = [0 90 180 270 360];
ax.XGrid= 'on';
ax.YGrid = 'on';
ax.Box='on';
```

APPENDIX C.

DEM GRADIENT DIRECTION AND MAGNITUDE PLOTS

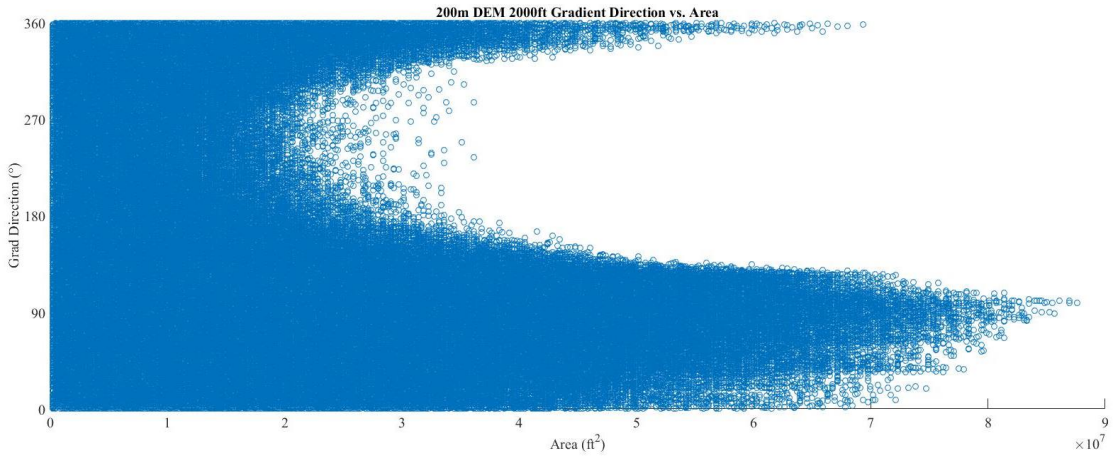
200m DEM 2000ft Gradient Direction vs. Area
Grad Direction (°)
360
270
180
90
0
0
1
2
3
4
5
6
7
8
9
Area (ft²)
×10⁷

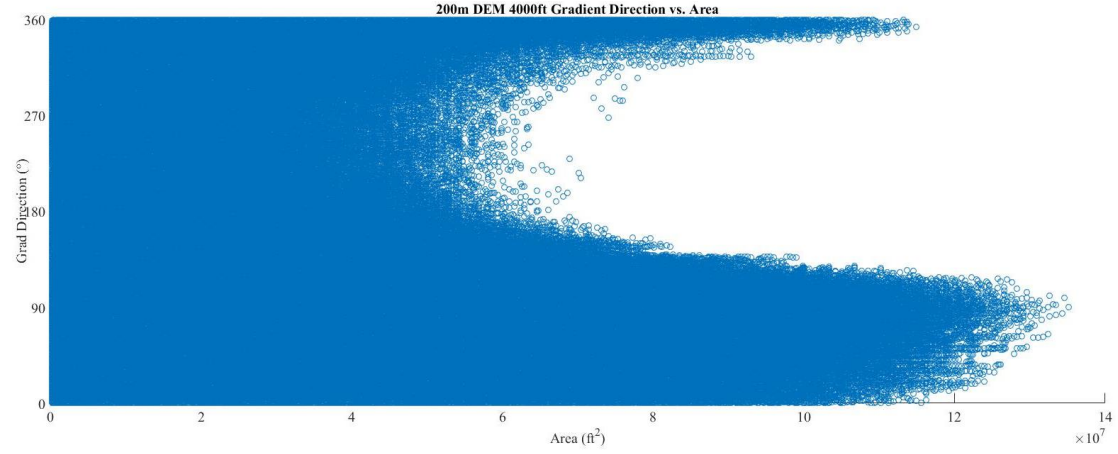
200m DEM 4000ft Gradient Direction vs. Area
Grad Direction (°)
360
270
180
90
0
0
2
4
6
8
10
12
14
Area (ft²)
×10⁷

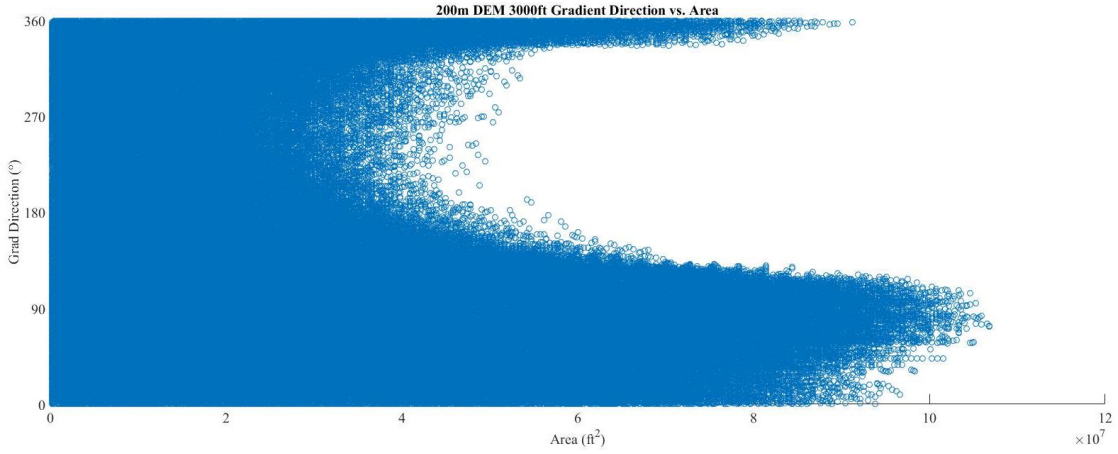
200m DEM 3000ft Gradient Direction vs. Area
Grad Direction (°)
360
270
180
90
0
0
2
4
6
8
10
12
Area (ft²)
×10⁷

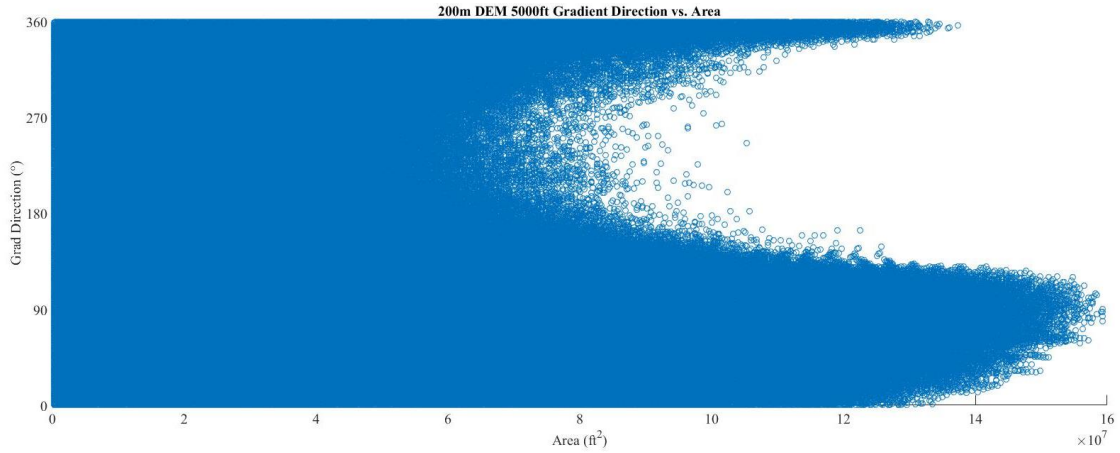
200m DEM 5000ft Gradient Direction vs. Area
Grad Direction (°)
Area (ft²)
×10⁷

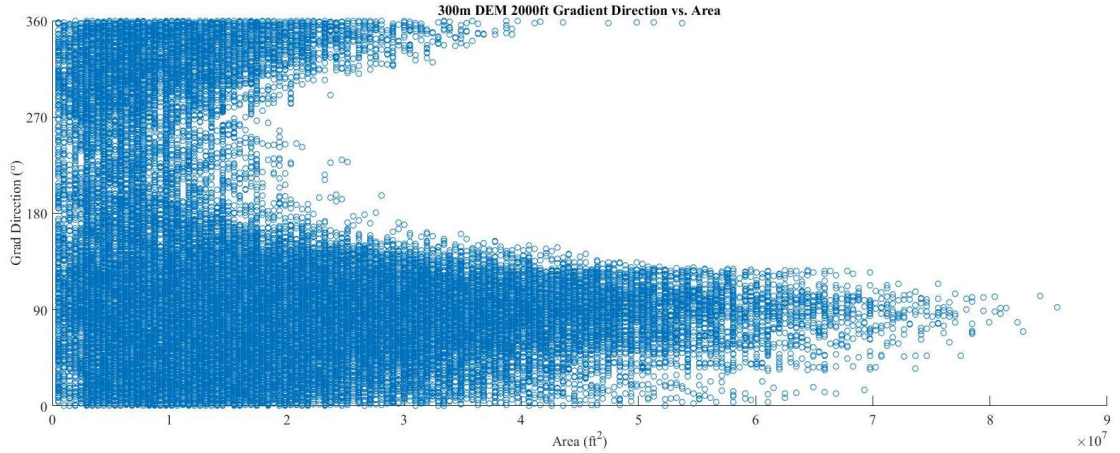
300m DEM 2000ft Gradient Direction vs. Area
Grad Direction (°)
Area (ft²)
×10⁷

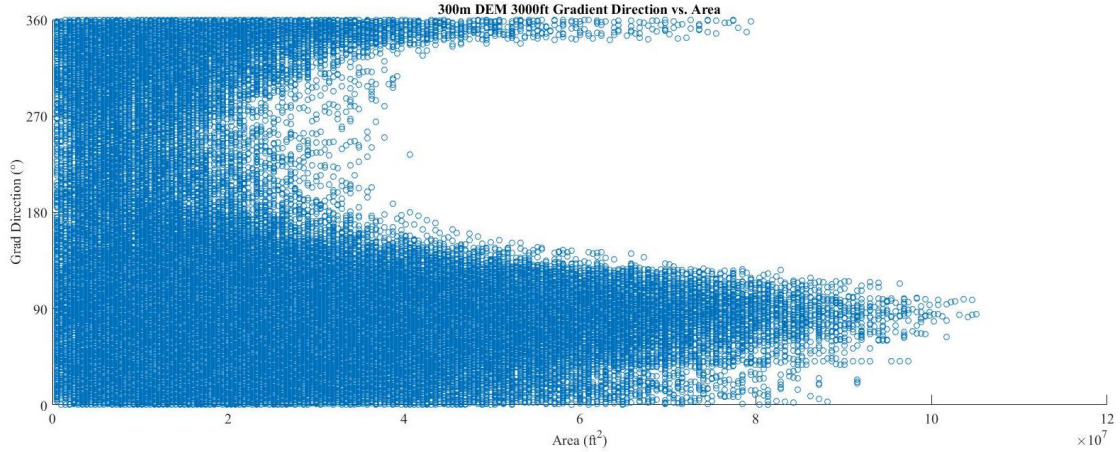
300m DEM 3000ft Gradient Direction vs. Area
Grad Direction (°)
Area (ft²)
×10⁷

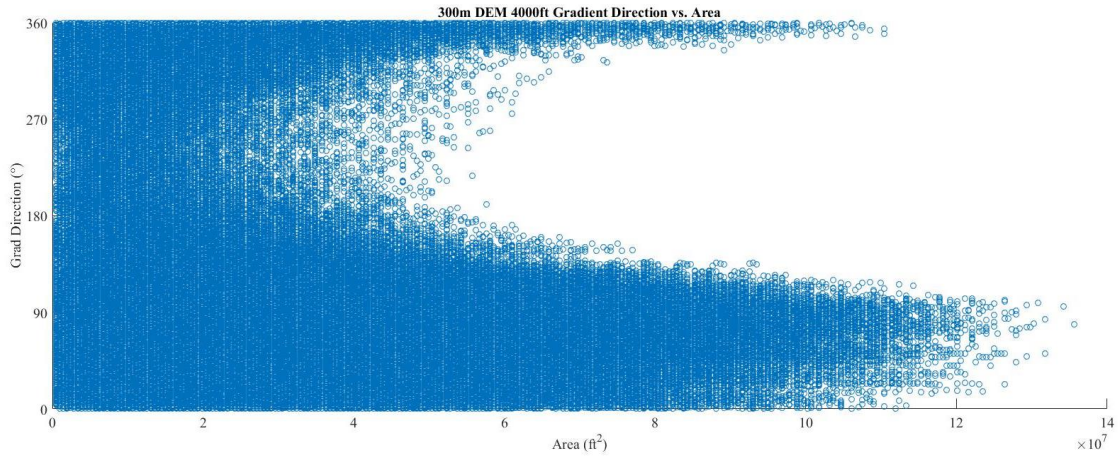
300m DEM 4000ft Gradient Direction vs. Area
Grad Direction (°)
360
270
180
90
0
0
2
4
6
8
10
12
14
Area (ft²)
×10⁷

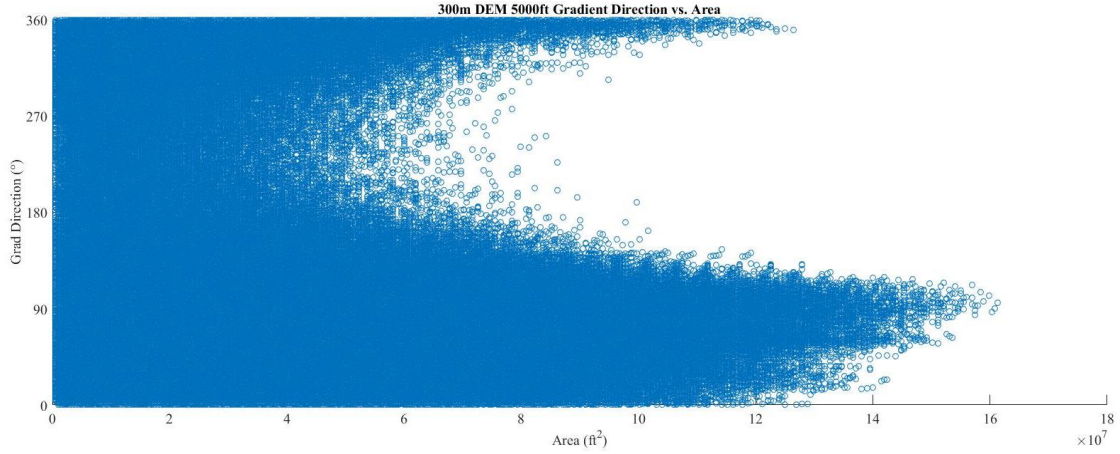
300m DEM 5000ft Gradient Direction vs. Area
Grad Direction (°)
360
270
180
90
0
0
2
4
6
8
10
12
14
16
18
Area (ft²)
×10⁷

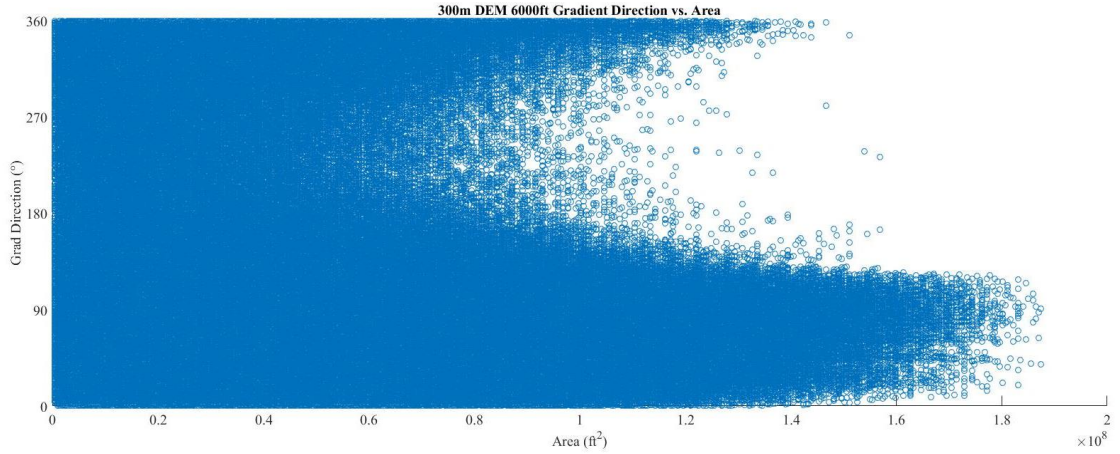
300m DEM 6000ft Gradient Direction vs. Area
Grad Direction (°)
360
270
180
90
0
0
0.2
0.4
0.6
0.8
1
1.2
1.4
1.6
1.8
2
Area (ft²)
×10⁸

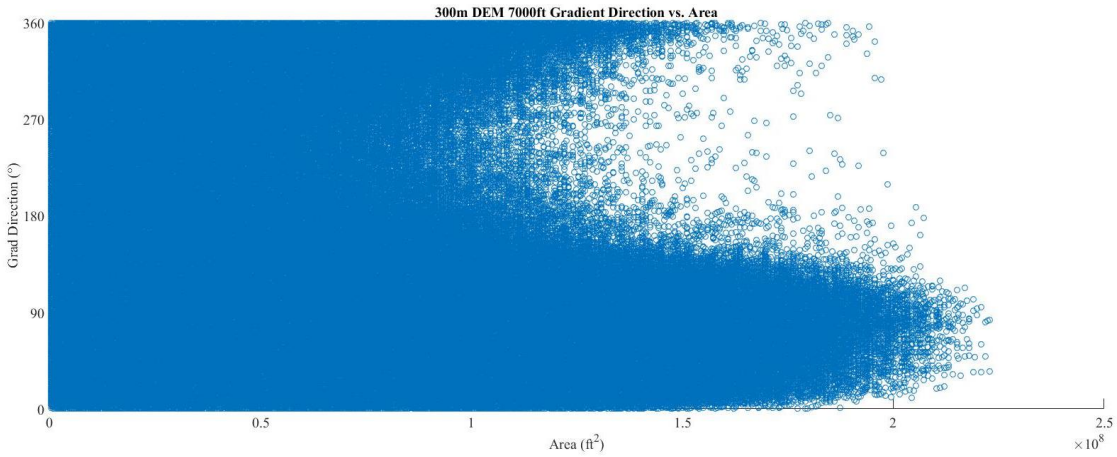
300m DEM 7000ft Gradient Direction vs. Area
Grad Direction (°)
Area (ft²)
×10⁸

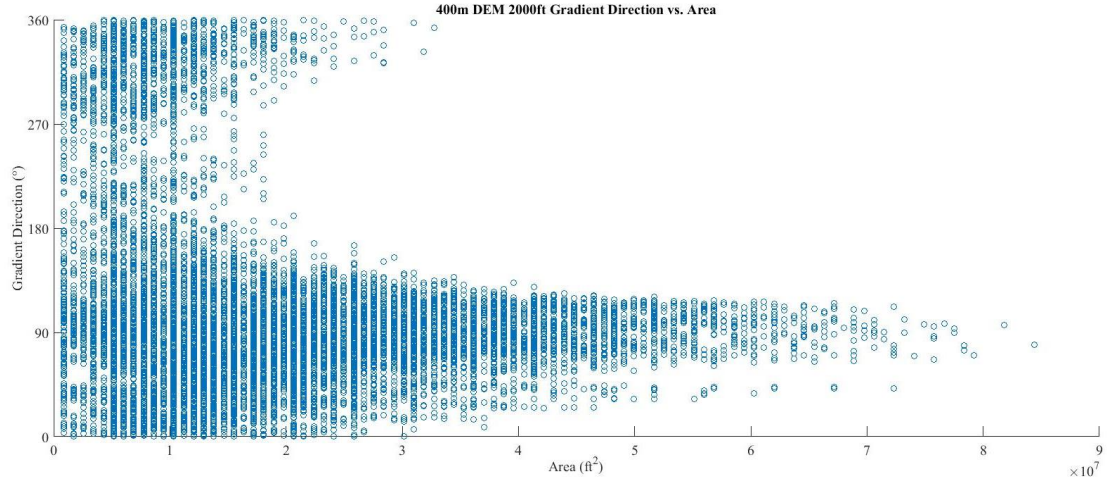
400m DEM 2000ft Gradient Direction vs. Area
Gradient Direction (°)
Area (ft²)
×10⁷

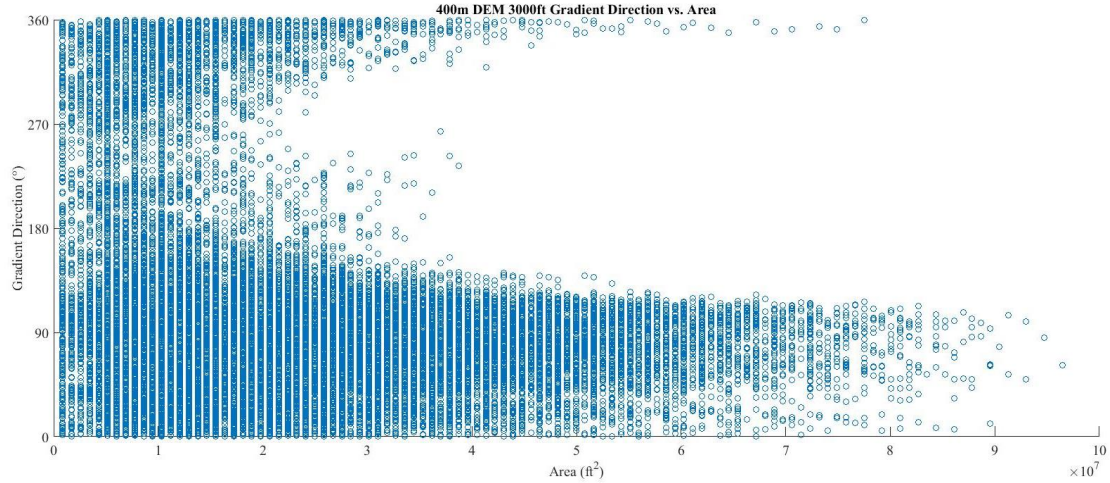
400m DEM 3000ft Gradient Direction vs. Area
Gradient Direction (°)
Area (ft²)
×10⁷

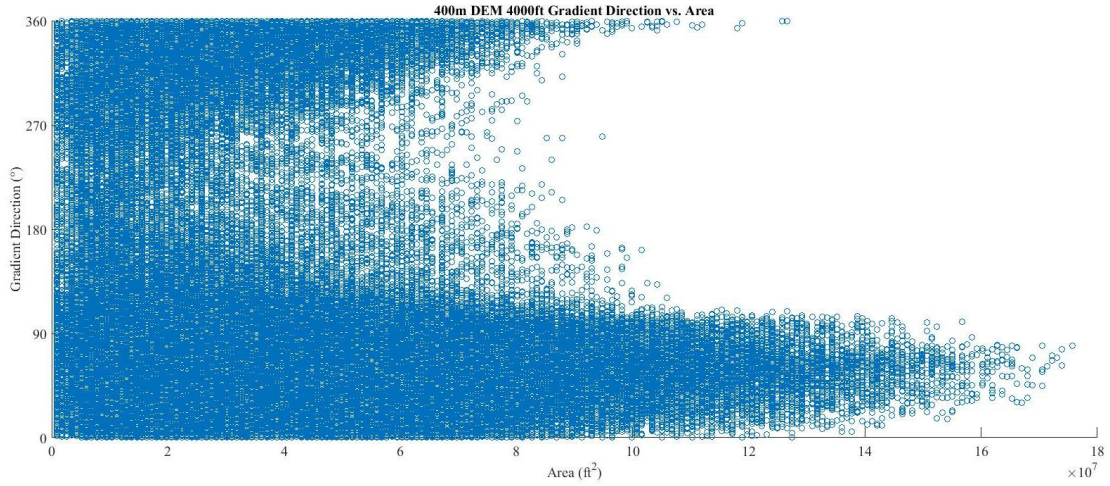
400m DEM 4000ft Gradient Direction vs. Area
Gradient Direction (°)
360
270
180
90
0
0
2
4
6
8
10
12
14
16
18
Area (ft²)
×10⁷

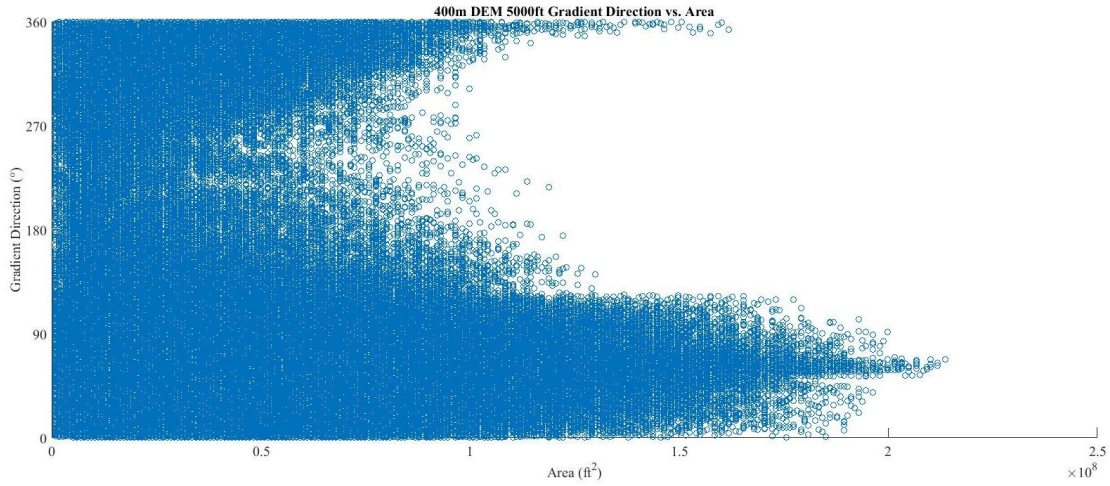
400m DEM 5000ft Gradient Direction vs. Area
Gradient Direction (°)
360
270
180
90
0
0
0.5
1
1.5
2
2.5
Area (ft²)
×10⁸

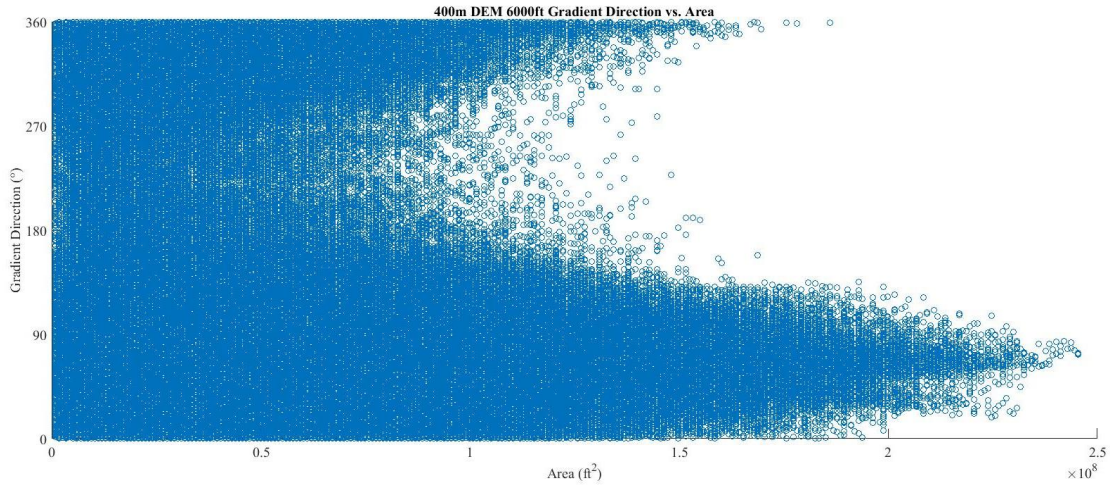
400m DEM 6000ft Gradient Direction vs. Area
Gradient Direction (°)
360
270
180
90
0
0
0.5
1
1.5
2
2.5
Area (ft²)
×10⁸

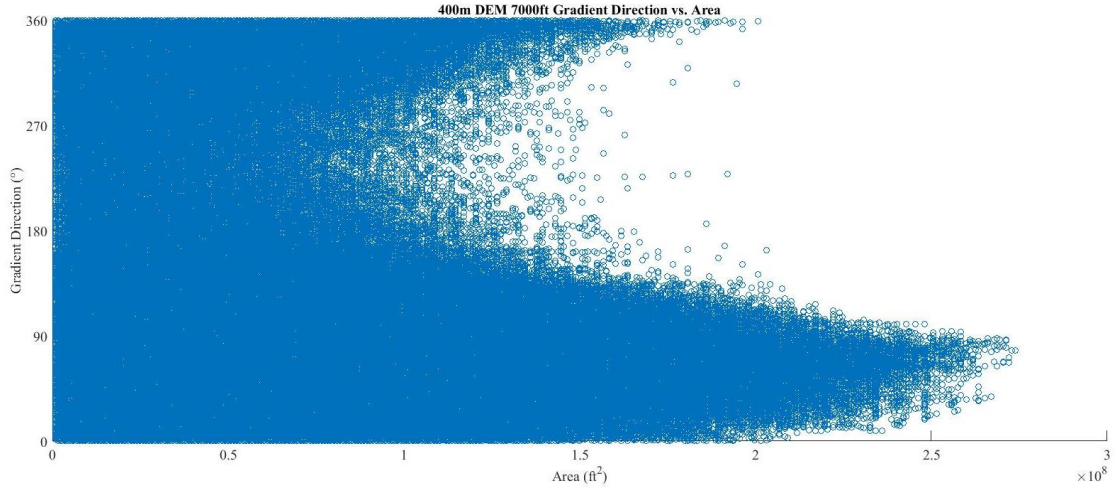
400m DEM 7000ft Gradient Direction vs. Area
Gradient Direction (°)
Area (ft²)
×10⁸

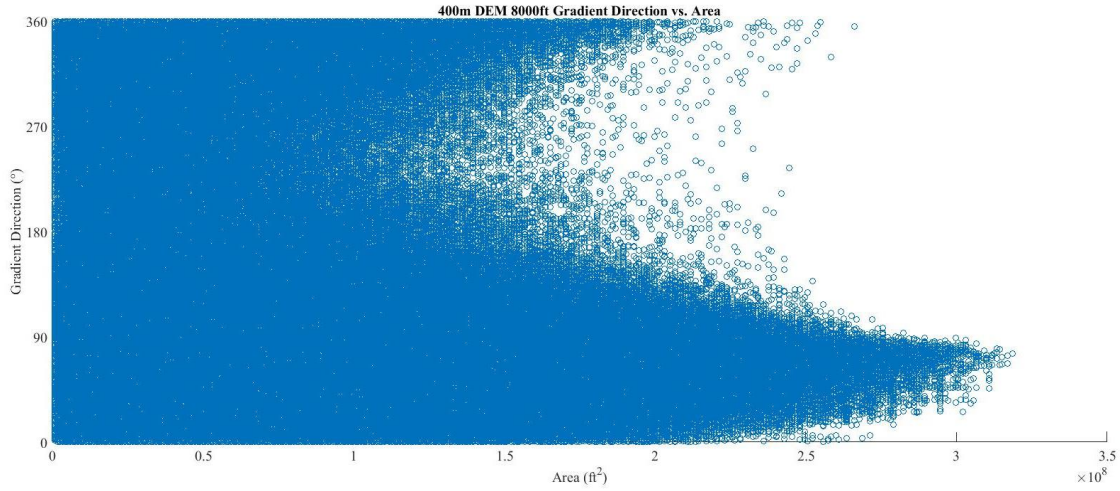
400m DEM 8000ft Gradient Direction vs. Area
Gradient Direction (°)
Area (ft²)
×10⁸

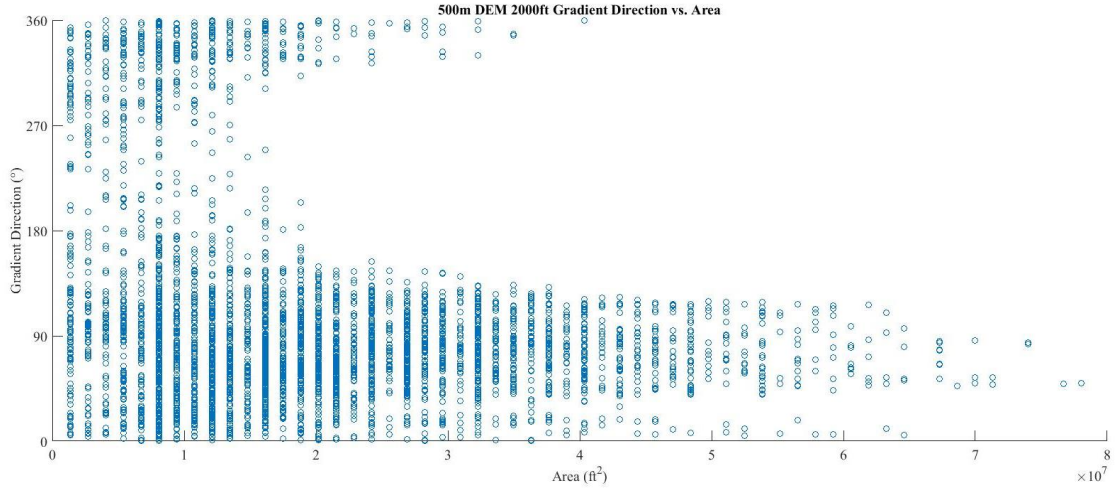
500m DEM 2000ft Gradient Direction vs. Area
Gradient Direction (°)
Area (ft²)
×10⁷

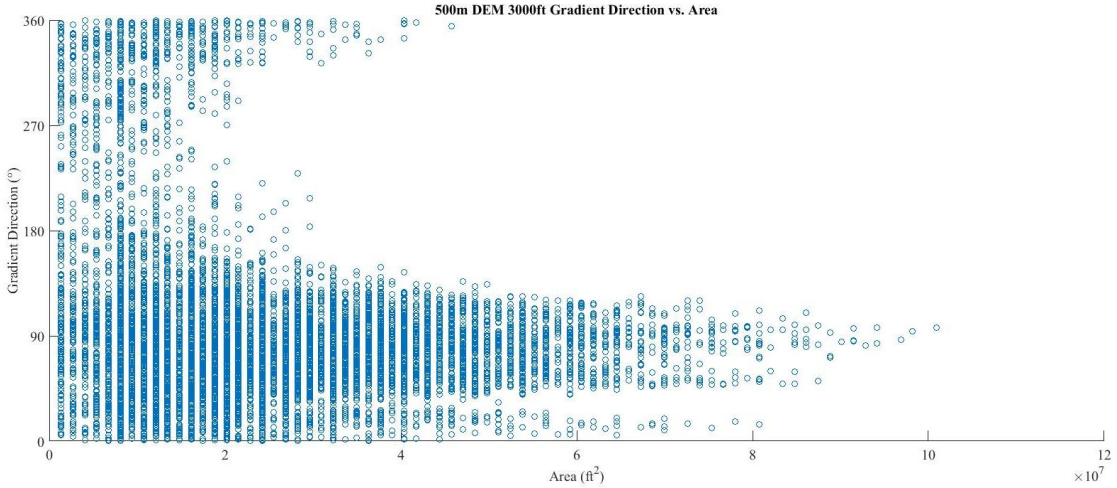
500m DEM 3000ft Gradient Direction vs. Area
Gradient Direction (°)
Area (ft²)
×10⁷

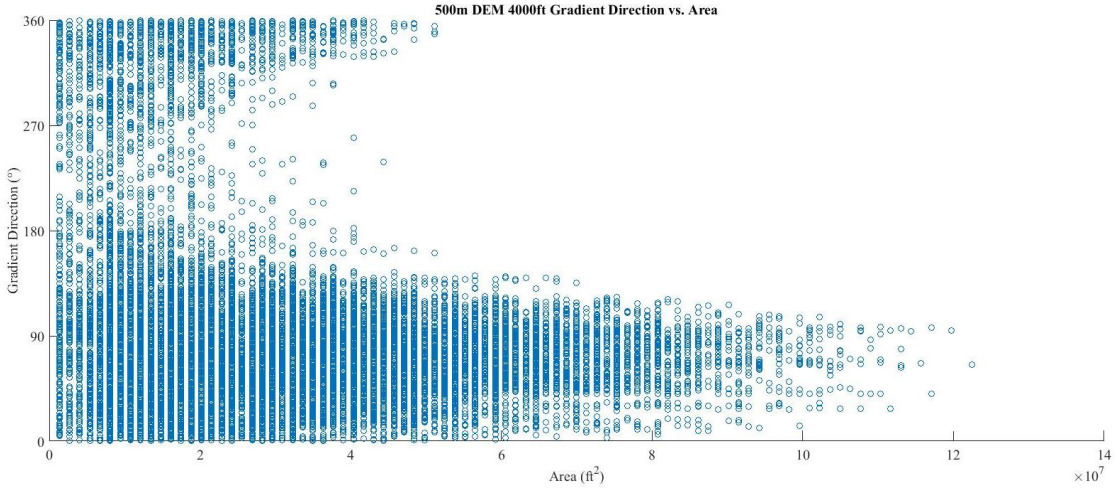
500m DEM 4000ft Gradient Direction vs. Area
Gradient Direction (°)
Area (ft²)
×10⁷

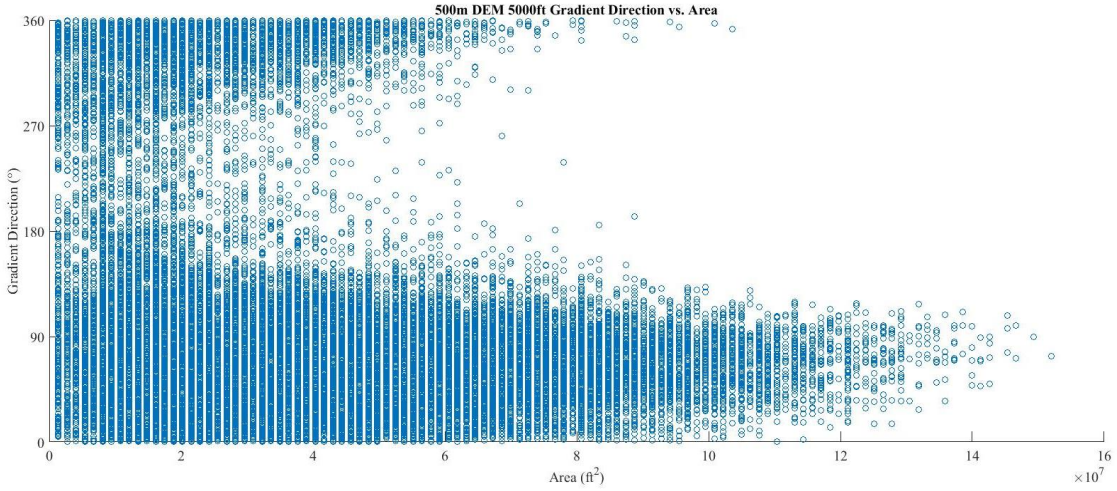
500m DEM 5000ft Gradient Direction vs. Area
Gradient Direction (°)
Area (ft²)
×10⁷

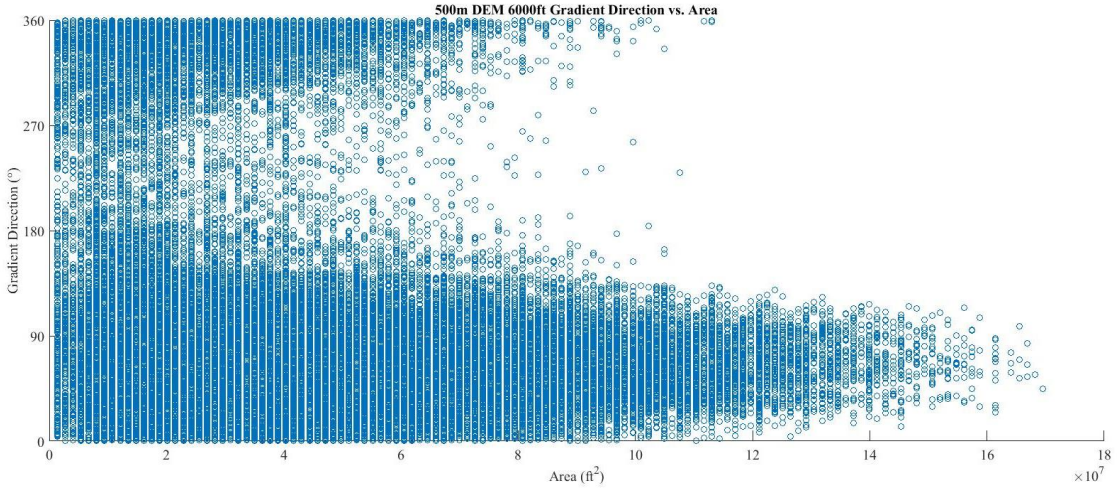
500m DEM 6000ft Gradient Direction vs. Area
Gradient Direction (°)
Area (ft²)
×10⁷

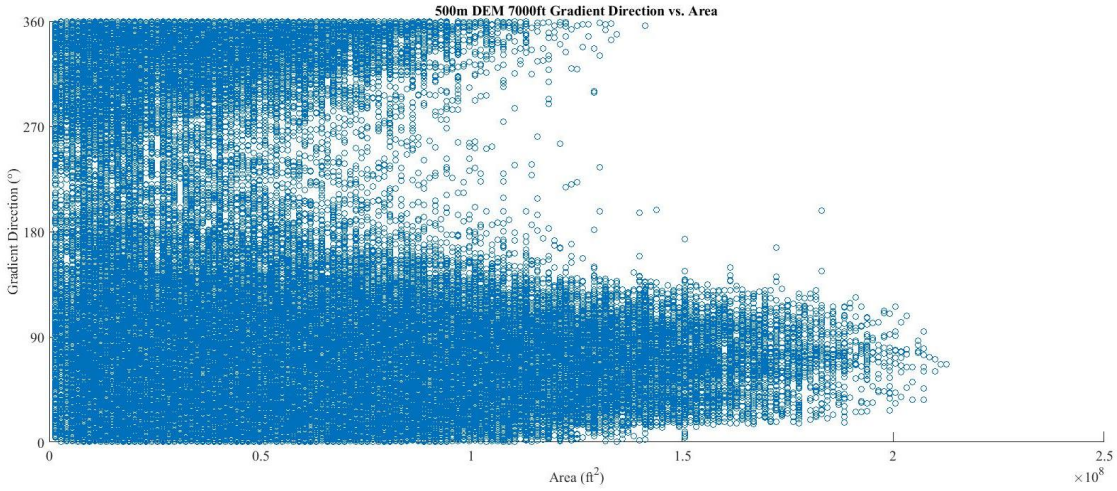
500m DEM 7000ft Gradient Direction vs. Area
Gradient Direction (°)
Area (ft²)
×10⁸

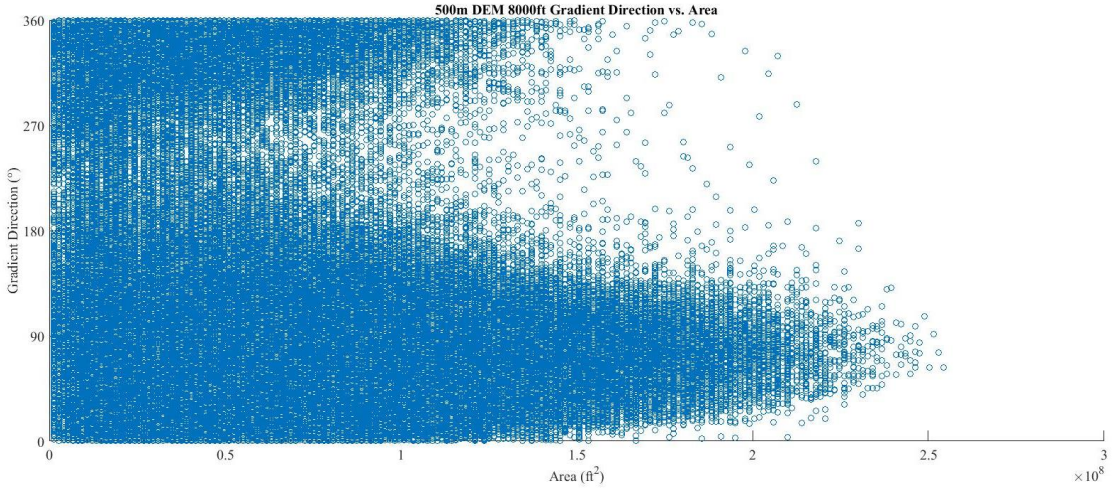
500m DEM 8000ft Gradient Direction vs. Area
Gradient Direction (°)
Area (ft²)
×10⁸

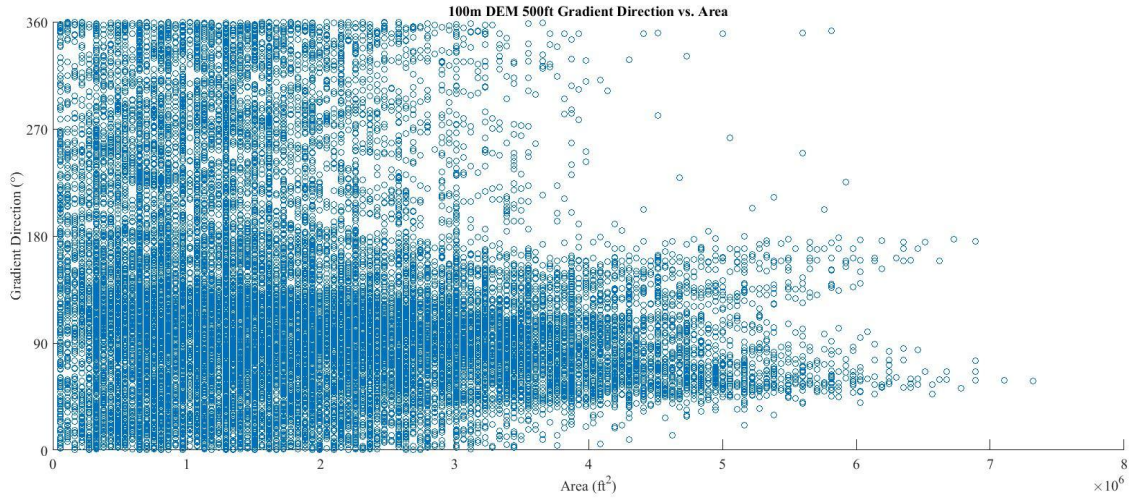
100m DEM 500ft Gradient Direction vs. Area
Gradient Direction (°)
360
270
180
90
0
0
1
2
3
4
5
6
7
8
Area (ft²)
×10⁶

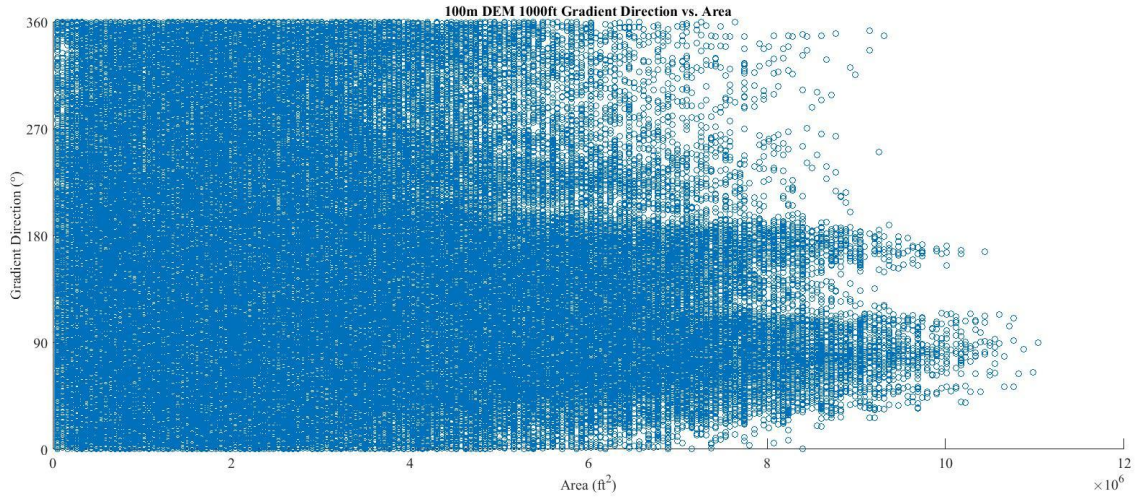
100m DEM 1000ft Gradient Direction vs. Area
Gradient Direction (°)
360
270
180
90
0
0
2
4
6
8
10
12
Area (ft²)
×10⁶

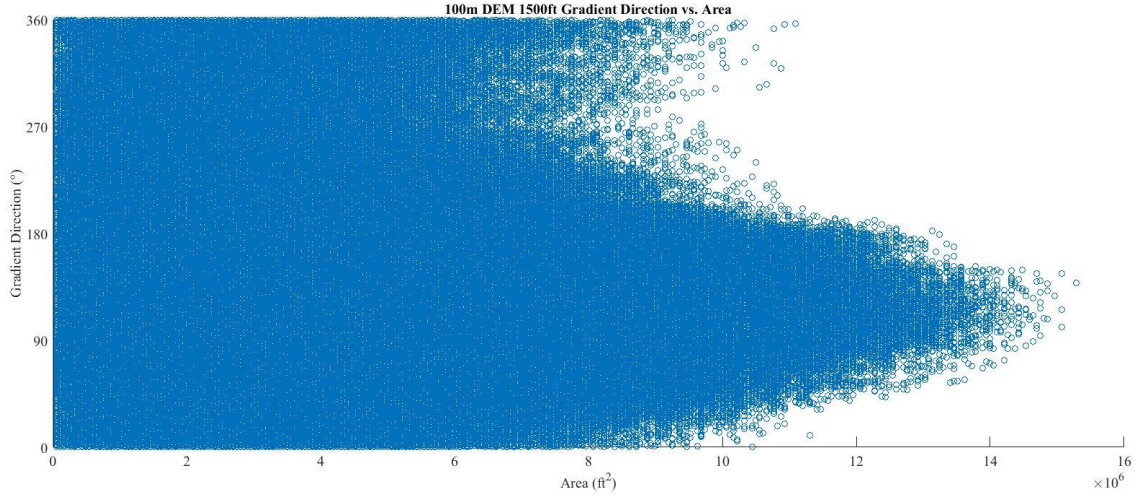
100m DEM 1500ft Gradient Direction vs. Area
Gradient Direction (°)
360
270
180
90
0
0
2
4
6
8
10
12
14
16
Area (ft²)
×10⁶

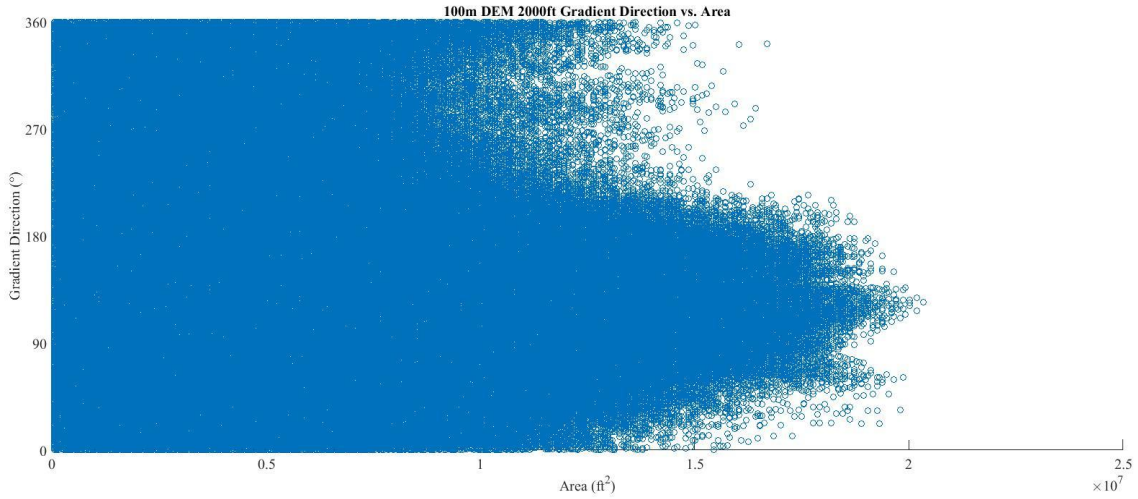
100m DEM 2000ft Gradient Direction vs. Area
Gradient Direction (°)
Area (ft²)
×10⁷

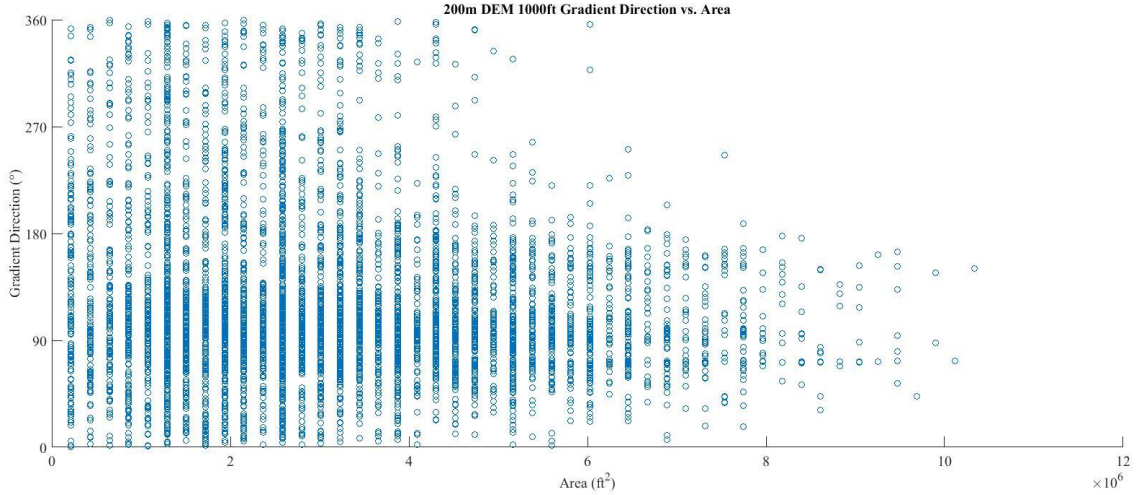
200m DEM 1000ft Gradient Direction vs. Area
Gradient Direction (°)
Area (ft²)
×10⁶

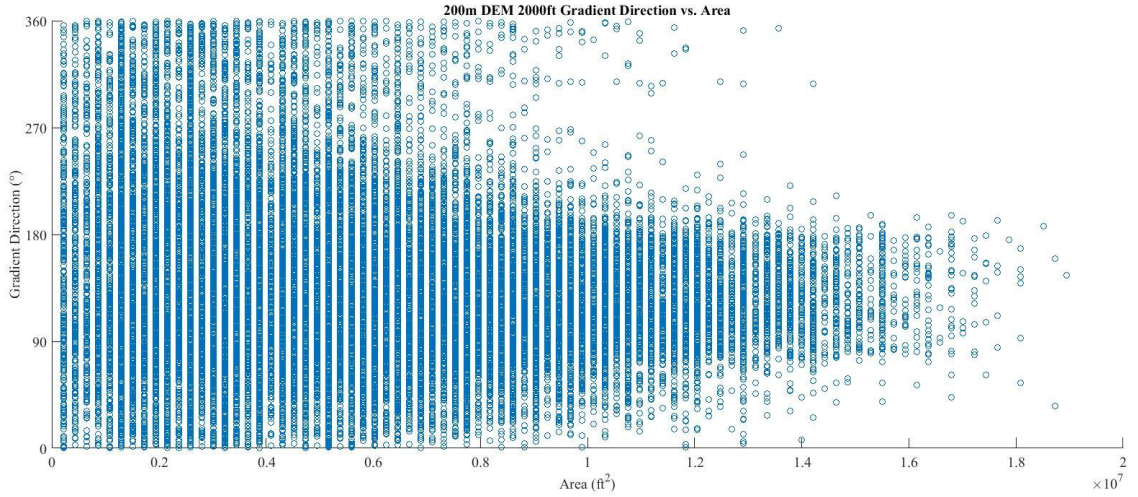
200m DEM 2000ft Gradient Direction vs. Area
Gradient Direction (°)
Area (ft²)
×10⁷

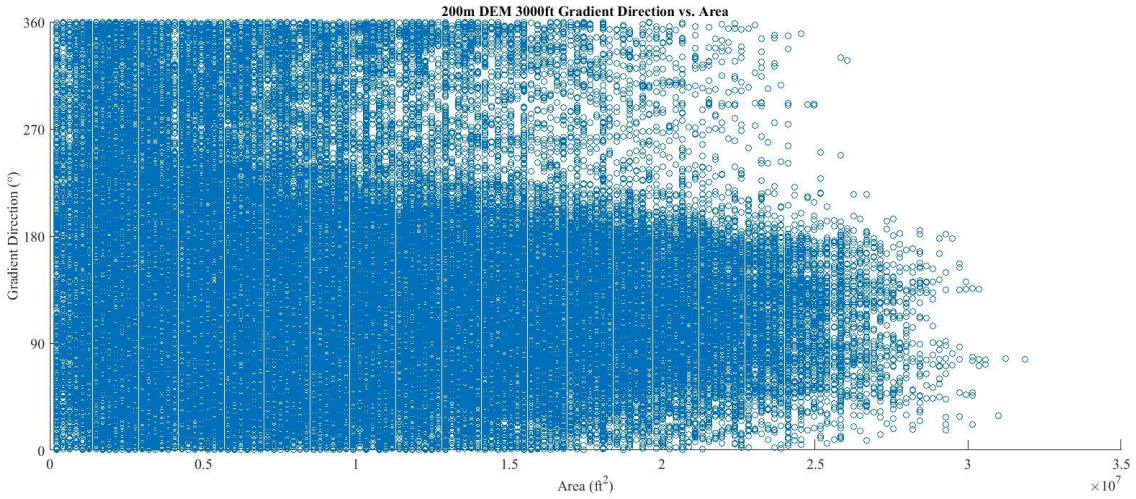
200m DEM 3000ft Gradient Direction vs. Area
Gradient Direction (°)
Area (ft²)
×10⁷

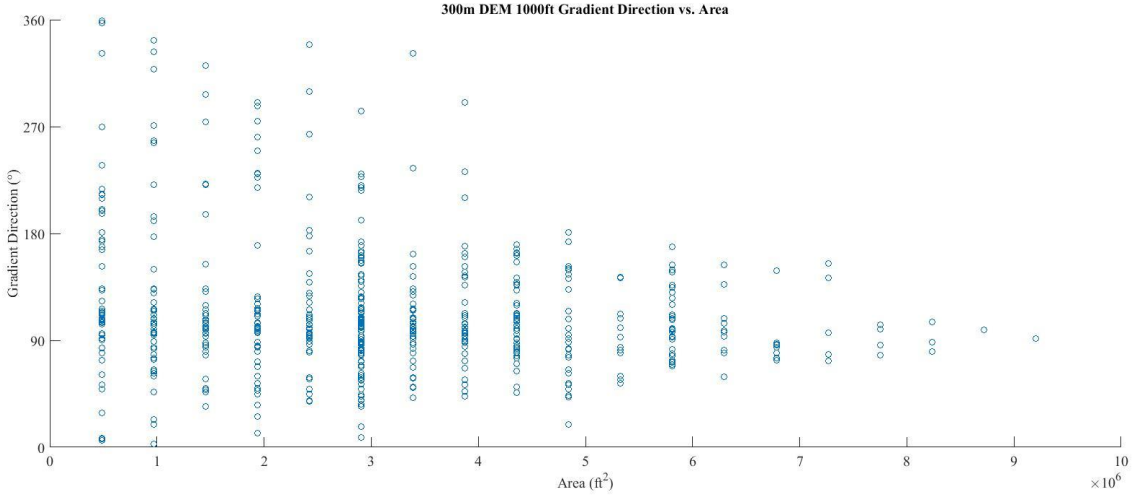
300m DEM 1000ft Gradient Direction vs. Area
Gradient Direction (°)
Area (ft²)
×10⁶

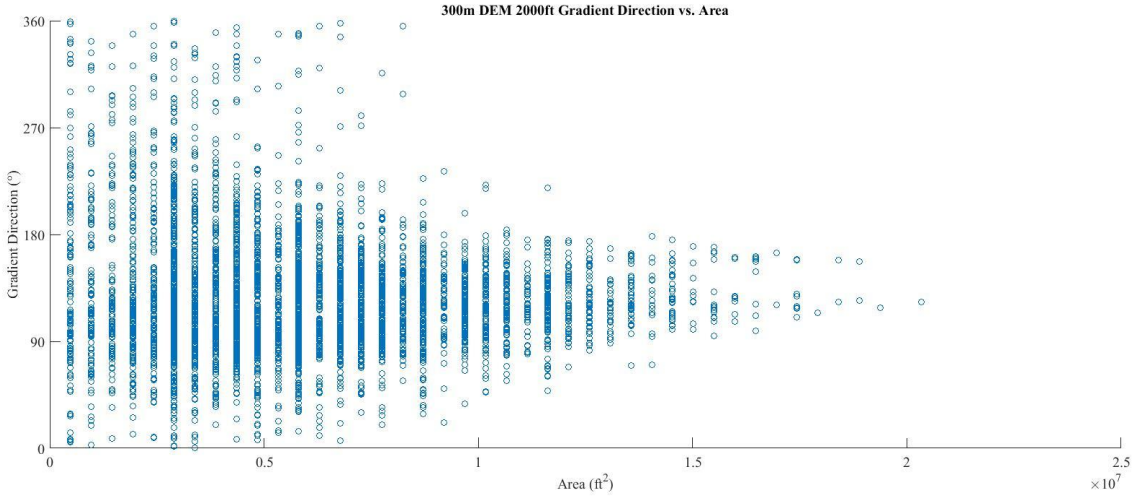
300m DEM 2000ft Gradient Direction vs. Area
Gradient Direction (°)
Area (ft²)
×10⁷

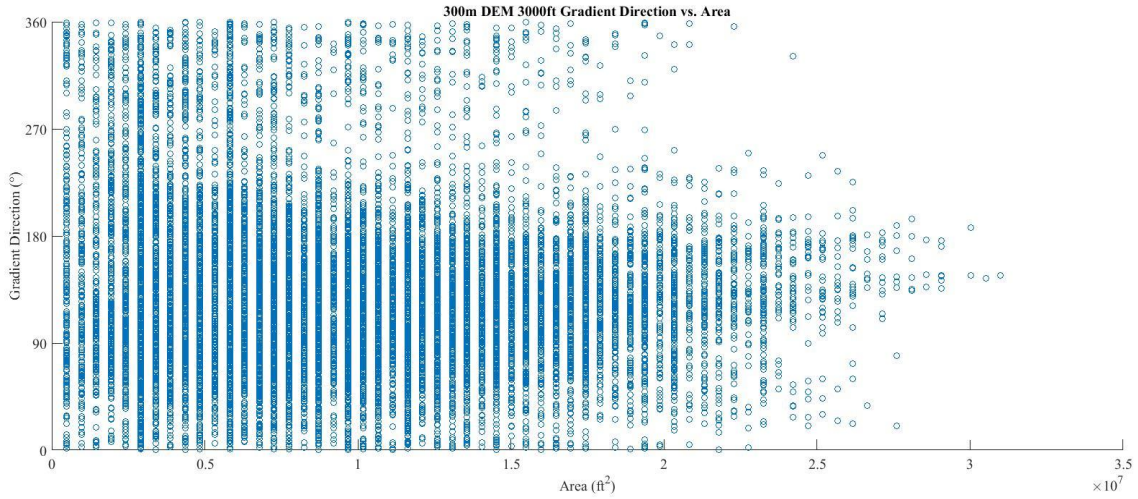
300m DEM 3000ft Gradient Direction vs. Area
Gradient Direction (°)
Area (ft²)
×10⁷

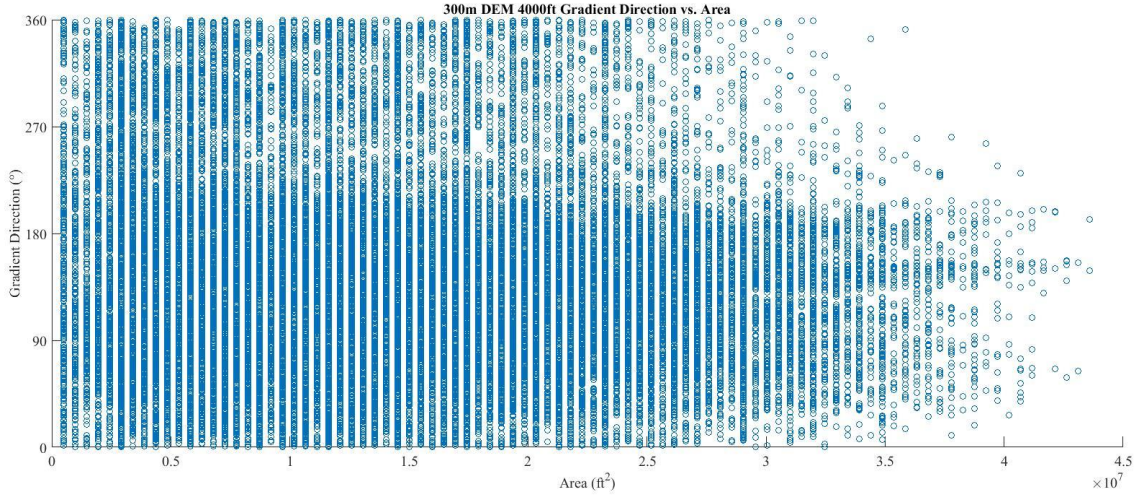
300m DEM 4000ft Gradient Direction vs. Area
Gradient Direction (°)
Area (ft²)
×10⁷

APPENDIX D.

SEASONAL ANALYSIS

MWG1A Gradient Direction Plots – Local Scale Defined by Vertical Dashed Line

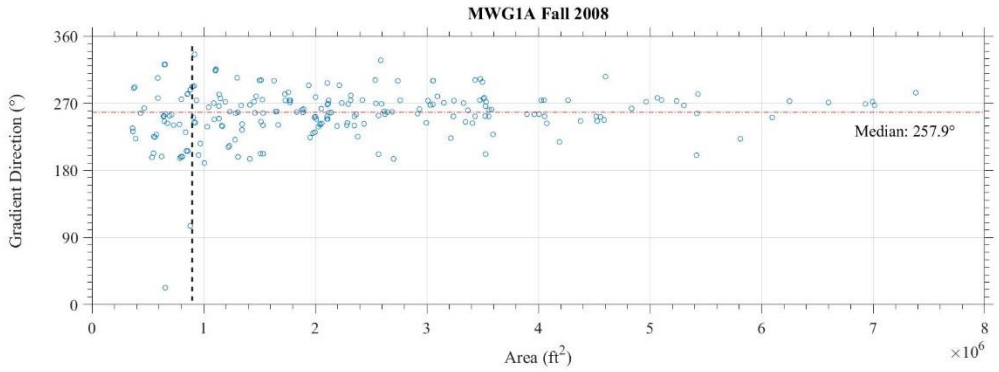

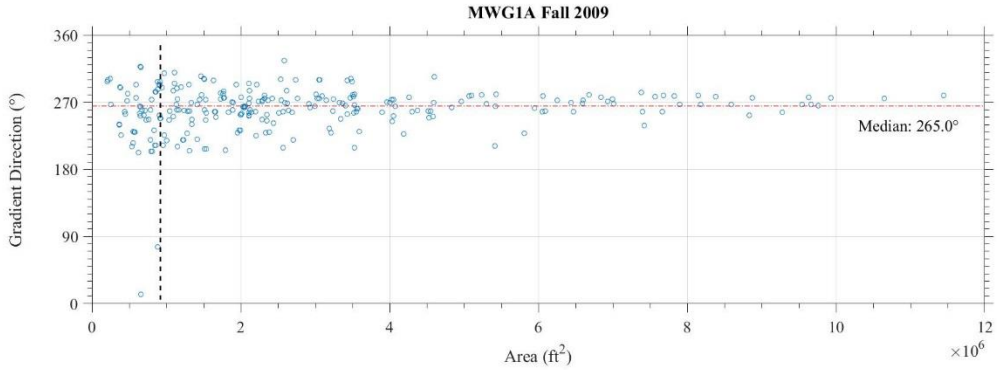

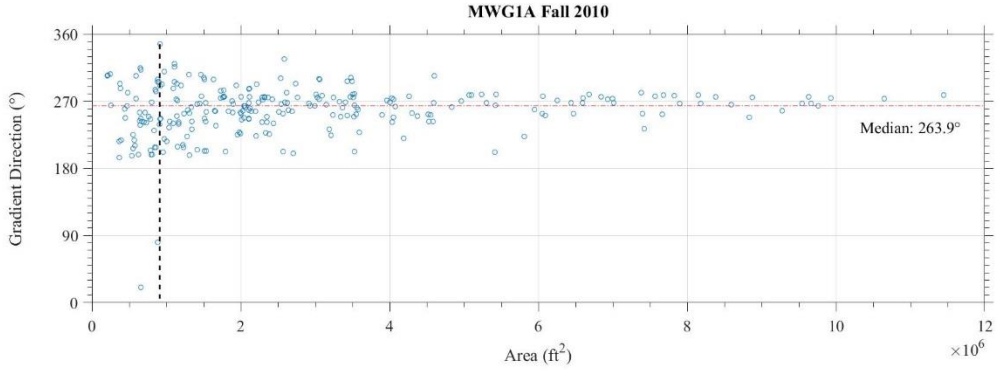

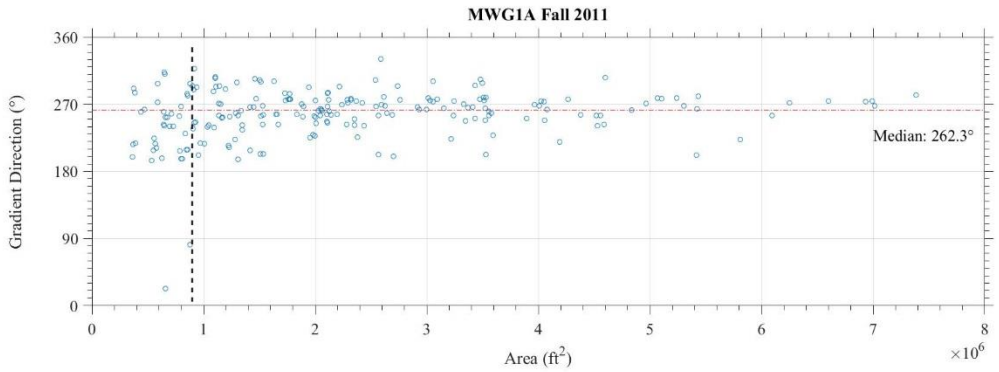
MWG1A Fall 2011
Gradient Direction (°)
360
270
180
90
0
Median: 262.3°
0
1
2
3
4
5
6
7
8
Area (ft²)
×10⁶

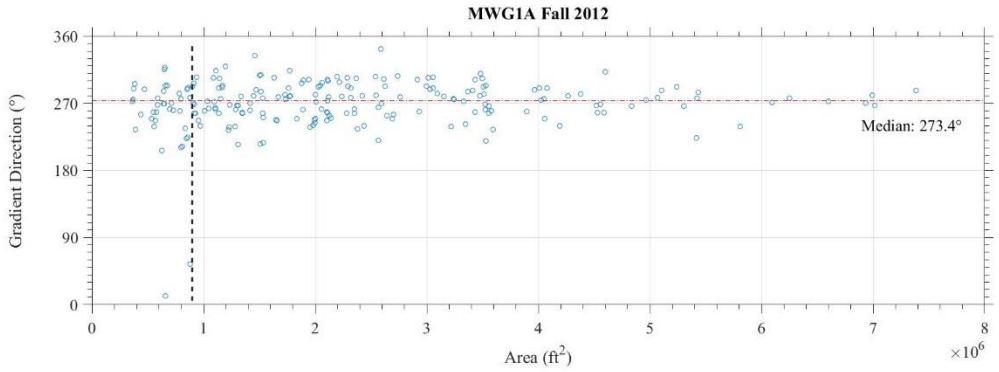
MWG1A Fall 2012
Gradient Direction (°)
360
270
180
90
0
Median: 273.4°
0
1
2
3
4
5
6
7
8
Area (ft²)
×10⁶

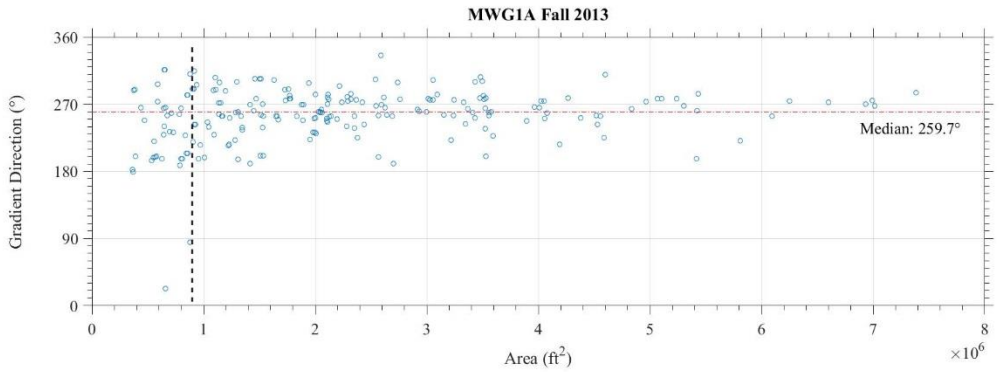
MWG1A Fall 2013
Gradient Direction (°)
360
270
180
90
0
Median: 259.7°
0
1
2
3
4
5
6
7
8
Area (ft²)
×10⁶

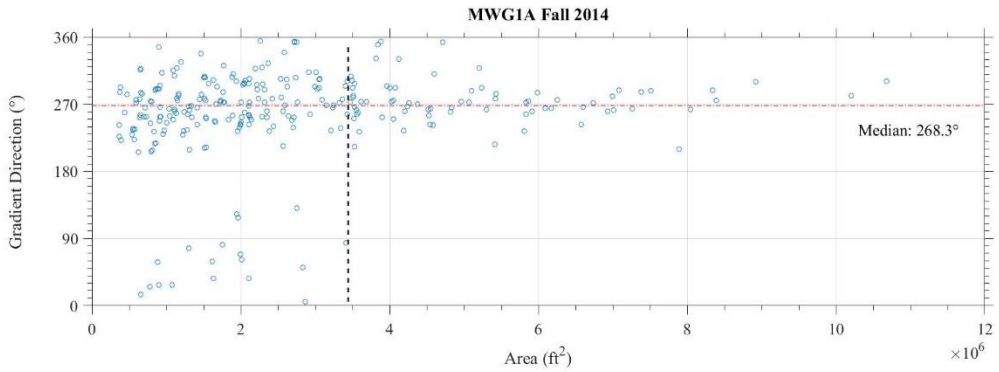
MWG1A Fall 2014
Gradient Direction (°)
360
270
180
90
0
Median: 268.3°
0
2
4
6
8
10
12
Area (ft²)
×10⁶

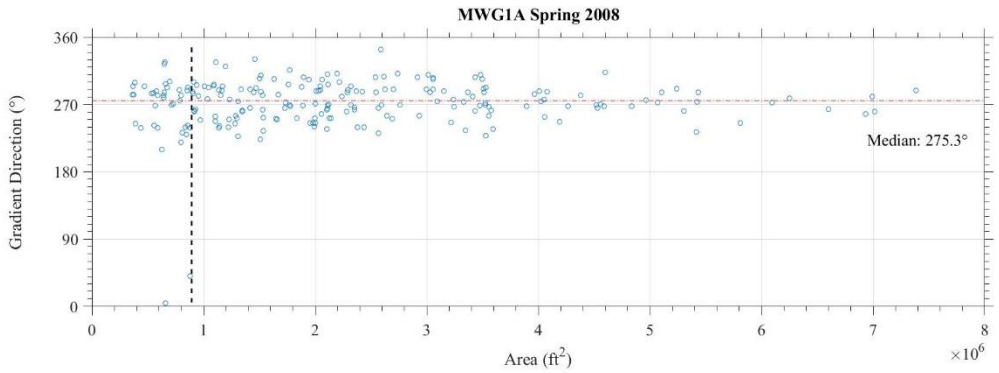
MWG1A Spring 2008
Gradient Direction (°)
360
270
180
90
0
Median: 275.3°
0
1
2
3
4
5
6
7
8
Area (ft²)
×10⁶

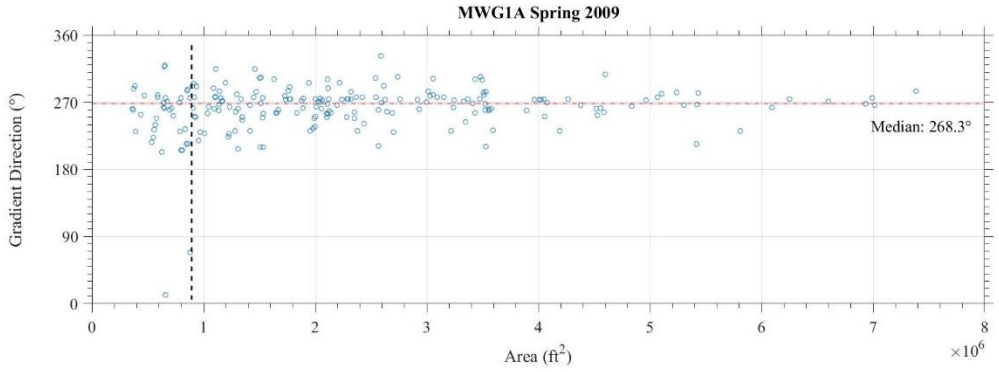
MWG1A Spring 2009
Gradient Direction (°)
360
270
180
90
0
Median: 268.3°
0
1
2
3
4
5
6
7
8
Area (ft²)
×10⁶

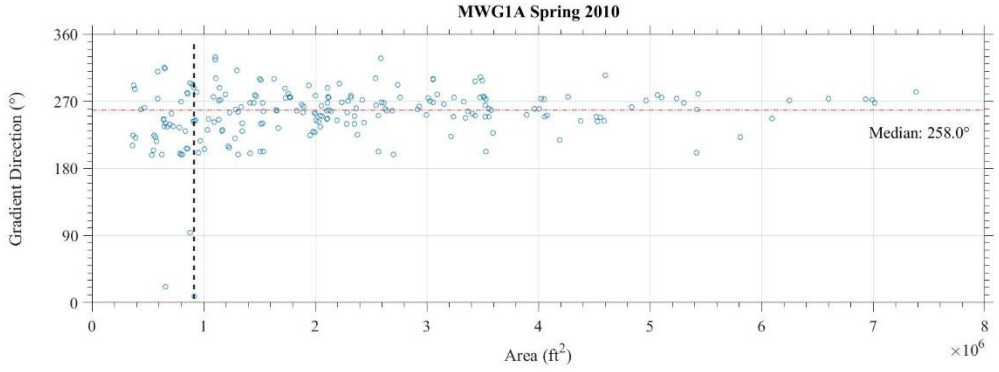
MWG1A Spring 2010
Gradient Direction (°)
360
270
180
90
0
Median: 258.0°
0
1
2
3
4
5
6
7
8
Area (ft²)
×10⁶

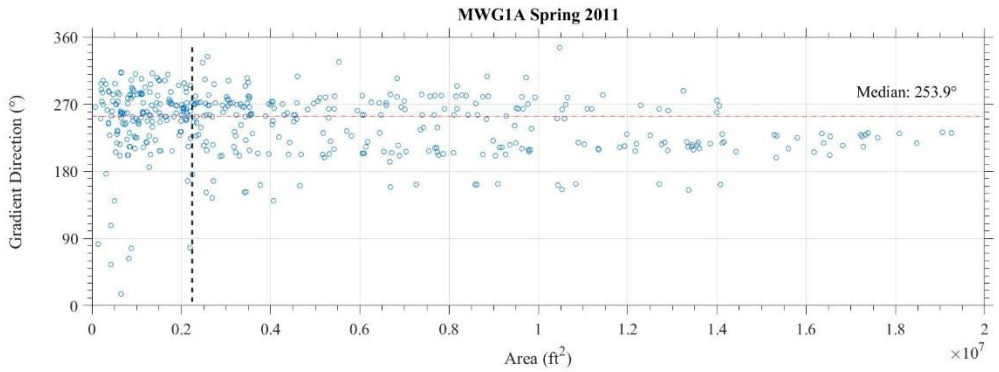
MWG1A Spring 2011
Median: 253.9°
Gradient Direction (°)
Area (ft²)
×10⁷

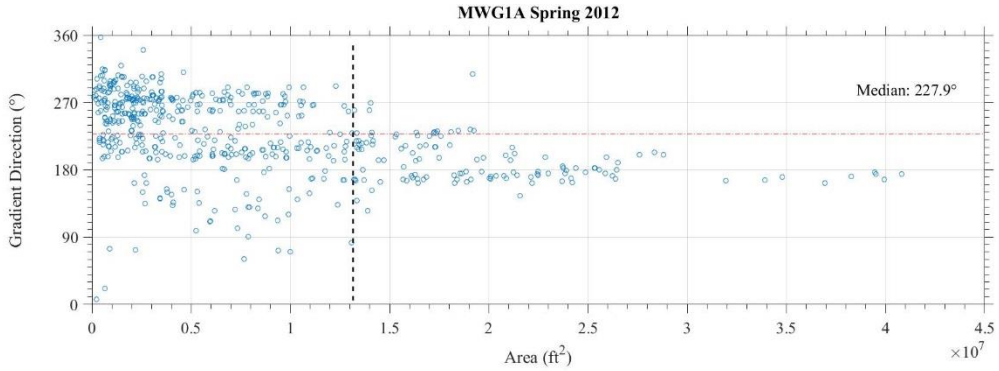
MWG1A Spring 2012
Median: 227.9°
Gradient Direction (°)
Area (ft²)
×10⁷

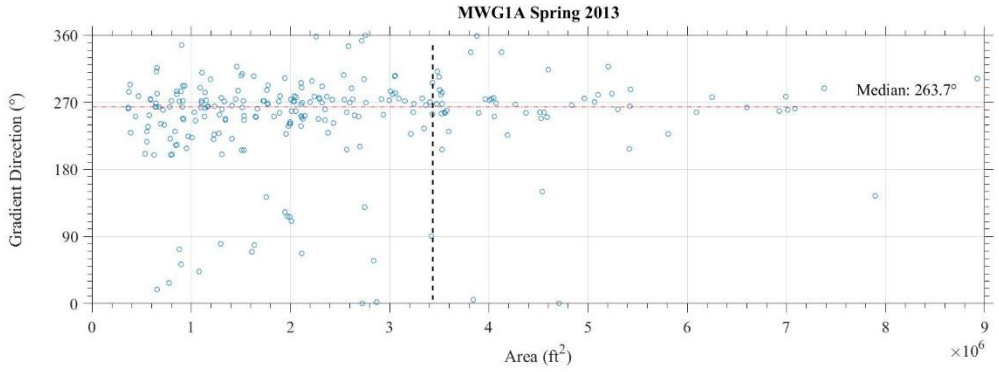
MWG1A Spring 2013
Median: 263.7°
Gradient Direction (°)
Area (ft²)
×10⁶

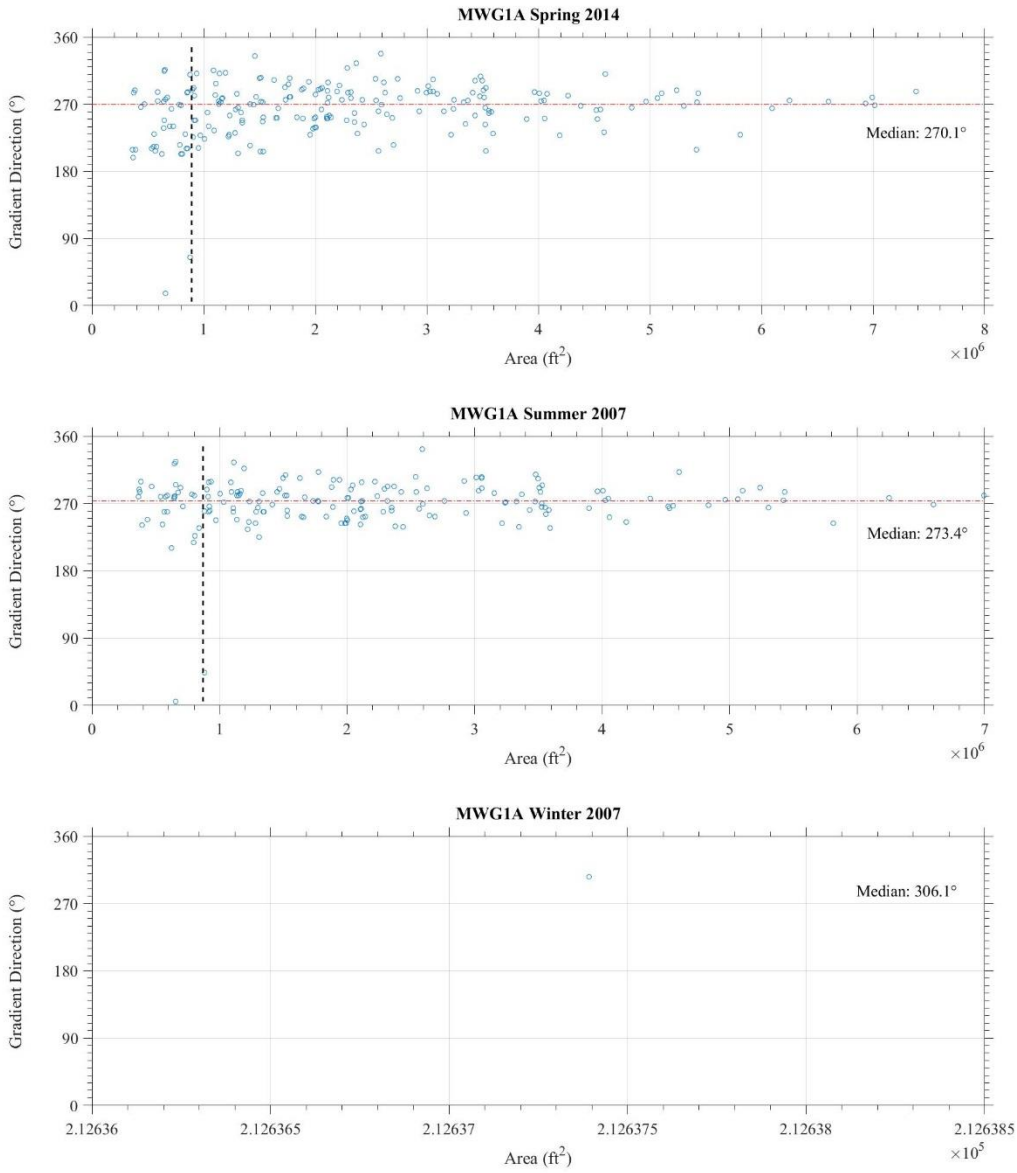
MWG1A Spring 2014
Gradient Direction (°)
Median: 270.1°
Area (ft²)
×10⁶
MWG1A Summer 2007
Gradient Direction (°)
Median: 273.4°
Area (ft²)
×10⁶
MWG1A Winter 2007
Gradient Direction (°)
Median: 306.1°
Area (ft²)
×10⁵

MWG1B Gradient Direction Plots – Local Scale approximated by maximum area

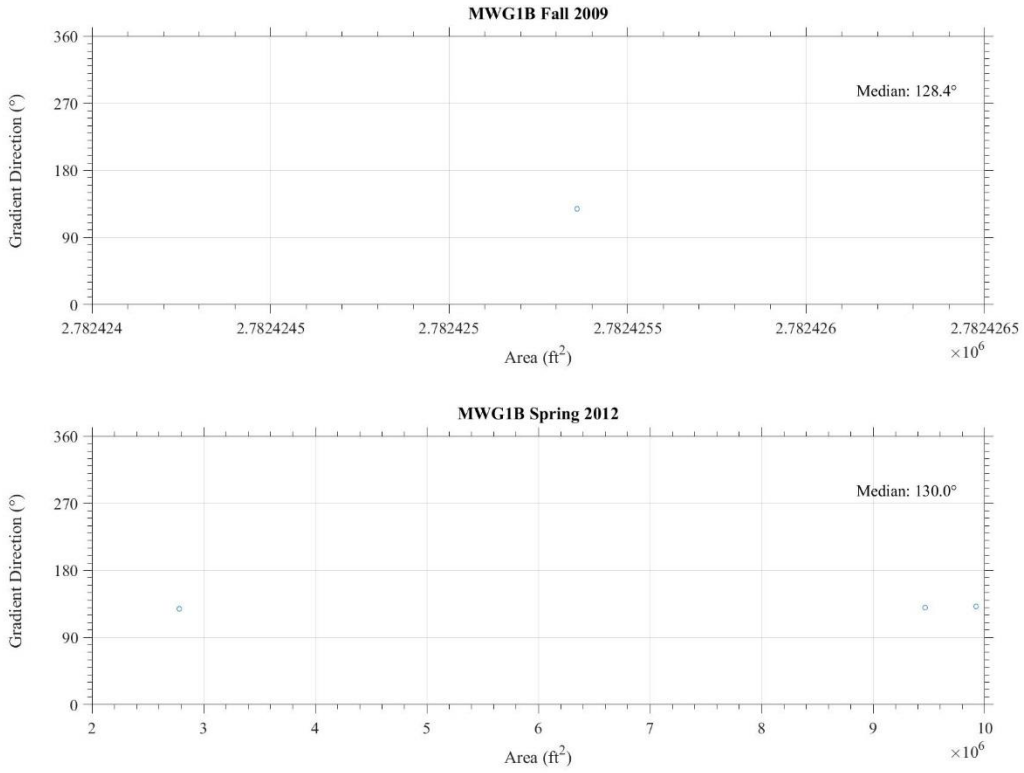

MWG2 Gradient Direction Plots – Local Scale Defined by Vertical Dashed Line

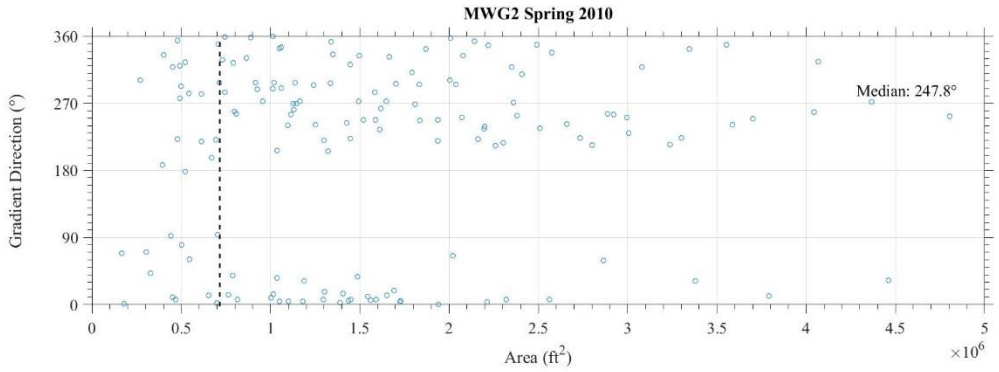

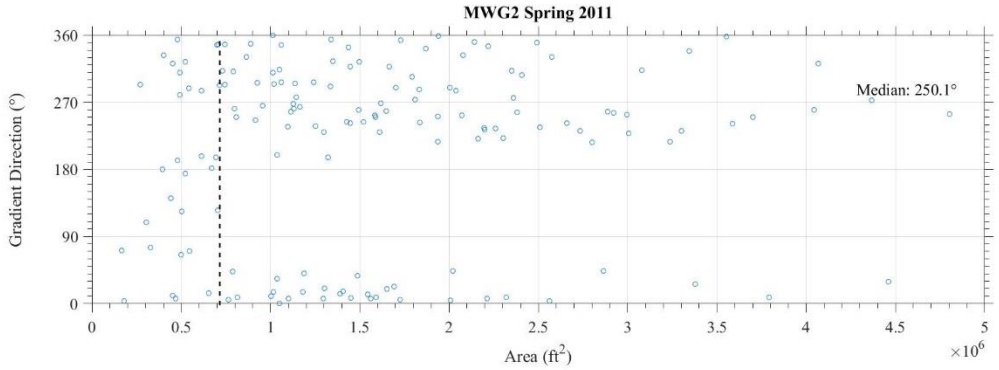

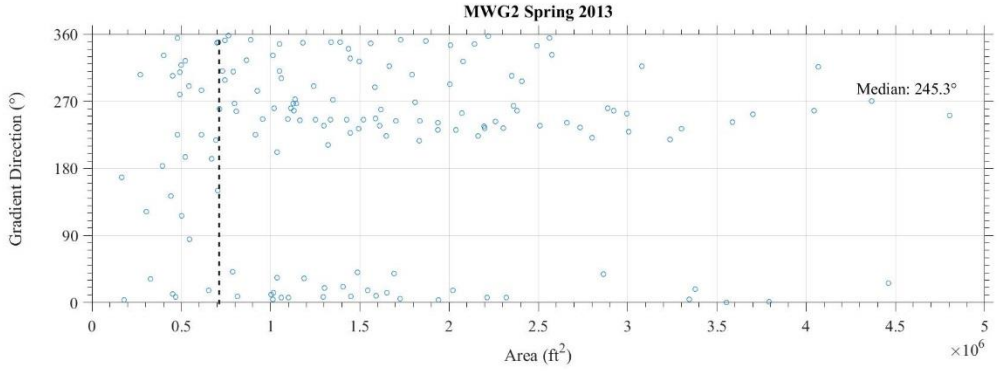

MWG3 Gradient Direction Plots – Local Scale Defined by Vertical Dashed Line

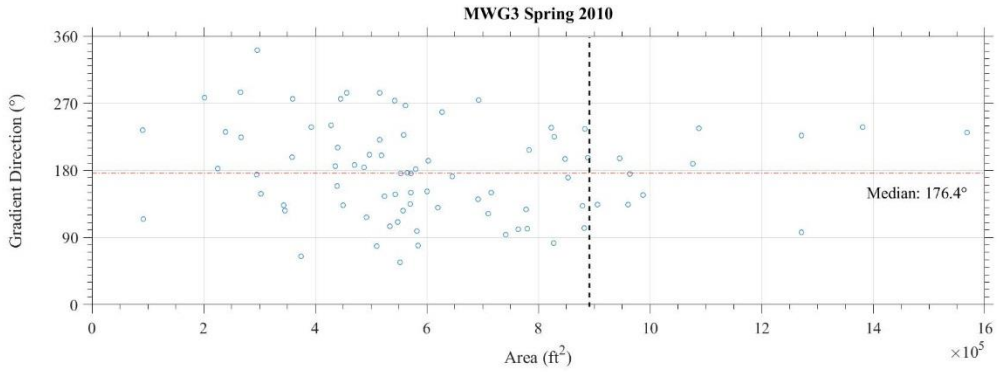

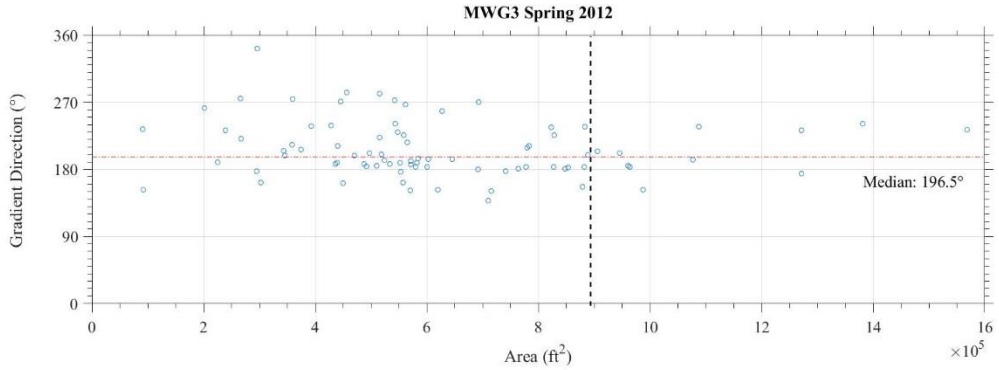

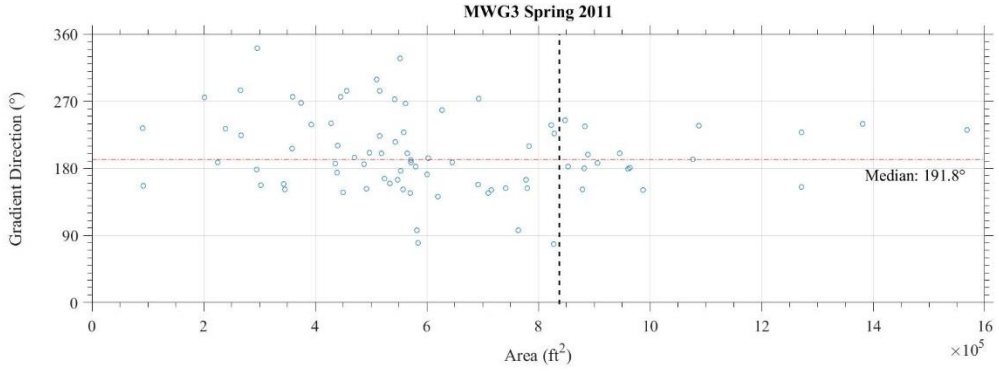

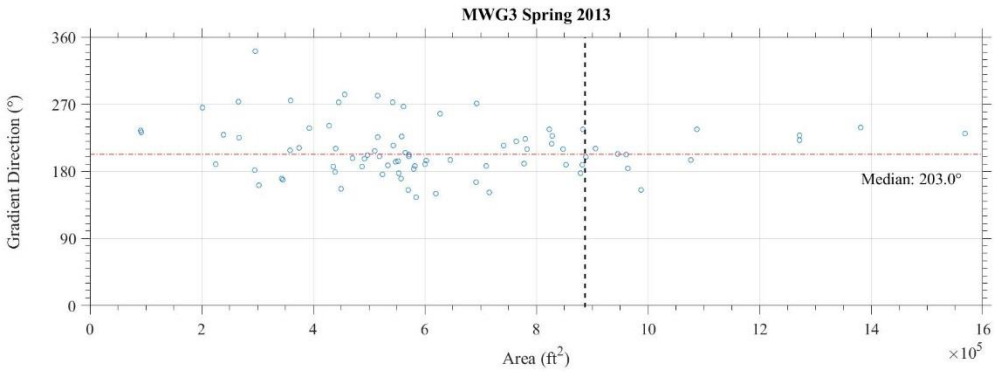

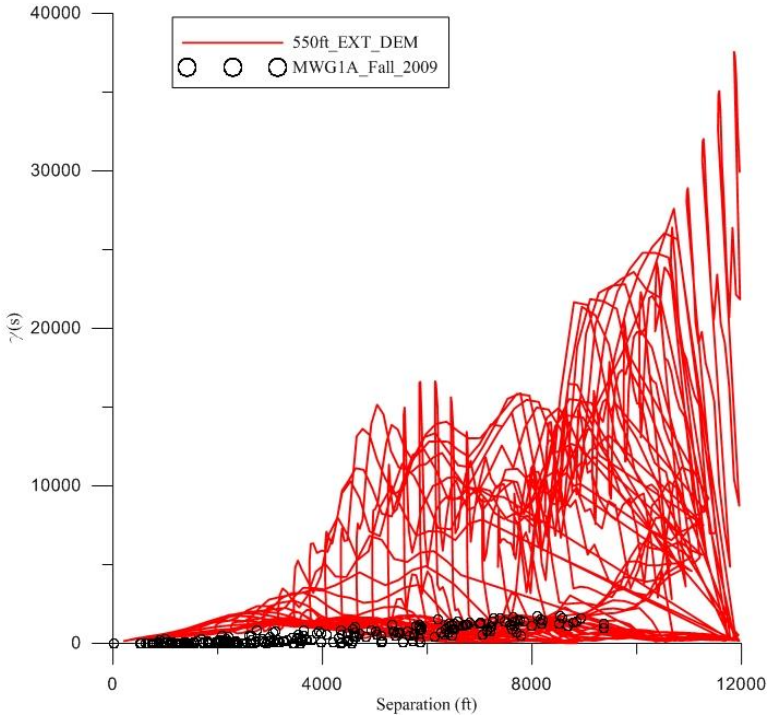

MWG1A Fall 2009 Variogram Comparison

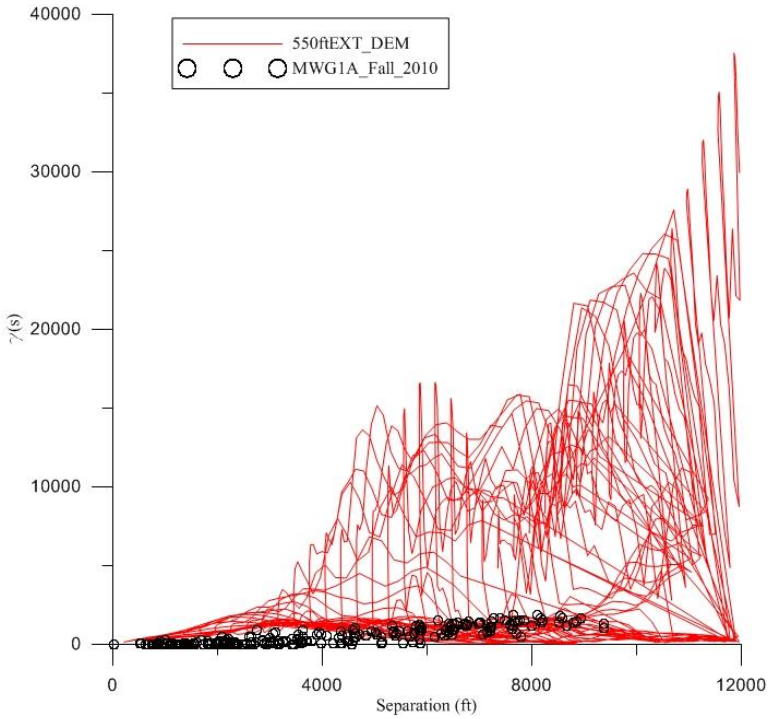

MWG1A Fall 2010 Variogram Comparison

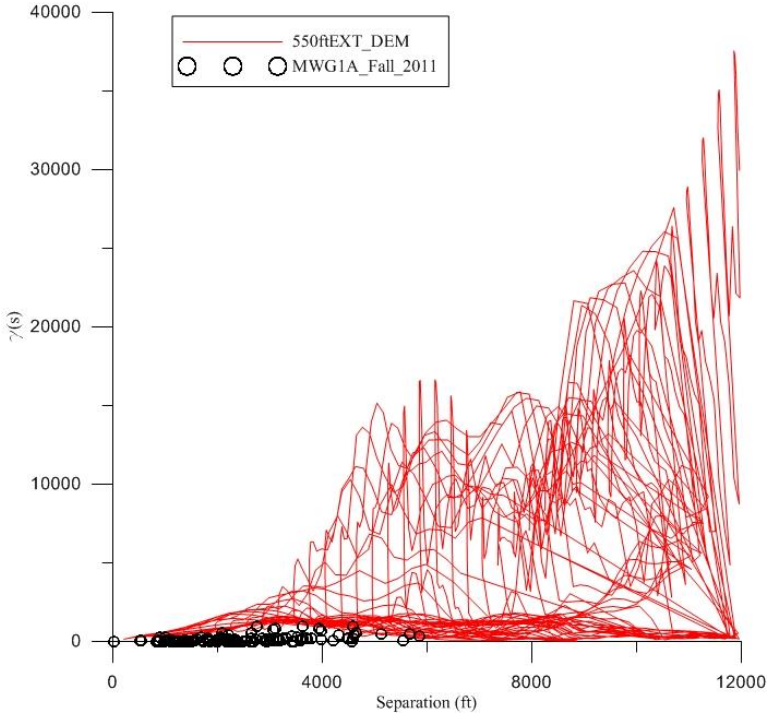

MWG1A Fall 2011 Variogram Comparison

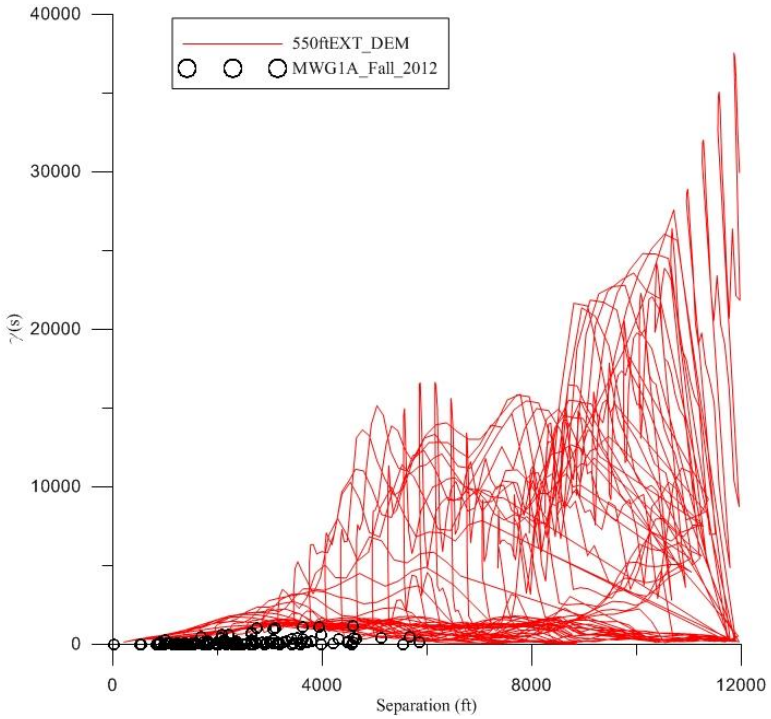

MWG1A Fall 2012 Variogram Comparison

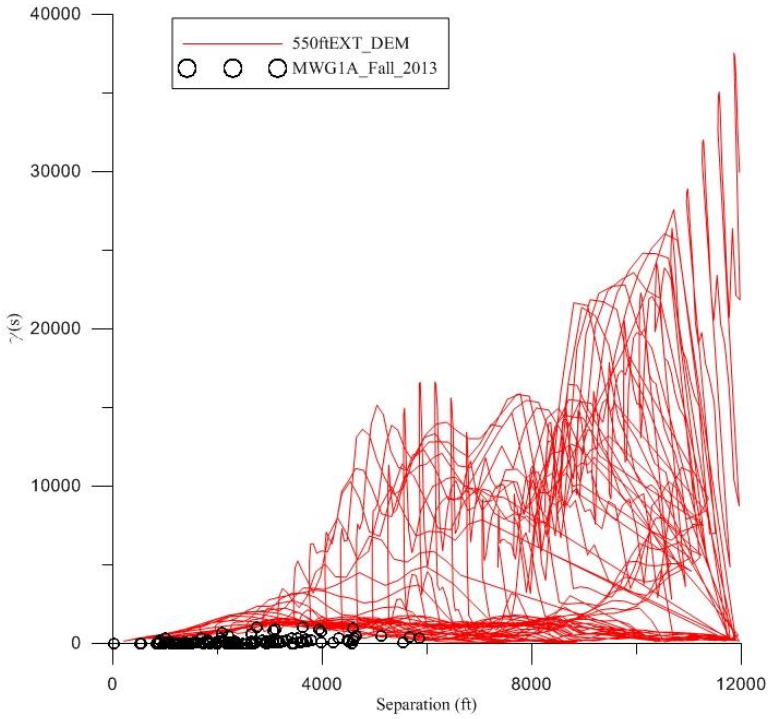

MWG1A Fall 2013 Variogram Comparison

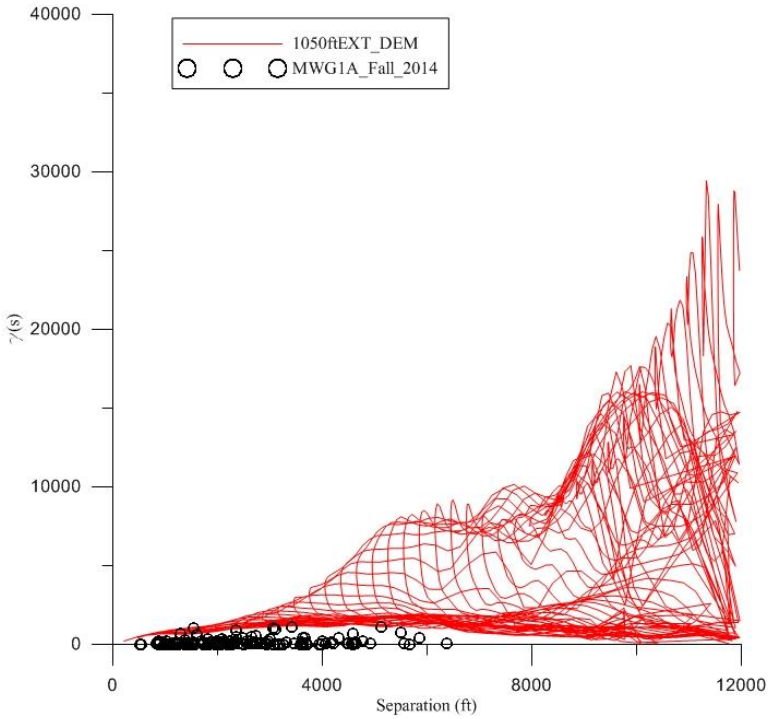

MWG1A Fall 2014 Variogram Comparison

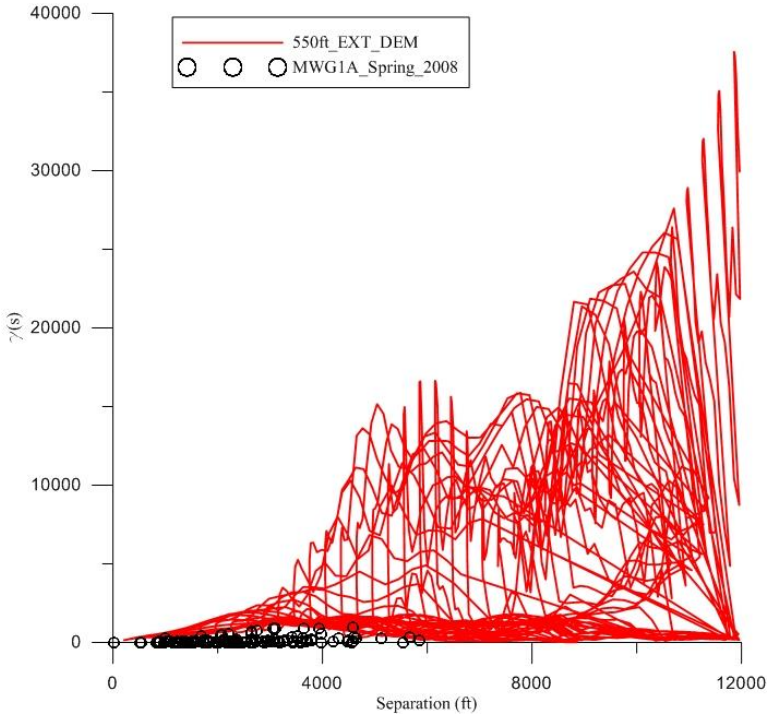

MWG1A Spring 2008 Variogram Comparison

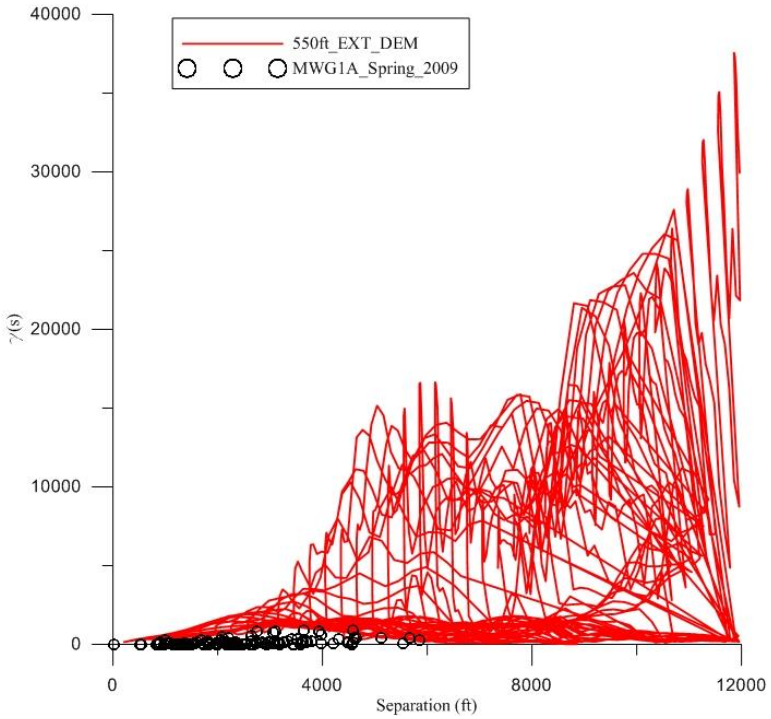

MWG1A Spring 2009 Variogram Comparison

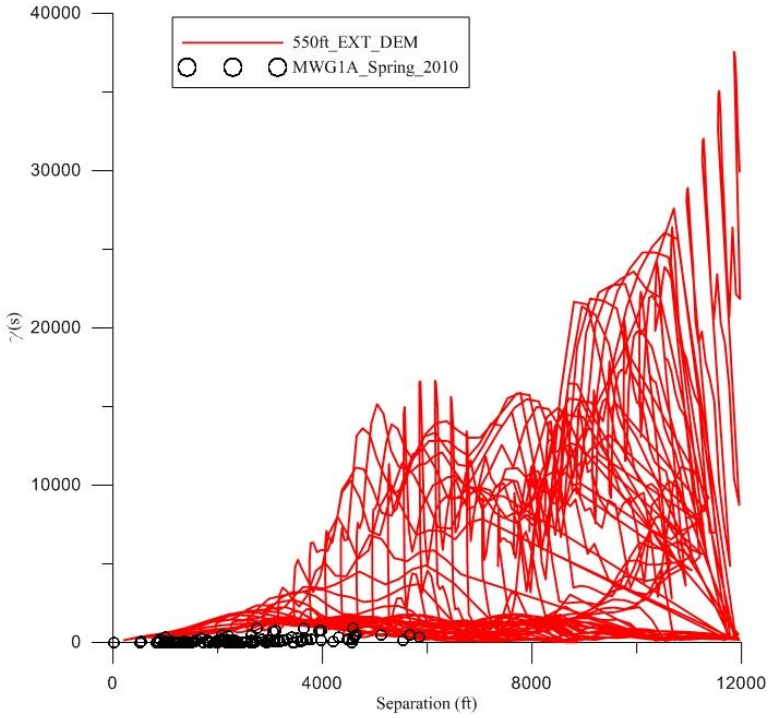

MWG1A Spring 2010 Variogram Comparison

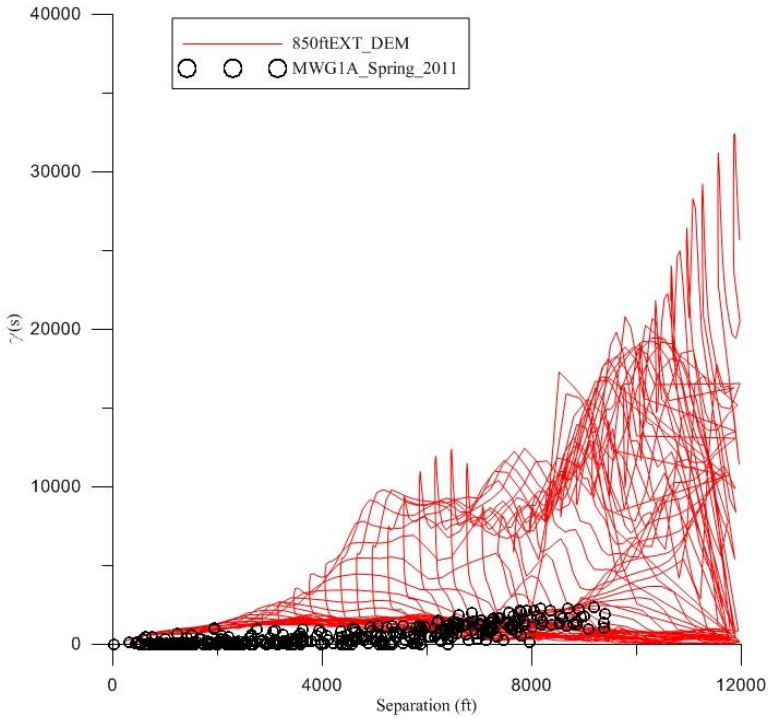

MWG1A Spring 2011 Variogram Comparison

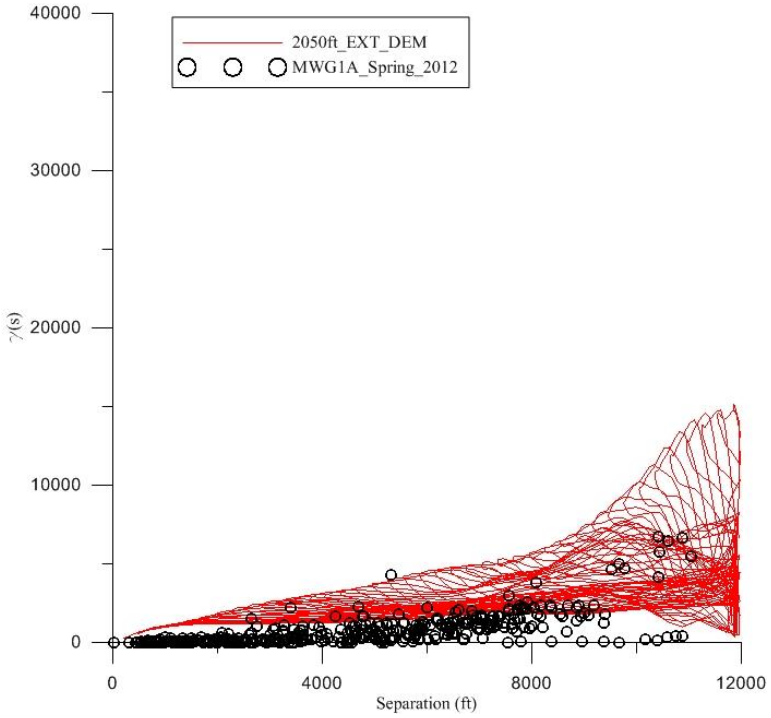

MWG1A Spring 2012 Variogram Comparison

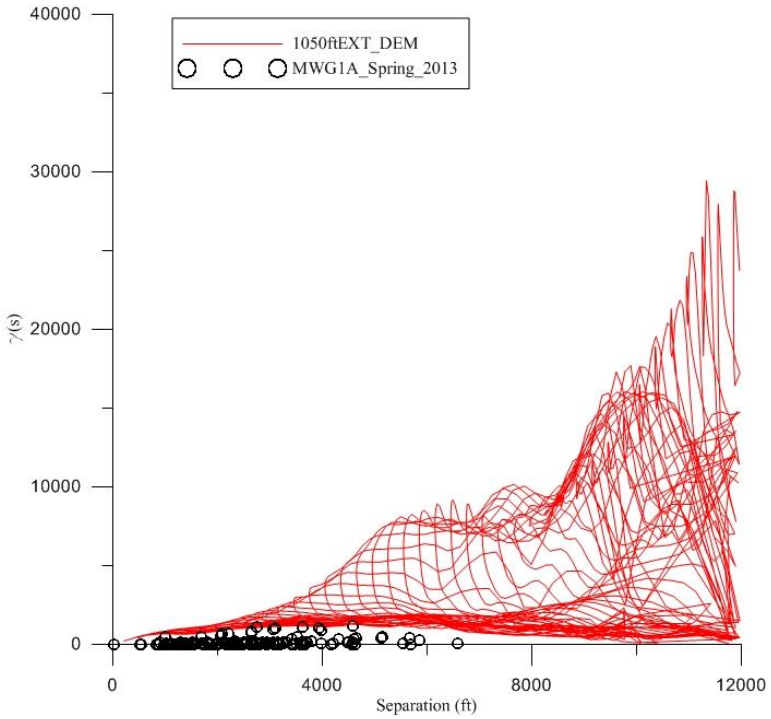

MWG1A Spring 2013 Variogram Comparison

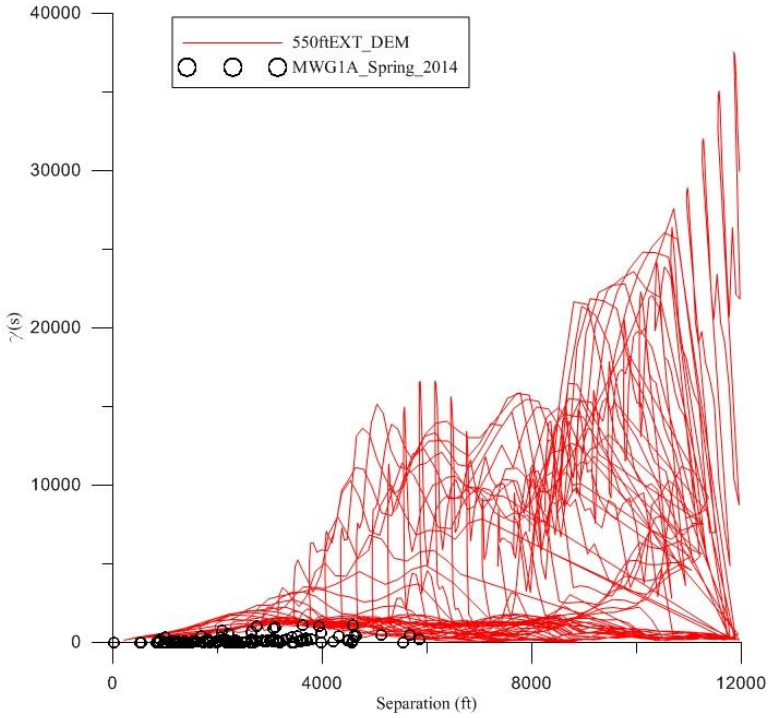

MWG1A Spring 2014 Variogram Comparison

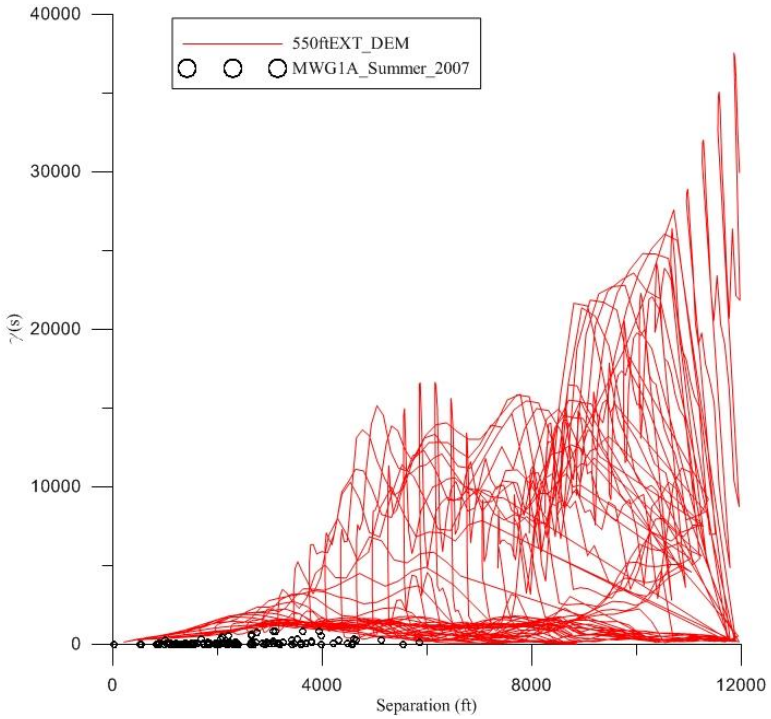

MWG1A Summer 2007 Variogram Comparison

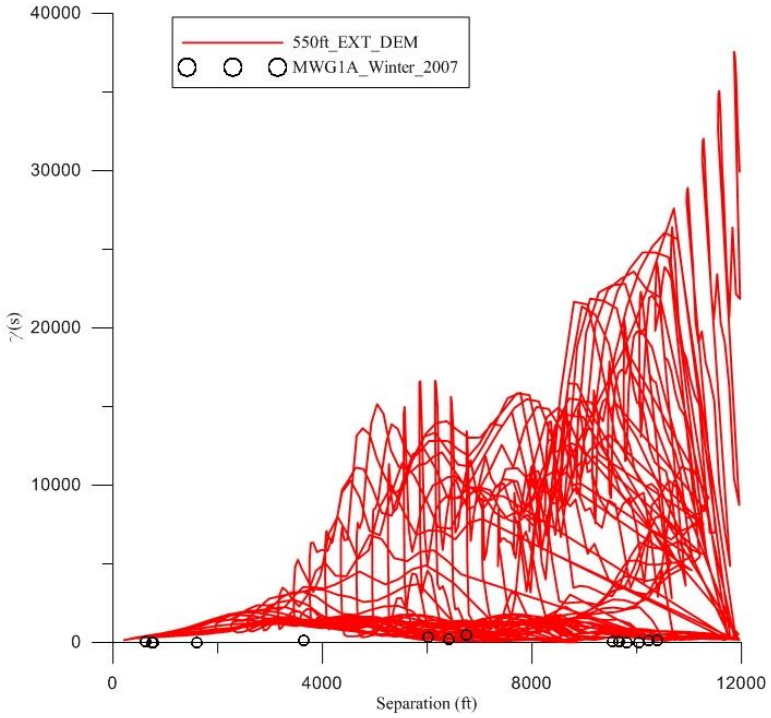

MWG1A Winter 2007 Variogram Comparison

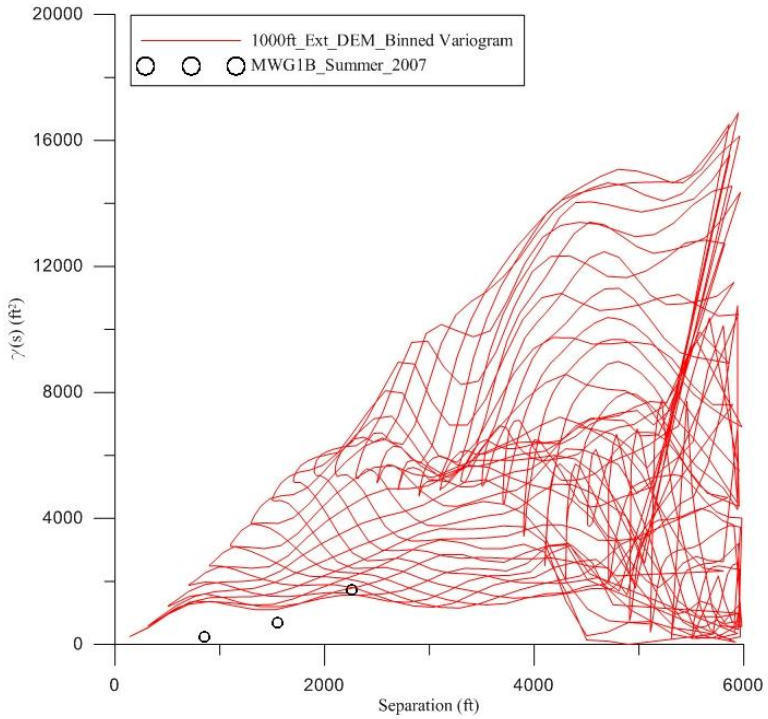

MWG1B Summer 2007 Variogram Comparison

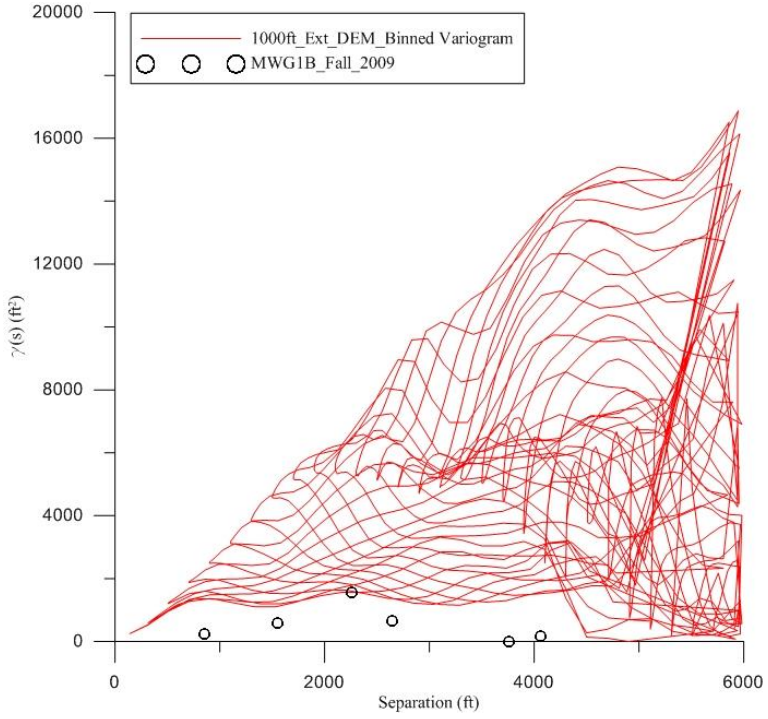

MWG1B Fall 2009 Variogram Comparison

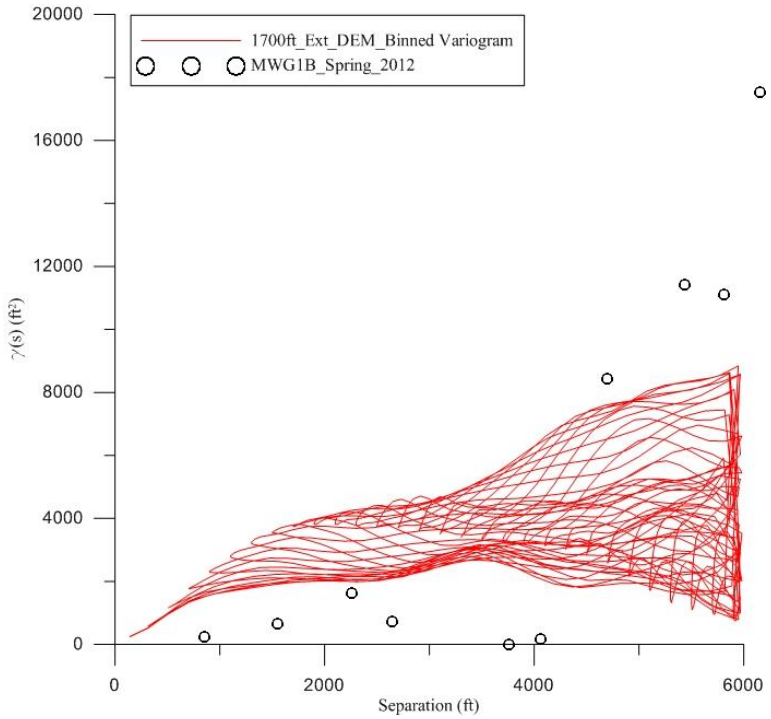

MWG1B Spring 2012 Variogram Comparison

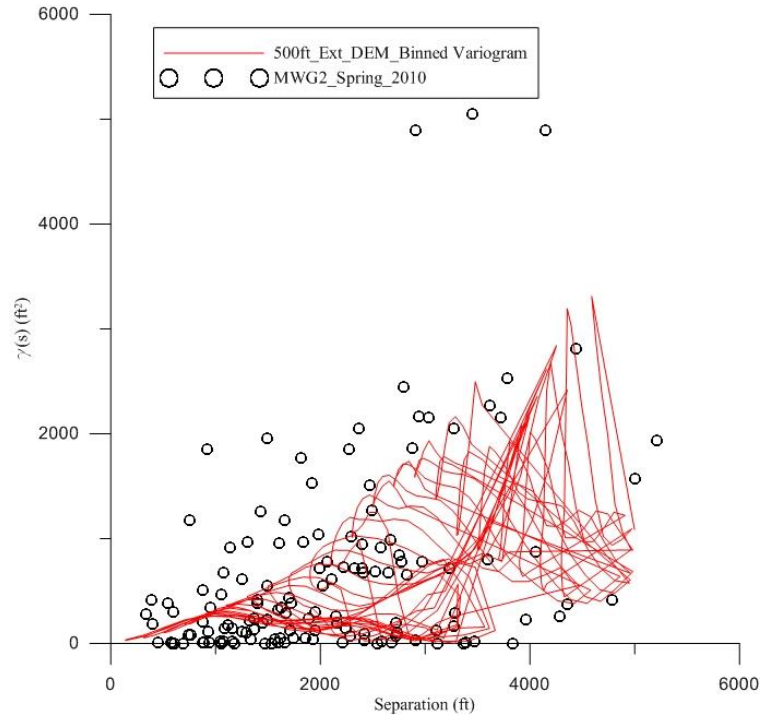

MWG2 Spring 2010 Variogram Comparison

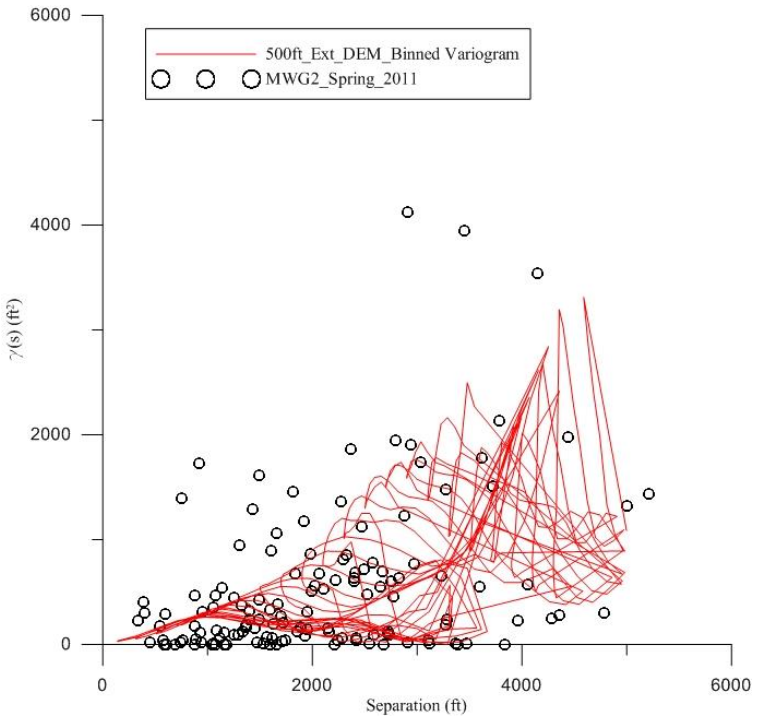

MWG2 Spring 2011 Variogram Comparison

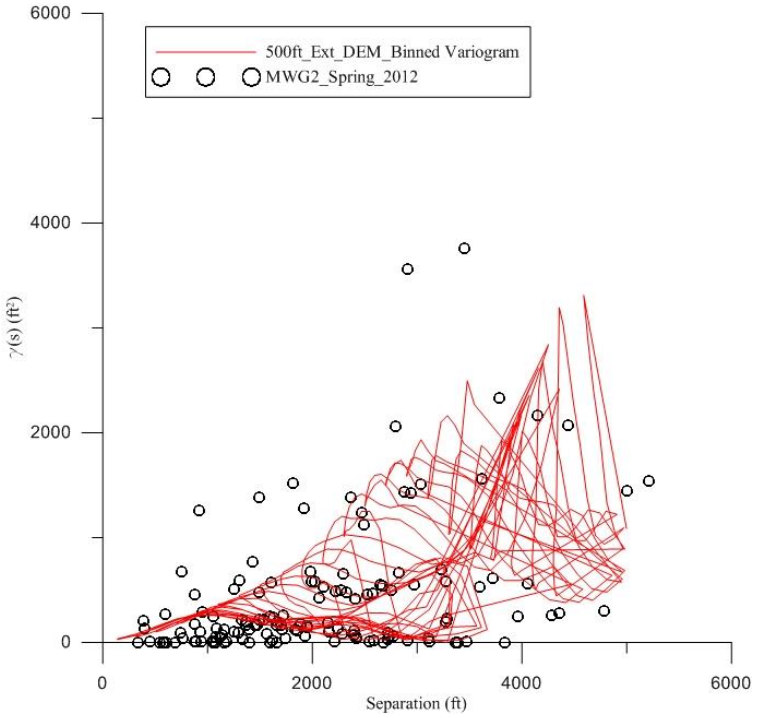

MWG2 Spring 2012 Variogram Comparison

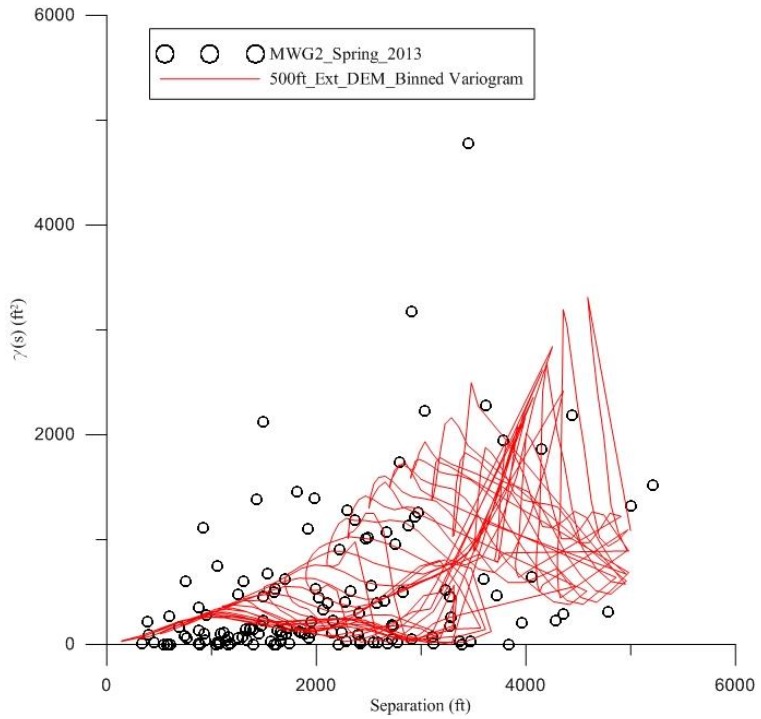

MWG2 Spring 2013 Variogram Comparison

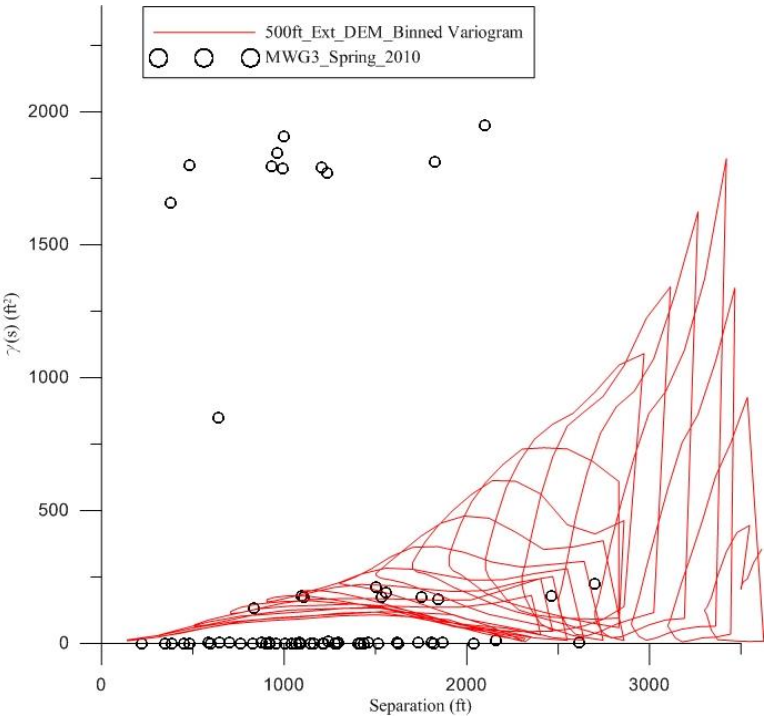

MWG3 Spring 2010 Variogram Comparison

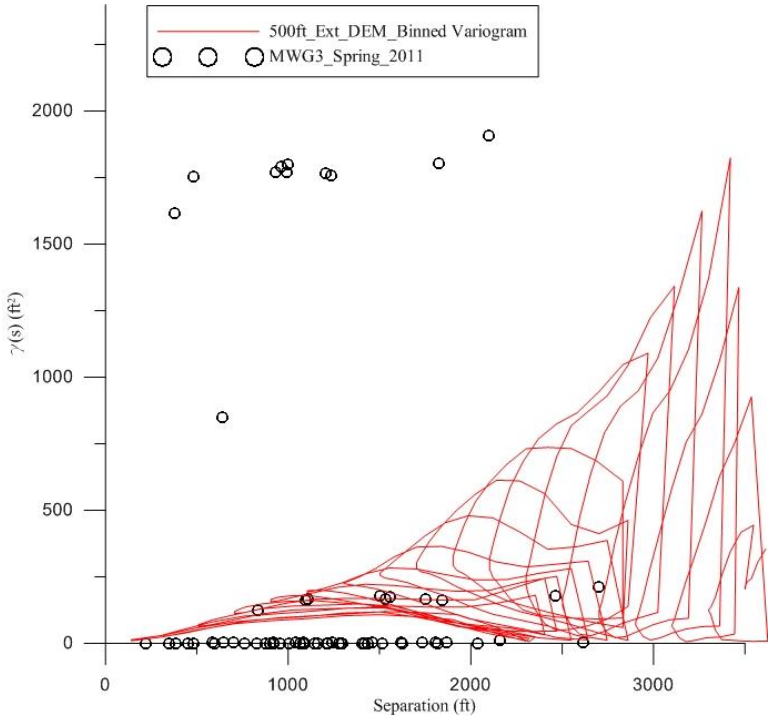

MWG3 Spring 2011 Variogram Comparison

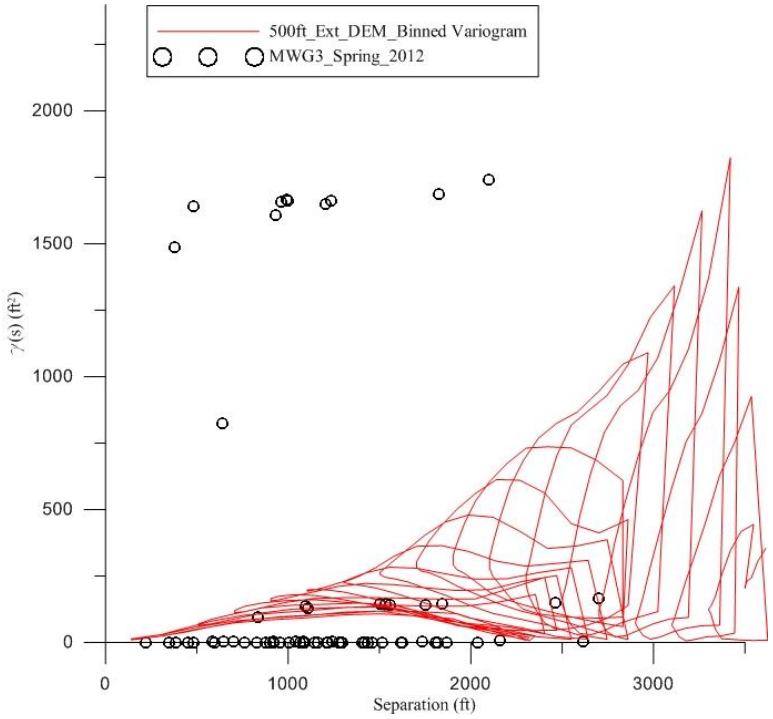

MWG3 Spring 2012 Variogram Comparison

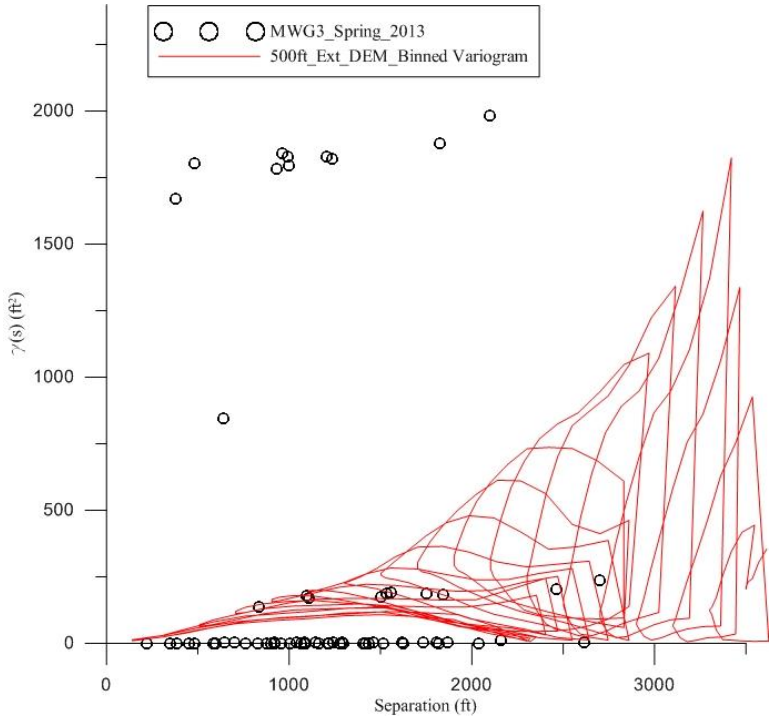

MWG3 Spring 2013 Variogram Comparison

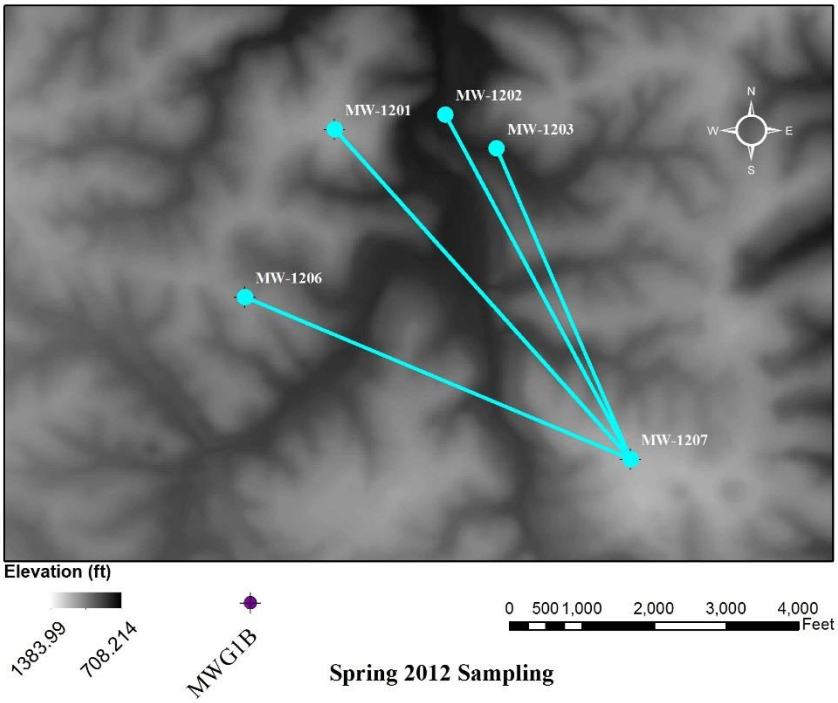

MWG1B Spring 2012 Variogram Links

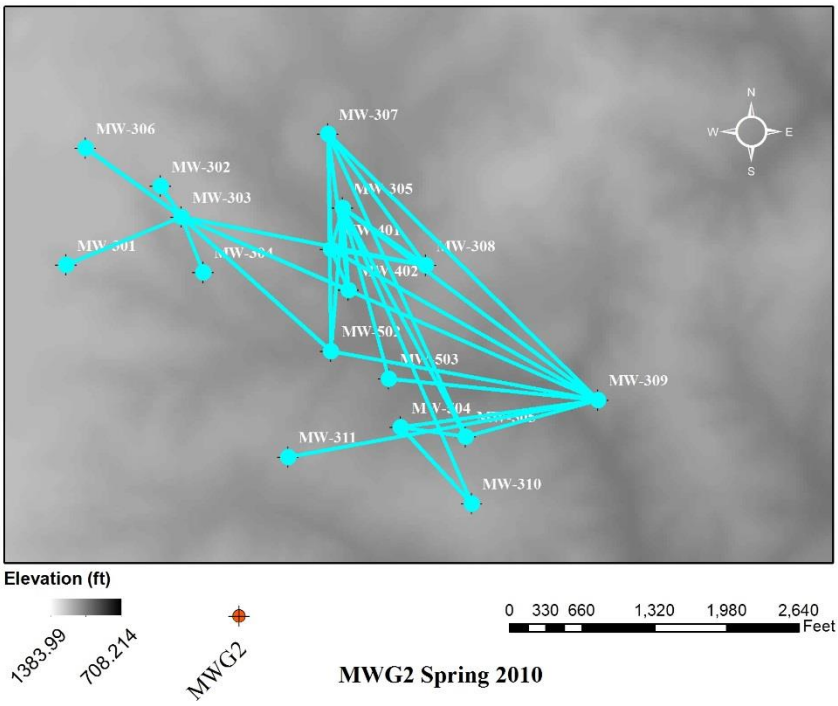

MWG2 Spring 2010 Variogram Links

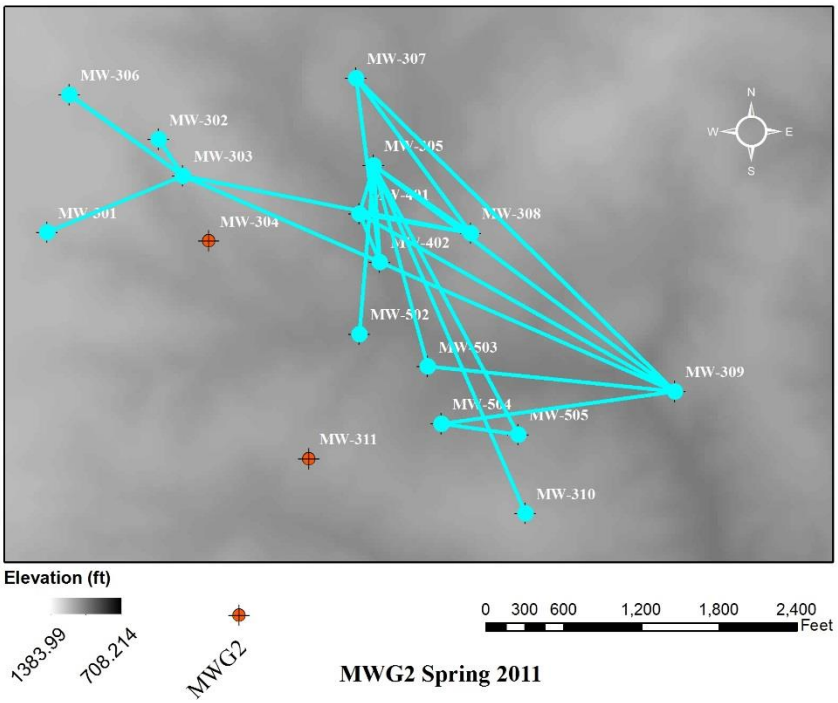

MWG2 Spring 2011 Variogram Links

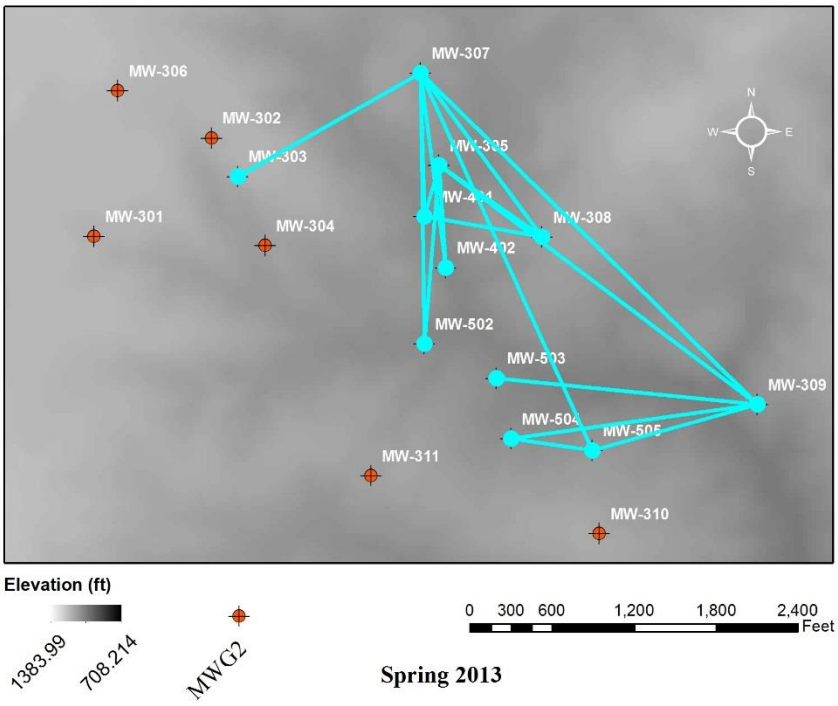

MWG2 Spring 2013 Variogram Links

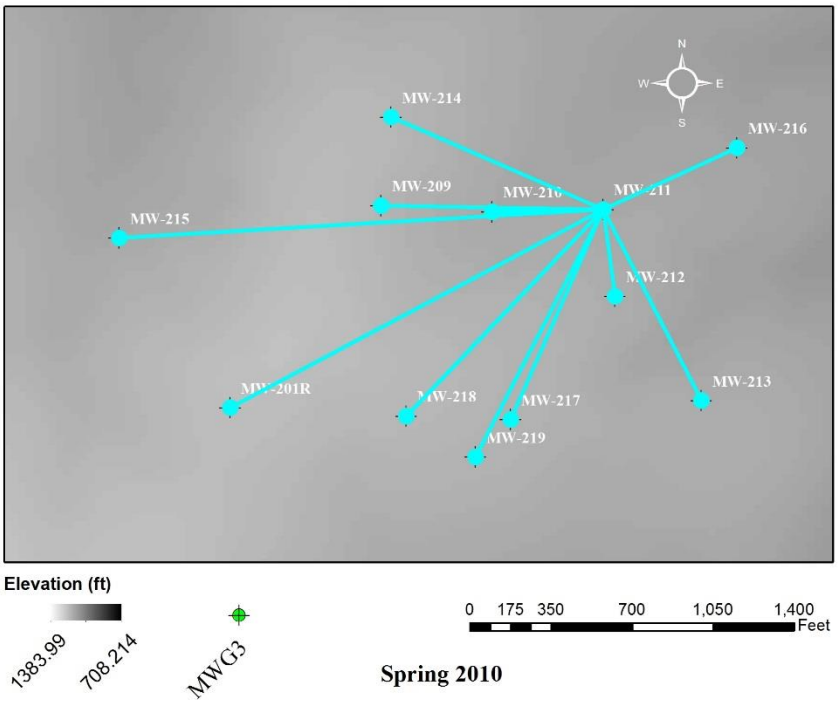

MWG3 Spring 2010 Variogram Links

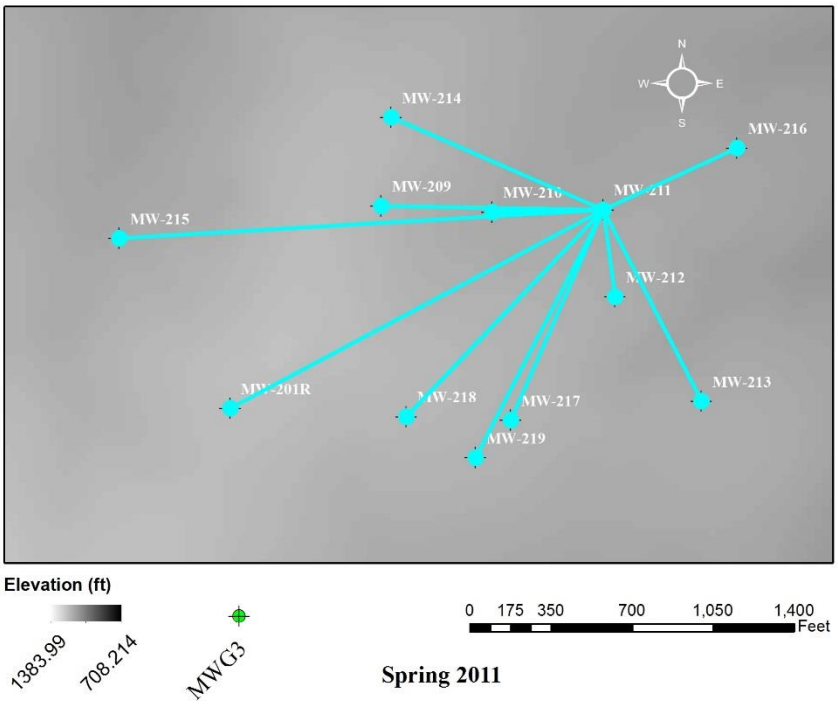

MWG3 Spring 2011 Variogram Links

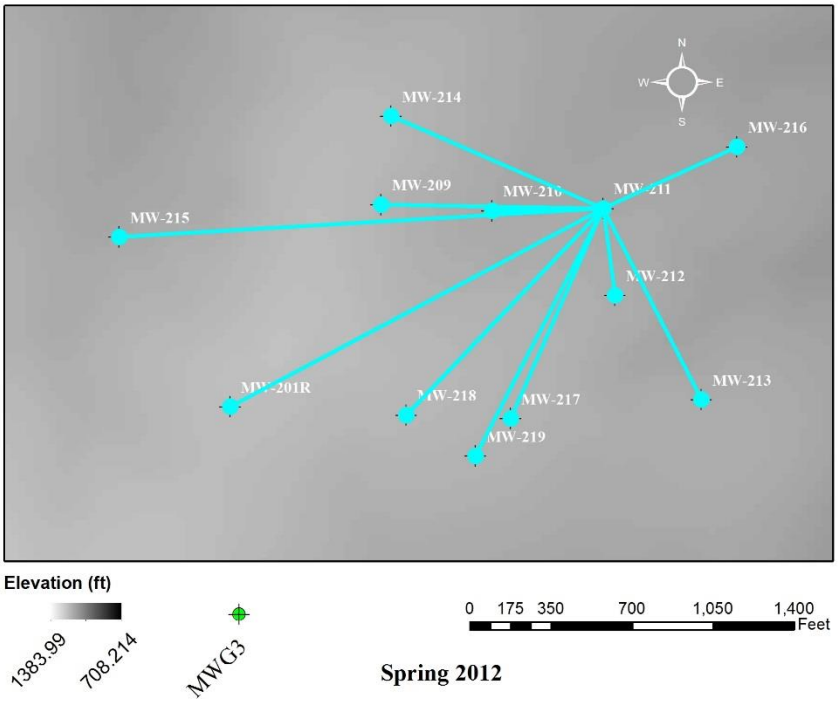

MWG3 Spring 2012 Variogram Links

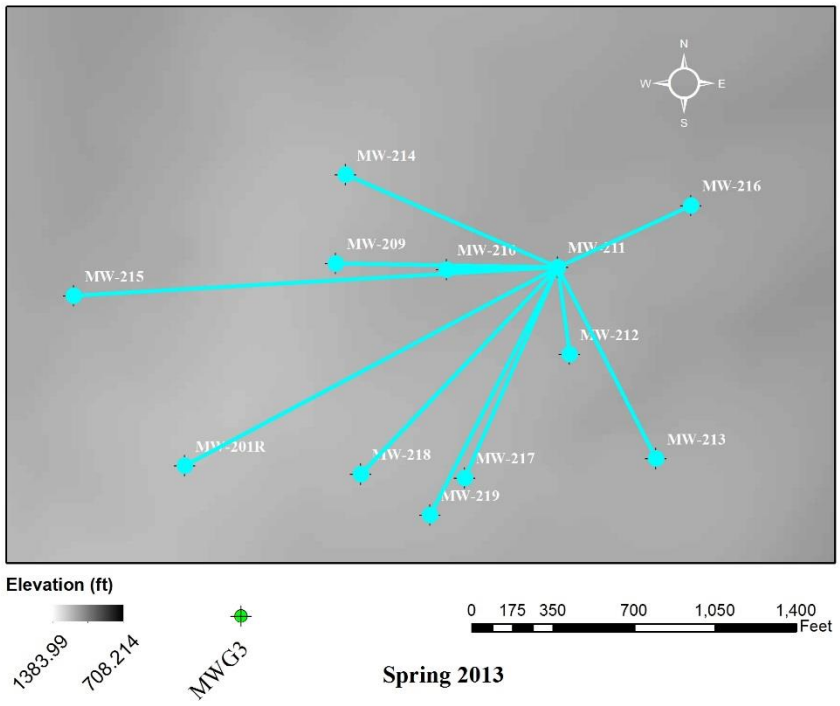

MWG3 Spring 2013 Variogram Links

REFERENCES

Bardossy, A. and Kundzewicz Z. W. (1990). "Geostatistical methods for detection of outliers in groundwater quality spatial fields." *Journal of Hydrology*. 115, 343-359.

Blauvelt, R. P. and Fullmer, D. (2011). "The Use of Topography as an Indicator of Ground Water Flow Direction and Its Implications for Due Diligence." *Journal of ASTM International*, 8(3), 103115.

Chen D., Lu, C.-T., Kou, Y., Chen, F. (2008). "On detecting spatial outliers." *Geoinformatica*. 12, 455-475.

Domenico, P. A., and Schwartz, F. W. (1998). *Physical and chemical hydrogeology*. Wiley, New York.

Goovaerts, P. (1997). *Geostatistics for natural resources evaluation*. Oxford University press, New York, N.Y.; Oxford.

Hannah, M.J., (1981). "Error detection and correction in digital terrain models." *Photogrammetric Engineering and Remote Sensing*. 47(1), 63-69.

Journel, A. G., and Huijbregts, C. J. (1997). *Mining geostatistics*. Acad. Press, London.

King, F.H., (1899). Principle and conditions of the movements of groundwater. US Geol. Survey 19th Ann. Rep. Part 2, 59-294.

Liu, H., Jezek, K. C., O'Kelly, M. E. (2001). "Detecting outliers in irregularly distributed spatial data sets by locally adaptive and robust statistical analysis and GIS." *Int. J. Geographical Information Science*. 15(8), 721-741.

Miller. R.D., Davis, J.C., Olea, R.A. (1997). "Acquisition Activity, Statistical Quality Control, and Spatial Quality Control for 1997 Annual Water Level Data Acquired by the Kansas Geological Survey." Open-file Report 97-33, Kansas Geological Survey.

Shekhar, S., Lu, C.-T., Zhang, P. (2003). "A unified approach to detecting spatial outliers." *GeoInformatica*. 7(2), 139-166.

Silliman, S. E., and Frost, C. (1998). "Monitoring Hydraulic Gradient Using Three-Point Estimator." *Journal of Environmental Engineering*, 124(6), 517–523.

Tremblay, Y., Lemieux, J.-M., Fortier, R. Molson, J., Therrien, R., Therrien, P., Comeau, G., Marie-Catherine, T. P. (2015). "Semi-automated filtering of data outliers to improve spatial analysis of piezometric data." *Hydrogeology Journal*. 23, 851-868.

Vacher, H. L. (2005). "Computational geology 12 - Cramer's Rule and the Three-Point Problem." *Journal of Geoscience Education*, 48(4), 522–532.

VITA

Zane Helwig was born to David Helwig and Deborah Spick in Oklahoma City, Oklahoma. In December 2015 he graduated Cum Laude with a B.S. degree in Geological Engineering and obtained his M.S. in Geological Engineering in July 2017 from Missouri University of Science and Technology.

Zane worked as a GIS intern at the Missouri Department of Natural Resources in Jefferson City, Missouri during the summer of 2015. He is an Engineering intern and 40-Hour Hazardous Waste Operations and Emergency Response certified. An extended abstract of Zane's work has been accepted for the ASCE-EWRI Hydraulic Measurements & Experimental Methods conference.